Preparation and Characterization of Flyash Based Catalyst for Transesterification of Mustard Oil

Thesis submitted in partial fulfillment of the requirements for the degree of

DOCTOR OF PHILOSOPHY

by

Vikranth Volli

Department of Chemical Engineering

Indian Institute of Technology Guwahati

Guwahati - 781039, India

Preparation and Characterization of Flyash Based Catalyst for Transesterification of Mustard Oil

Vikranth Volli

Preparation and Characterization of Flyash Based Catalyst for Transesterification of Mustard Oil

Thesis submitted in partial fulfillment of the requirements for the degree of

DOCTOR OF PHILOSOPHY

by

Vikranth Volli
Roll No.: 11610701

Department of Chemical Engineering
Indian Institute of Technology Guwahati
Guwahati - 781039, India

July, 2015

Dedicated To

Deepu

Department of Chemical Engineering
Indian Institute of Technology Guwahati
Guwahati - 781039, India

CERTIFICATE

This is to certify that the thesis entitled ***"Preparation and Characterization of Flyash Based Catalyst for Transesterification of Mustard Oil"*** being submitted by ***Vikranth Volli*** for the award of PhD degree has been carried out under my guidance and supervision. The work documented in this thesis has not been submitted to any other University or Institute for the award of any degree or diploma.

(Dr. Mihir Kumar Purkait)

Professor

Department of Chemical Engineering,

Indian Institute of Technology Guwahati

Guwahati - 781039, India.

Acknowledgements

I would like to express my gratitude to all those who helped me in different ways in completing this research work within the time span of four years directly or indirectly. First and foremost, I would like to express my deep felt gratitude to my supervisor, **Dr. Mihir Kumar Purkait** for providing me continuous inspiration and guidance throughout the entire course of work. I am indebted to him for his useful suggestions and constant encouragement throughout the entire period.

I am grateful to **Dr. Mihir Kumar Purkait** for his continuous support, interesting discussions and giving me freedom in handling different issues. His uncompromising approach to complete the experimental part, data analysis, writing manuscripts as well as thesis within the stipulated time period helped me a lot in completing my research work. His flexibility and openness in dealing with the specific and general needs of this research work helped me in improving the quality of the articles. I thank him for his patience and helping nature. It has been a great privilege to work with him.

I must also thank my doctoral committee members **Dr. S.K. Majumder, Dr. Vimal Katiyar** of the Department of Chemical Engineering and **Dr. Ramesh Aiyagari** of the Department of Biosciences and Bioengineering, for their valuable suggestions and contribution towards the improvement of my research work.

I also thank all the faculty members of the Department of Chemical Engineering for their kind cooperation during my stay in the department. I am also thankful to all the staff members and scientific officers of the Chemical Engineering Department for their genuine help during my entire research period. I also acknowledge the financial support provided by the **DST, New Delhi.**

I am thankful to the Central Instruments Facility of IIT Guwahati for allowing me to carry out **TGA-DSC, FESEM and Raman** analysis, which has been very important in this research work. In this regard, I should acknowledge the help of **Mr. K. K. Senapati,** Scientific Officer, Central Instruments Facility, IIT Guwahati.

I was fortunate enough to get excellent batchmates like**, Ravi Bhandari, Manish, Harsha, Randeep, Shyam, Anjali, Ravi Kiran, Venu Babu, Rupak, Abhik, Abhipsa, Nevin, Chaitanya, Dhanaraj and Deepthi** for their friendly support, timely assistance and co – operation throughout my research work.

Last but not the least; I would like to express my deepest sense of gratitude to my parents and family members. Their love, care, sacrifice and encouragement have made it possible for me to come so far. I appreciate the courage, understanding and dedicated support shown by all of them despite many testing times at their end.

Vikranth Volli

(Email: vikranthvolli@gmail.com)

Abstract

Development of suitable technologies for the production of alternate source of energy has become a daunting task in the recent decades. The depletion of fossil fuels and increasing population further increased these complexities. Biodiesel, a suitable alternative to conventional energy system has attracted the attention of the scientific community. Though there are many ways for biodiesel production, transesterification has gained a lot of importance due to renewability, higher cetane number and combustion efficiency. Transesterification is often performed in presence of catalyst (homogeneous, heterogeneous and enzymatic) and development of these catalysts (heterogeneous) from industrial wastes with high basic properties is the main objective of this study. This work presents the use of flyash as starting material for the synthesis of heterogeneous catalyst for transesterification of mustard oil. The entire work carried out in this research was divided into five major parts. The abstract of each part is highlighted below

Physico-chemical properties and thermal degradation studies of commercial oils in nitrogen atmosphere

Thermal properties and reaction kinetics of commercial oils play prominent role in design, operation and modeling of systems with various industrial applications including cosmetics, lubrication, fuel and food processing. Thermogravimetric analysis (TGA) and differential thermogravimetric analysis (DTG) techniques were used to study the thermo-chemical behavior of four varieties of oils (mustard, soybean, olive and karanja). The thermal degradation was studied in an inert (N_2) atmosphere from ambient temperature to a temperature of 600 °C using a heating rate of 10, 20, 30, 50, 100 ^{o}C min^{-1}. The chemical composition and thermal properties were investigated by measuring FTIR, DSC, CHNS and ^{1}H NMR. Physical properties such as moisture content, viscosity, ash content, flash, fire, pour and cloud points were also determined. The model-free iso-conversional methods were used to determine kinetic parameters without making any assumptions about the reaction function and reaction order which avoids the risk of obtaining wrong kinetic parameters, especially activation energy, due to pre-assumption of inappropriate reaction function. Four degradation models including modified Coats and Redfern, Friedman, Kissinger and Flynn–Wall–Ozawa methods were used to determine the apparent activation energy.

Utilization of flyash as heterogeneous catalyst for transesterification

The work reconnoitres the feasibility of utilizing flyash supported hydroxyapatite as heterogeneous catalyst for transesterification. Conventional wet-impregnation method was used to synthesize a strong base catalyst from bone powder (milled animal bone) calcined at 900 ^{o}C for 2 h in order to convert the calcium phosphate present in it to hydroxyapatite. Three different catalysts (viz. C10, C20 and C30) were synthesized by varying the ratio of bone powder to flyash (0.5:4.5, 1:4 and 1.5:3.5), respectively. The synthesized catalyst was characterized for its chemical composition by (TGA, XRD, XRF, LPSA, SEM and BET) and their activity was evaluated through transesterification of mustard oil. Response surface methodology (RSM) with three factors - three level central composite design (CCD) was employed to statistically assess and optimize biodiesel production. The predicted values from the statistical model to achieve highest conversion of biodiesel would be 90.4% at CBP loading of 10 wt %, 9.6 wt % catalyst concentration and 5.5:1 methanol/oil molar ratio. The synthesized catalyst was reused for 5 times without any significant reduction in its activity. Results showed that calcium enriched waste materials when impregnated in flyash might be a good potential source of catalyst in biodiesel production.

Selective preparation of zeolite X and A from flyash and its use as catalyst for biodiesel production.

The utilization of flyash for synthesis of heterogeneous catalyst for transesterification was explored. Different types of zeolites were synthesized from alkali fusion followed by hydrothermal treatment of coal flyash as source material. The synthesis conditions were optimized to obtain highly crystalline zeolite based on degree of crystallinity and cation exchange capacity (CEC). The effect of CEC, acid treatement, Si/Al ratio and calcination temperature (800, 900 and 1000 ^{o}C) on zeolite formation was also studied. Pure, single phase and highly crystalline zeolite was obtained at flyash/NaOH ratio (1:1.2), fusion temperature (550 ^{o}C), fusion time (1 h), hydrothermal temperature (110 ^{o}C) and hydrothermal time (12 h). The synthesized zeolite was ion-exchanged with potassium and was used as catalyst for transesterification of mustard oil to obatin a maximum conversion of 84.6% with 5 wt % catalyst concentration, 12:1 methanol to oil molar ratio, reaction time of 7 h at 65 ^{o}C. The catalyst was reused for 3 times with marginal reduction in activity.

Preparation and characterization of hydrotalcite with bifunctional properties from flyash for transesterification

Attempts were made to synthesize Mg-Al hydrotalcite like materials with bifunctional properties from flyash and flyash zeolite by co-precipitation method. The synthesized hydrotalcite and their corresponding Mg-Al mixed oxides obtained after calcination were characterized for their structural, compositional, thermal and morphological properties by XRD, XRF, TGA, FESEM, BET, FTIR, Raman spectroscopy and H_2-TPR. The synthesized hydrotalcite had Mg/Al ranging from 1.3 to 2.3. The activity of the synthesized catalyst was estimated in transesterification of mustard oil and the effect of reaction time, catalyst concentration and methanol to oil molar ratio on biodiesel production was also investigated. A maximum yield of 93.4% was obtained with methanol to oil molar ratio of 12:1, 7 wt % catalyst concentration for 6 h of reaction at 65 ^{o}C. The study showed the potential application of flyash and its use in modified Mg-Al hydrotalcite materials as heterogeneous catalyst in biodiesel production.

Thermal stability, physical properties, chemical composition and degradation kinetics of biodiesel: A comparative study.

This study discusses the physical properties of synthesized mustard oil methyl ester (MOME) using ASTM standards and are compared with raw mustard oil and standard biodiesel. The thermal stability and degradation kinetics of MOME produced was estimated by using thermogravimetric analysis at 10, 20, 30, 50 and 100 ^{o}C min^{-1} heating rates using iso-conversional methods. The values of onset temperatures and activation energy was compared with mustard oil. The average values of activation energy were determined as 142.4, 117.3, 131.9 and 129.1 KJ mole^{-1} with regression coefficients of 0.95, 0.99, 0.96 and 0.95 for Friedman, Kissinger, Flynn - Wall - Ozawa and modified Coats - Redfern methods, respectively. When compared with the activation energy of mustard oil (149.5 KJmole^{-1}), the activation energy of MOME was found to be less (130.5 KJ mole^{-1}).

In summary, the thesis outlines the efficacy of flyash based catalyst for transesterification of mustard oil. The obtained data is anticipated to serve as reference data for furthering research in the field of catalysis and its application.

Table of Contents

List of Tables

List of Figures

Nomenclature

Abbreviations

AAS	Atomic adsorption spectroscopy
BET	Brunauer-Emmet-Teller
CEC	Cation exchange capacity
CHNS	Carbon hydrogen nitrogen sulfur
DSC	Differential scanning calorimetry
EDX	Energy dispersive X ray spectroscopy
FTIR	Fourier transform infrared spectroscopy
FFA	Free fatty acid
FESEM	Field emission scanning electron microscopy
GC-MS	Gas chromatography – Mass spectroscopy
LPSA	Laser particle size analyzer
NMR	Nuclear magnetic resonance
SEM	Scanning electron microscopy
TPR	Temperature programmed reduction
TGA	Thermogravimetric analysis
XRD	X- ray diffraction
XRF	X- ray fluoresce

Notations

X	Conversion
t	Time (sec)
K	Specific rate constant
n	Reaction order
W_0	Initial weight (mg)
W_t	Weight after time t (mg)
W_∞	W_∞ is the weight after pyrolysis (mg)
A	Frequency factor,
E_a	Activation energy (KJ $mole^{-1}$)
T	Temperature (^oC)
R	Universal gas constant (J $mole^{-1}$ K^{-1})
β	Heating rate (^oC min^{-1})
T_{onset}	Onset temperature (^oC)
T_{peak}	Peak temperature (^oC)
T_{offset}	Offset temperature (^oC)

Chapter 1

Introduction and Literature Review

Background;

State -of- the- art;

Objectives;

Organization of thesis.

In this chapter, a brief discussion of energy sources, requirements, alternatives and suitable conversion technologies in biodiesel production along with their properties was presented. The focus in this chapter has been towards the identification of suitable raw materials (oil and industrial wastes) for synthesis and characterization of heterogeneous base catalyst. Subsequently, the possible scope for further research has been elaborated. Finally, the objectives of the thesis and its organization was summarized.

1.1 Background

India is a mineral store house and the primary source for power generation is coal. The life of these convectional energy sources (coal, petroleum and natural gas) has become limited in the present era, where the use of energy and their source has been growing faster than world population. It is expected that the world population would increase by 1.3% per year, from 7238 million in 2014 to 9683 million in 2050. Indian population may increase from 1296.2 million to 1656.9 million from the year 2014 to 2050 with an annual average percent change of 1.3% from 2014 to 2050. Along with increase in population, the energy needs are also increasing. The world energy consumption would increase by 0.4 percent per year, from 97.1 quadrillion Btu in 2011 to 106.3 quadrillion Btu in 2040 [1, 2].

The major energy demand is fulfilled from the conventional energy resources like coal, petroleum and natural gas. These sources are in the verge of getting extinct. With declining petroleum resources and increased demand for petroleum products, there is an urgent need to develop economical and energy-efficient processes for production of fuels and chemicals. Biodiesel, a clean, environment friendly and renewable fuel source, could be considered as the best candidate for a diesel fuel substitute. Vegetable oils are promising feed

stocks for biodiesel production since they are renewable in nature and can be produced on a large scale and are environment friendly. Vegetable oils are two types edible and non-edible. More than 95% of biodiesel production feed stocks comes from edible oils since they are mainly produced in many regions and the properties of biodiesel produced from these oils are much suitable to be used as diesel fuel substitute [3, 4].

Table 1.1 Different methods of producing bio-diesel

Method	Definition	Advantage	Dis-advantage
Direct use and blending	Direct use as diesel fuel or blend with diesel fuel	liquid nature portability Heat content (80% diesel fuel) Readily available; renewability.	Higher viscosity Lower volatility Reactivity of unsaturated hydrocarbon chains
Micro-emulsions	A colloidal equilibrium dispersion of optically isotropic fluid generally in the 1-150 nm range formed spontaneously from two immiscible liquids.	Better spray patterns during combustion Lower fuel viscosities	Lower cetane number Lower energy content
Thermal cracking (pyrolysis)	The conversion of long-chain and saturated substance (biomass basis) to biodiesel by means of heat	Chemically similar to petroleum derived gasoline and diesel fuel	Energy intensive and hence higher cost
Trans-esterification	The action of a fat or oil with an alcohol in the presence of catalyst to form esters and glycerol	Renewability; higher cetane number; lower emissions; higher combustion efficiency	Disposal of byproduct (glycerol and waste water)

1.2 Biodiesel and their properties

As a well-known fact, a major substitute for these conventional sources is biodiesel. Biodiesel refers to a vegetable oil or animal fat-based diesel fuel consisting of long-chain alkyl (methyl, propyl or ethyl) esters. There are many ways of producing this biodiesel. Table 1.1 shows the different methods of biodiesel production. These are; by direct use and the use

of blends of available edible and non-edible oils, making micro-emulsions, thermal cracking (pyrolysis) and transesterification. Specifications of biodiesel [4, 5] are given in Table 1.2. The most commonly used method for converting oils to biodiesel is through transesterification of animal fat or vegetable oils.

Table 1.2 Specifications of biodiesel as per ASTM and EN standards.

Property	Units	Limits and test method	
		ASTM	EN
Flash point	^oC	130 min	101 min
Kinematic viscosity at 40°C	mm^2/s	1.9-6.0	3.5 - 5
Cetane number	--	47 min	51
Copper strip corrosion	--	NO.3 max	Class 1
Acid value	mgKOH/g	0.80 max	0.5 max
Free glycerol	% (m/m)	0.020 max	--
Phosphorous content	% (m/m)	0.001 max	0.01 max
Carbon residue (100% sample)	% (m/m)	0.050 max	0.3 max
Distillation	^oC	360 max	---
Water and sediment	%vol	0.050 max	--
Ash content	% (m/m)	0.02 max	--
Sulfur content	mg Kg^{-1}	--	10 max
Water content	% vol	0.05	--
Oxidation stability at 110 ^oC	H	--	6 min
Iodine value	--	--	120 max
Linolenic acid methyl ester	% (m/m)	--	12
Ester content	% (m/m)	--	96.5 min
Methanol content	% (m/m)	--	0.2 max
Monoglyceride content	% (m/m)	--	0.8 max
Diglyceride content	% (m/m)	--	0.2 max
Triglyceride	% (m/m)	--	0.2 max
Alkaline metals (Na+K)	mg Kg^{-1}	--	5 max

1.3 Transesterification and its history

Transesterification is the most effective way of producing biodiesel by using different sources of oils (edible, non-edible, animal and poultry fat). In transesterification of vegetable oils, a triglyceride reacts with an alcohol in the presence of a strong acid or base or enzymes (catalyst), producing a mixture of fatty acids alkyl esters and glycerol.

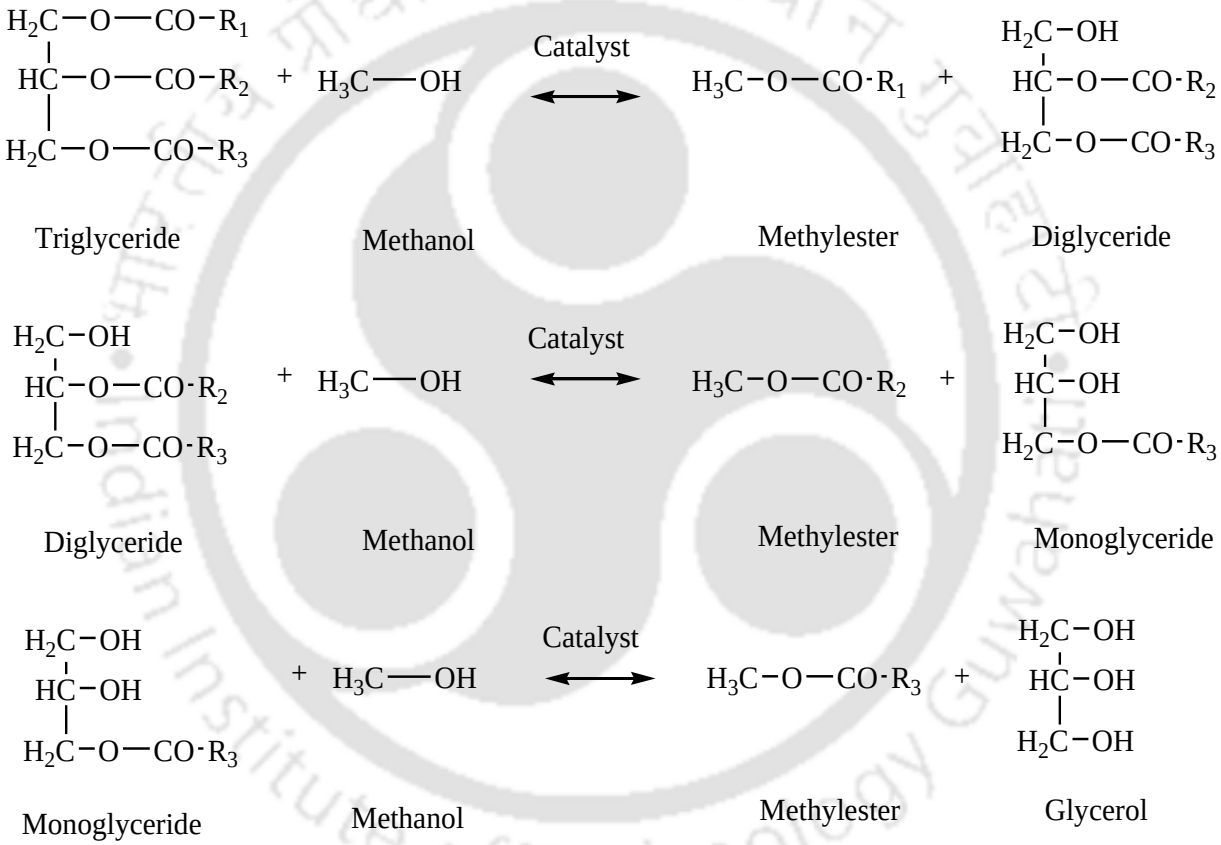

Fig. 1.1 General three stage transesterification process

Two chemists, E. Duffy and J. Patrick [6], were credited first with experimenting vegetable oils for transesterification to make soap in 1853. The resultant biofuel by-product was later named "biodiesel". Rudolph Diesel [6], on August 10, 1893, first demonstrated the

use of peanut oil to run his compression ignition engine. This date has since come to be known as "International Biodiesel Day". Henry Ford designed his 1908 Model T automobile [6] so that it could be powered with ethanol, a common biofuel made from hemp or corn.

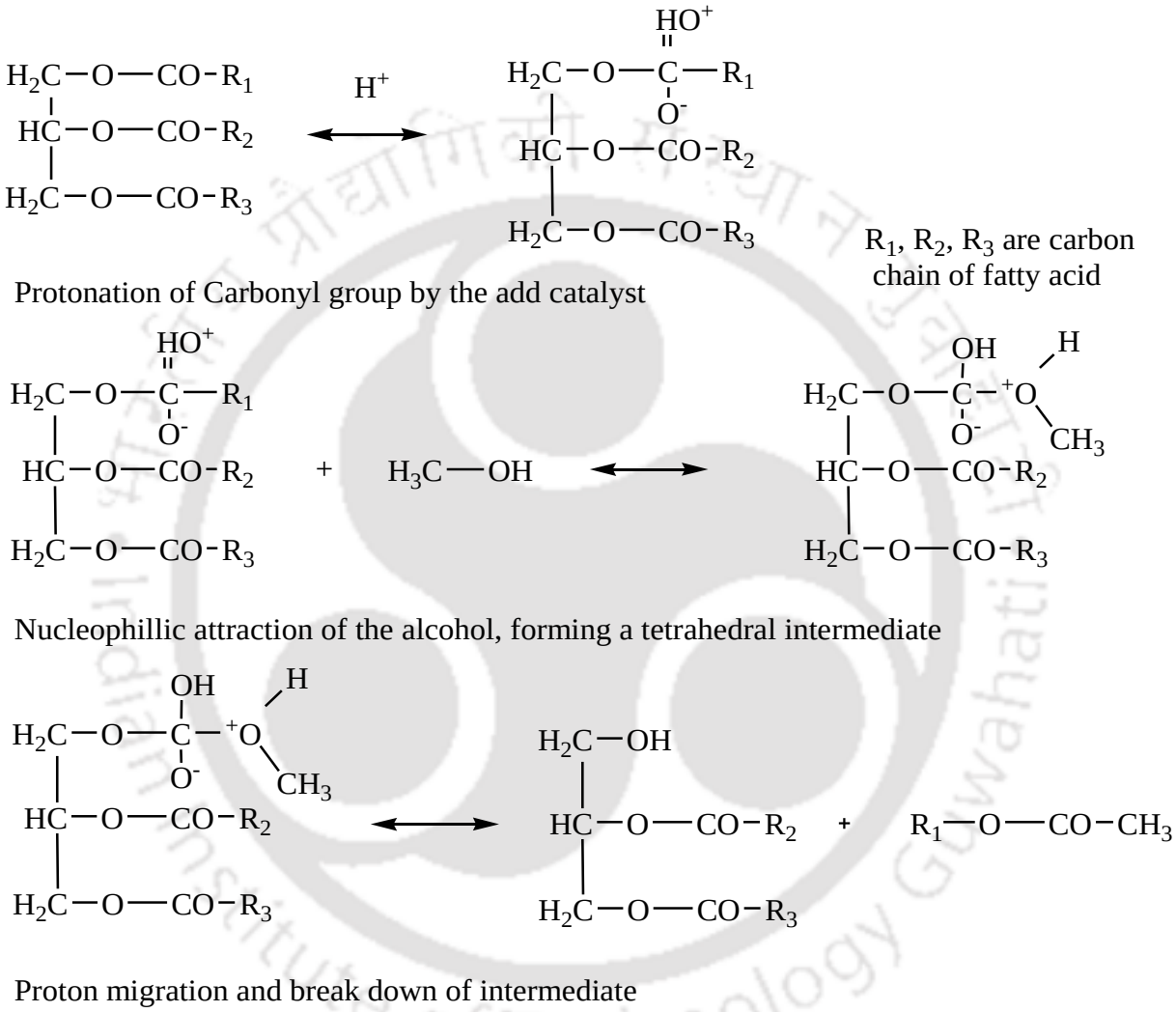

Fig. 1.2 Acid catalyzed reaction mechanism

The general mechanism for the process of transesterification is given in Fig. 1.1. Transesterification is always accompanied by the use of catalyst. The catalyst used can be either homogeneous-heterogeneous acid/base or enzyme catalyst. Figs. 1.2 and 1.3 show the mechanism for acid and base catalyzed transesterification, respectively. Higher free fatty acid

(FFA) content present in the oils restricts the use of these catalysts. Enzymatic transesterification not only increases the process cost but also restricts its application to laboratory scale. Fig. 1.4 shows the general flow sheet for the transesterification process [5]. However, the use of bi-functional catalyst in transesterification was a major breakthrough. The advantages and disadvantages of using these catalysts are given in Table 1.3.

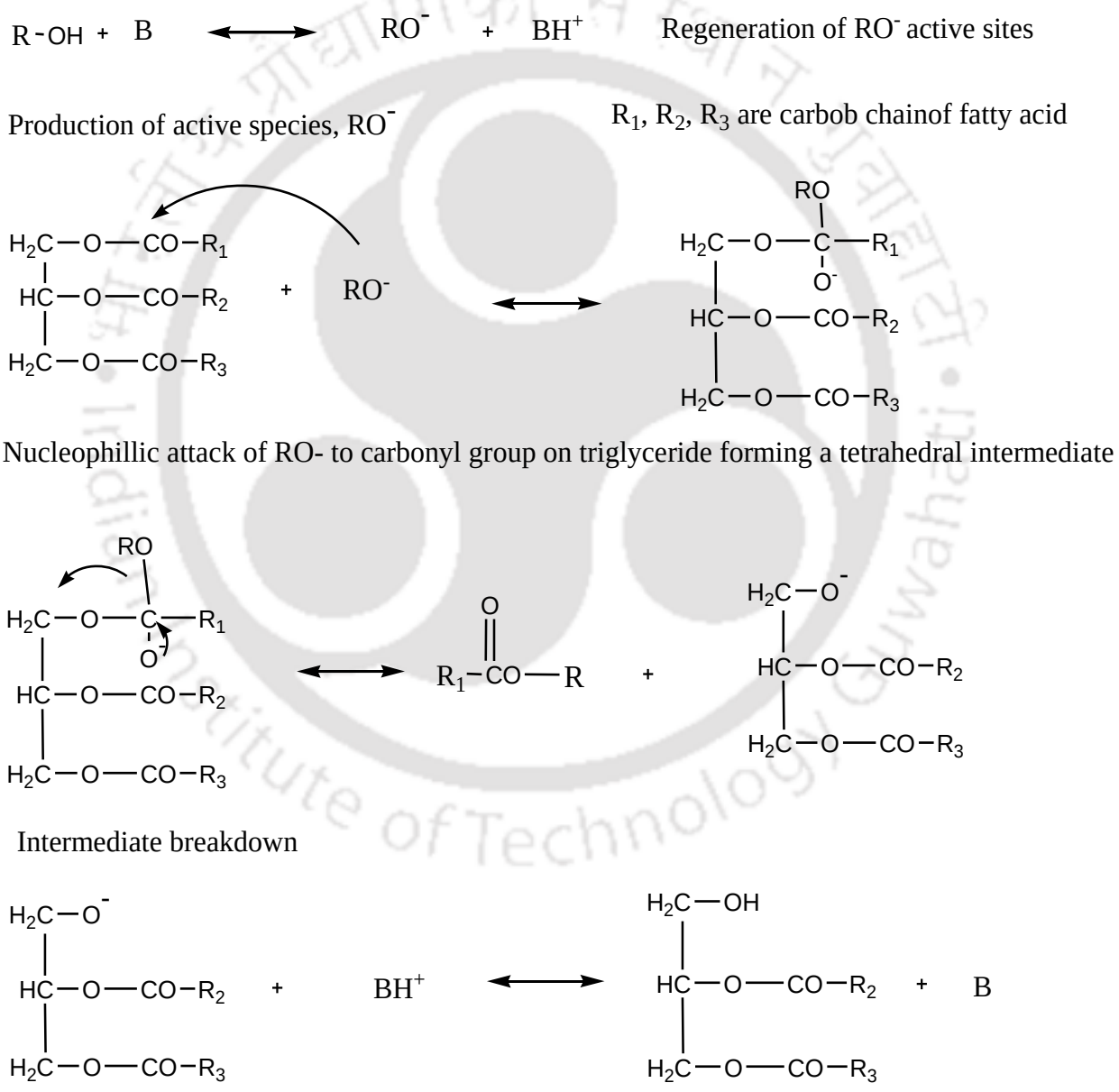

Fig. 1.3 Base catalyzed reaction mechanism

Table 1.3 Advantages and dis-advantages of different types of catalysts.

Type of catalyst	Advantages	Disadvantages
Homogeneous base catalyst (NaOH, KOH)	Very fast reaction rate 4000 times faster than acid catalyzed transesterification	Soap will formed if the FFA content in the oil is more than 2 wt %
	Reaction can occur at mild reaction condition	Too much soap formation will decrease the biodiesel yield huge amount of wastewater
Heterogeneous base catalyst ($CaTiO_3$, $CaZrO_3$, Cao-CeO_2, $CaMnO_3$, $Ca_2Fe_2O_5$, ETS-10 zeolite)	Relatively faster reaction rate than acid-catalyzed transesterification	Poisoning of the catalyst when exposed to ambient air
	Easy separation of catalyst from product	Sensitive to FFA content in the oil due to its basicity property
	High possibility to reuse and regenerate the catalyst	Leaching of catalyst active sites may result to product contamination
Homogeneous acid catalyst (H_2SO_4)	Insensitive to FFA and water content in the oil	Very slow reaction rate
	Preferred-method if low-grade oil is used	Corrosive catalyst
	Esterification and transesterification occur simultaneously	Separation of catalyst from product is problematic
Heterogeneous acid catalyst (carbon-based solid acid catalyst, carbohydrate- derived catalyst)	Separation of catalyst from product	Complicated catalyst synthesis lead to higher cost
	High possibility to reuse and regenerate the catalyst	Energy intensive
		Leaching of catalyst active sites may result to product contamination
Enzyme (Candida antarctica fraction B lipase, Rhizomucor mieher lipase)	High possibility to reuse and regenerate the catalyst	Very slow reaction rate
	Insensitive to FFA and water content in the oil	High cost
	Transesterification can be carried out at low reaction temperature	Sensitive to alcohol, typically methanol that can deactivate the enzyme.

1.4 Main factors affecting the yield of biodiesel

The main factors that affect the yields of bio-diesel are [3–5]:

a. Alcohol quantity

b. Reaction time

c. Reaction temperature

d. Catalyst concentration

1.4.1 Alcohol quantity

One of the main factors affecting the yield of biodiesel is molar ratio of alcohol to triglyceride. Theoretically, transesterification reaction requires 3 moles of alcohol for 1 moles of triglyceride to produce 3 moles of fatty acid ester and 1 moles of glycerol. An excess of alcohol is used in biodiesel production to ensure that the oils or fats will be completely converted to esters and a higher alcohol triglyceride ratio can result in a greater ester conversion in a shorter time [4, 5]. The yield of biodiesel increases when the alcohol triglyceride ratio is raised beyond 3 and reaches a maximum. Further increasing the alcohol amount beyond the optimal ratio will not increase the yield but will increase cost for alcohol recovery. In addition, the molar ratio is associated with the type of catalyst used and the molar ratio of alcohol to triglycerides in most investigations is 6:1.

1.4.2 Reaction time

The conversion rate of fatty acid esters increases with reaction time. At the beginning, the reaction is slow due to the mixing and dispersion of alcohol into the oil. After a while, the reaction proceeds very fast [3, 5]. Normally, the yield reaches maximum at a reaction time of < 90 min, and then remains relatively constant with a further increase in the reaction time.

Moreover, excess reaction time will lead to a reduction in the product yield due to the backward reaction of transesterification, resulting in loss of esters as well as causing more fatty acids to form soaps.

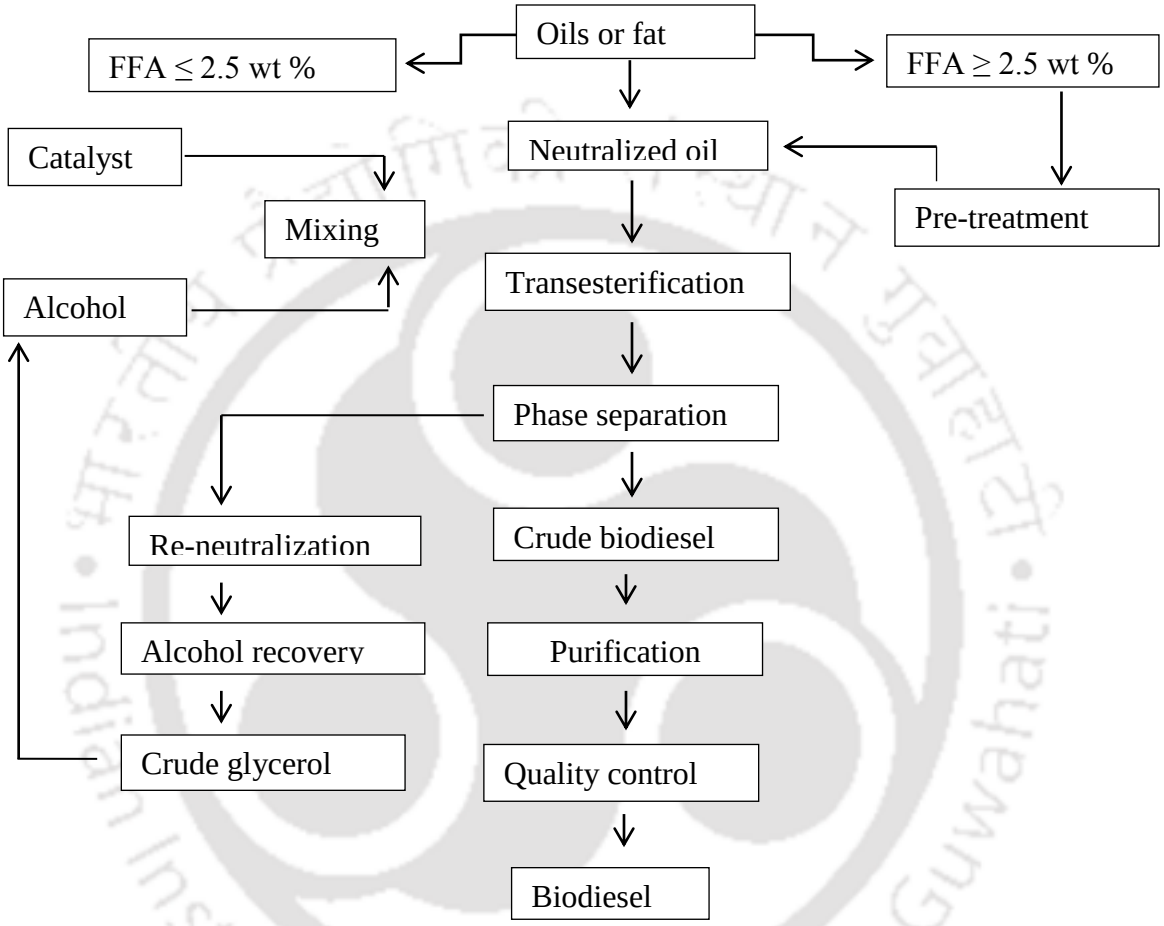

Fig. 1.4 General process flow sheet of transesterification

1.4.3 Temperature

A higher reaction temperature can decrease the viscosities of oils and results in increased reaction rate, and shortened reaction time. When the reaction temperature increases beyond the optimal level, the yield of biodiesel decreases because higher reaction temperature accelerates the saponification reaction of triglycerides [4, 5]. The reaction temperature must

be less than the boiling point of alcohol in order to ensure that the alcohol will not leak out through vaporization. Depending on the oil used, the optimal temperature ranges from 50 to 60 ^{o}C.

1.4.4 Catalyst concentration

Catalyst concentration can affect the yield of biodiesel product. As the catalyst concentration increases the conversion of triglyceride and the yield of biodiesel increase. This is because an insufficient amount of catalysts result in an incomplete conversion of the triglycerides into the fatty acid esters. Usually, the yield reaches an optimal value when the catalyst (NaOH) concentration reaches 1.5 wt % and then decreases a little with a further increase in catalyst concentration. The reduction of the yield of the biodiesel is due to the addition of excessive alkali catalyst causing more triglycerides to react with the alkali catalyst and form more soap [3, 5]. Table 1.4 shows the comparison of the above mentioned reaction conditions and their performance for various types of catalysts used in transesterification.

Though there are numerous publications reporting the use of catalysts (Table 1.4), considering the cost of production and complex behavior, use of flyash as starting material for catalyst synthesis has received considerable attention. Further, only a few literatures [43- 51] have reported the use of flyash as catalyst for transesterification.

Chaturvedi et al. [43] reported the use of flyash as catalyst in biodiesel production from pongamia oil. Molar ratios of feed stock to the alcohol was 4.5:45. Transesterification was carried out at elevated temperatures of 120- 250 ^{o}C under auto generated pressure for 8 h. Greater than 99% conversion was achieved at 10 wt % catalyst concentration.

Chakraborty et al. [44] developed flyash supported eggshell as solid base catalyst for transesterification of soybean oil. The optimal process conditions to obtain maximum

biodiesel yield (96.9%) were, CaO loading of 30 wt %, catalyst concentration 1.0 wt % of oil and 6.9:1 methanol to oil molar ratio.

Babajide et al. [45] synthesized class F flyash based zeolite FA/Na-X catalyst and studied the catalytic activity in the conversion of sunflower oil with methanol. Biodiesel yield of 83.53 and 85.5% was obtained at reaction times of 8 and 24 h, respectively using the ion-exchanged zeolite catalyst (FA/KX) at methanol: oil ratio of 6:1, 3 wt % catalyst concentration at 65 ^{o}C.

Suppes et al. [46] performed transesterification of soybean oil with methanol at 60, 120, and 150 ^{o}C using Na-X faujasite, ETS-10 zeolite and metal catalysts. Conversion to methyl esters in excess of 90% were achieved at temperatures of 150 and 120 ^{o}C with residence times of 24 h.

Supamathanon et al. [47] has developed K/Na-Y zeolite catalyst with high activity for the production of biodiesel from Jatropha seed oil. The highest yield of 73.4% was obtained at the condition including methanol to oil molar ratio of 16:1, a catalyst amount of 4 w/w %, reaction time of 3 h and reaction temperature of 65 ^{o}C.

Shu et al. [48] prepared La/zeolite beta by an ion exchange method for biodiesel production. Results showed that transesterification can proceed efficiently at 60 ^{o}C, the methanol/ soybean oil molar ratio 14.5:1, and catalyst/oil mass ratio of 0.011, the conversion of triglyceride 48.9 wt % was obtained in 4 h from these reaction conditions.

Ojha et al. [49] studied the tert-butylation (alkylation) of phenol over zeolite prepared from flyash and to compare its activity with commercially available Na-X zeolite. The effects of various parameters, such as temperature, reactant composition, catalyst loading on phenol conversion as well as product selectivity were studied.

Table 1.4 Comparison of reaction conditions and performance for various types of catalysts used in transesterification.

Oil	Catalyst	Reaction conditions				Yield (%)	References
		Temperature (°C)	methanol: oil molar ratio	Catalyst loading (%)	Time (h)		
Soybean oil	KOH, NaOH	60	6:1	0.2 - 1	2	94	Dias et al. [7]
	KI impregnated mesoporous silica	70	16:1	2.5 - 7.5	6 - 10	90	Samart et al. [8]
	CaO	60	1:2	0.78 g	1	93	Kouzu et al. [9]
	Thermomyces lanuginosus (TLL) and Rhizomu-cormiehei (RML)	30	7.5:1 (ethanol:oil)	25	10	90	Rodrigues et al. [10]
Jatropa	KOH, NaOH	70	14:1 (ethanol:oil)	2.5	2 - 6	97	Ginting et al. [11]
	CaMgO and CaZnO	65	15:1	4	6	83	Taufiq-Yap et al.[12]
	Aluminium modified (Mg–Zn) oxide	182	11:1	8.68	6	92	Olutoye et al. [13]
	Mg/Al Hydrotalcite	45	4:1	1	1.5	95	Veljkovic et al. [14]
	Rhizopus oryzae (ROL)	30	3:1	0.2 g	60	80	Tamalapudi et al. [15]

Cotton seed	Dicationic ionic liquids	55	12:1	0.4	4	99	Liang et al. [16]
	NaOH	40	13:1	0.1	3	98	Qian et al. [17]
	Sulfonated vegetable oil pitch	260	14:23	0.2	3	89	Shu et al. [18]
	Pancreatic lipase	37	15:1	5	4	80	Chattopadhayya et al. [19]
Palm oil	KF/ZnO	65	11:1	5.5	9.72	89	Hameed et al. [20]
	SO_4^{2-}/SnO_2	200	6:1	25	250	95	Jitputti et al. [21]
	KOH/Al_2O_3 KOH/NaY	70	15:1	3-6	2-3	91	Noiraj et al. [22]
Rapeseed oil	Waste slag (MgO-CaO/SiO_2)	68	6.5:1	3.5	3.5	98	Zhang et al. [23]
	Liquid organic amines	250	24:1	3.34 moles	1	89	Wang et al. [24]
	KOH	65	6:1	1.5	2	96	Rashid et al. [25]
	Ca/Al/Fe_3O_4 magnetic composite	65	15:1	6	3	98	Tang et al. [26]
	Alkylguanidines	70	1:4	1	1	90	Schuchardt et al. [27]

Sunflower	Alumina/silica supported K_2CO_3	120	15:1	2	<1.7	97	Lukic et al. [28]
	Gem-diamines	150	10:1	10	7	85	Alarcon et al. [29]
	Mg–Al hydrotalcites	60	12:1	2	24	78	Navajas et al. [30]
	Na-X zeolite	60	6:1	10	7	95	Ramos et al. [31]
	Mesoporous Ca/ SBA-15	200	27:1	5	8	99	Sun et al. [32]
	WO_3 supported MCM- 41 silica	200	12:1	15	2.5	80	Lopez et al. [33]
Waste or once used oil	NaoH	60	7:1	1.1	0.33	88	Leung et al. [34]
	H_2SO_4	95	20:1	4	20	90	Wang et al. [35]
	K_3PO_4	60	6:1	4	2	97	Guan et al. [36]
	Starch derived catalyst	80	30:1	10	8	92	Lou et al. [37]
	Lipase	45	3.8:1	9	48	85	Azocar et al. [38]
Rubber seed oil	NaOH	45	6:1	1	0.5	95	Ramadhas et al. [39]
Polanga oil	KOH	65	6:1	1.5	5	85	Sahoo et al. [40]
Waste tallow	H_2SO_4	60	30:1	1.25g	24	98	Bhatti et al. [41]
Canola oil	Dolomite	67.5	6:1	1.5	3	91	Ilgen et al. [42]

Flyash has been proved to be a useful material for a number of applications with potential to conserve valuable minerals, improves the physical health of agriculture soil, provide micro nutrients and as a result increase the yield of cereals, oil seeds, pulses, cotton and sugarcane etc. by 10-15%, vegetables by about 20- 25% and root vegetable by about 30-40% waste lands. Though this flyash is being utilized in brick manufacture, agricultural fertilizer and substituted upto 66% of cement in construction of dams, an effective way of utilizing this waste so that it can be converted into a value added product is one of the daunting challenges faced by the scientific community. Planning commissions reports indicate that the coal requirement and generation of flyash during the year 2031- 32 would be around 1800 million tonnes and 600 million tonnes respectively. Table 1.5 shows the production and utilization of flyash in different countries [50]. The management of such a large volume of flyash and its mitigation would cause greater impact on environment as well as demand on land for deposition/storage is a huge task.

Table 1.5 Flyash generation and utilization in different countries.

S. No	Country	Annual ash production, MT	Ash utilization %
1	India	112	38
2	China	100	45
3	USA	75	65
4	Germany	40	85
5	UK	15	50
6	Australia	10	85
7	Canada	6	75
8	France	3	85
9	Denmark	2	100
10	Italy	2	100
11	Netherland	2	100

Table 1.6 Mineralogical composition of flyash.

Component	Range (wt %)				
	Europe	**US**	**China**	**India**	**Australia**
SiO_2	28.5 – 59.7	37.8 – 58.5	35.6 – 57.2	50.2 – 59.7	48.8 – 66.0
Al_2O_3	12.5 – 35.6	19.1 – 28.6	18.8 – 55.0	14.0 – 32.4	17.0 – 27.8
Fe_2O_3	2.6 – 21.2	6.8 – 25.5	2.3 – 19.3	2.7 – 14.4	1.1 – 13.9
CaO	0.5 – 28.9	1.4 – 22.4	1.1 – 7.0	0.6 – 2.6	2.9 – 5.3
MgO	0.6 – 3.8	0.7– 4.8	0.7 – 4.8	0.1 – 2.1	0.3 – 2.0
Na_2O	0.1 – 1.9	0.3 – 1.8	0.6 – 1.3	0.5 – 1.2	0.2 – 1.3
K_2O	0.4 – 4	0.9 – 2.6	0.8 – 0.9	0.8 – 4.7	1.1 – 2.9
P_2O_5	0.1 – 1.7	0.1 – 0.3	1.1 – 1.5	0.1 – 0.6	0.2 – 3.9
TiO_2	0.5 – 2.6	1.1 – 1.6	0.2 – 0.7	1.0 – 2.7	1.3 – 3.7
MnO	0.03 – 0.2	--	--	0.5 – 1.4	--
SO_3	0.1 – 12.7	0.1 – 2.1	1.0 – 2.9	--	0.1 – 0.6
LOI	0.8 – 32.8	0.2 – 11.0	--	0.5 – 5.0	--

In this context, use of flyash as raw material for catalyst synthesis is the major objective of this work. The mineralogical composition present in flyash (Table 1.6) makes it a suitable low cost industrial waste that can be used as starting material for catalyst synthesis [51]. Further, the major problem encountered during the transesterification process is the FFA. An oil source with higher FFA would either require pretreatment, requires different catalysts (acid catalysis followed by base catalysis) which increase operational and process cost. For a given FFA content, synthesis of catalyst which can be used for both acid and base transesterification would be of a greater advantage. Flyash which has some similar physical properties and chemical composition can be used as catalyst by bringing some major modifications in its chemical composition (controlling Si: Al and Mg: Al ratio).

1.5 State-of-the-art

1.5.1 Physico-chemical properties and thermal behavior of edible and non-edible oils.

India is one of the largest producers of commercial edible and non-edible oils and oil seeds as their major sources. About 90% of the vegetable oils produced from these sources are used for edible purpose and the rest are used for varieties of industrial applications. The depletion of petroleum resources lead to an energy crisis and as an alternative, the use of these commercial edible and non-edible oils has been proposed as a raw material in bio-diesel production. The use of these oils poses a great challenge because these are triglycerides (polyunsaturated, monounsaturated and saturated fatty acids) and tend to decompose or oxidize under conventional processing conditions. High viscosities of these oils cause durability problems along with poor atomization pattern when used as fuel [52]. Comprehensive knowledge regarding the thermal degradation of oils might result in development and establishment of technologies for various industrial applications.

The use of thermo-analytical techniques such as thermogravimetric analysis (TGA), differential thermogravimetric analysis (DTG) and differential scanning calorimetry (DSC) of oils has gained a lot of importance in recent times. Santos et al. [52] evaluated the decomposition kinetics and thermal stability of eight samples of commercial edible oils in air atmosphere at heating rate of 2, 5, 10 and 20 $^{o}C\ min^{-1}$. Integral and approximation methods were used to determine kinetic parameters. The order of stability was determined to be corn > sunflower > soybean > rice > soybean + olive > sunflower + olive > canola > olive. The effects of alpha-tocopherol (vitamin E) on thermal stability and the thermal degradation

behavior of sunflower, soybean oil and their blend in air atmosphere at 5, 10 and 20 ^{o}C min^{-1} heating rates were studied by Arora et al. [53] The sequence of thermal stability was found to be as (sunflower + soybean)> sunflower > soybean. Souza et al. [54] evaluated the thermo-analytic and kinetic parameters of sunflower oil with and without oxidants in air atmosphere at 5, 10 and 20 ^{o}C min^{-1} heating rates. Deterioration of sunflower oil under frying conditions were also studied using DSC and non-isothermal thermogravimetry in both air and nitrogen atmosphere.

Vecchio et al. [55] studied the thermoxidation of 12 varieties of olive oils by simultaneous TGA and DSC in air atmosphere at heating rates of 2.5, 5, 7.5 and 10 ^{o}C min^{-1}. The use of DSC to determine the iodine value (IV) of palm oil and its products was studied by Haryati et al. [56]. The DSC analysis showed a clear separation of the substances that have low and high melting points. Tan et al. [57] examined the thermal degradation profiles of 17 edible oils by DSC. Melting and crystallization curves of all the samples were reported. It was found that the oil samples with a high degree of saturation (IV < 65) showed DSC melting and crystallization profiles at higher temperature regions than the oil samples with high degree of unsaturation (IV > 65). Souza et al. [58] studied the thermal and kinetic behavior of methanol biodiesel derived from cotton oil. Non isothermal dynamic analysis method in both air and nitrogen atmosphere was used at heating rate of 10 ^{o}C min^{-1}. It was found that the activation energy of cotton seed oil was higher than its biodiesel. Studies on the oxidative kinetics of soybean oil/ anhydrous milk fat blends by DSC at heating rate of 2.5, 5, 7.5, 10 and 12.5 ^{o}C min^{-1} were done by Thurgood et al. [59] Arrhenius parameters were calculated by using Flynn - Wall- Ozawa method. It was reported that the activation energy varied from 58.5 to 117.4 KJ kg^{-1}. Jain et al. [60] studied the thermo-oxidative behavior of Jatropha

biodiesel with and without oxidant. Pyrogallol was found to have significant effect on onset temperature of biodiesel. Direct Arrhenius plot method was used to determine the kinetic parameters in air at 10 ^{o}C min^{-1} heating rate.

Scope for research

From the above literatures it may be depicted that the thermal degradation studies of commercials oils like soybean, sunflower, olive, corn, canola and rice bran were investigated in presence of air. However, to the best of knowledge of authors, thermal degradation studies in nitrogen atmosphere have not been studied. Again, thermal degradation of Mustard and Karanja oil has not been studied yet. Moreover, various models have been used to compute the kinetic parameters and the use of single heating rate in calculation of activation energy (E_a) gives unreliable result. Thermal degradation behavior of commercial oils along with the determination of activation energy using model-free iso-conversional methods including Coats and Redfern, Friedman, Kissinger and Flynn–Wall–Ozawa could provide valuable insight in developing kinetics of reaction. These methods calculate the reaction activation energy (E_a) without making any modelistic assumptions and hence accurate results can be obtained.

1.5.2 Identification of natural sources of calcium (municipal solid waste) for catalyst synthesis.

Among the several methods for production of biodiesel, catalyzed transesterification of triglycerides has gained lots of importance in recent time. The use of homogeneous catalyst causes environmental problems, produces large amount of waste water, difficult for catalyst separation after reaction and are corrosive resulting in reduction of ester yield [61]. In order to

overcome these drawbacks, heterogeneous base catalysts such as CaO [62], alkali/alkaline oxides and carbonate [63], basic zeolites [64] and amino-polysilica [65] were developed. But the synthesis of these catalysts would involve a lot of capital investment, their reusability and recycling is still a daunting task. Thus, development of heterogeneous base catalyst for transesterification from natural sources (wastes) could be better alternative. Several researchers have reported the synthesis of low cost calcium based heterogeneous catalyst from fish scales [66], wood ash [67], rice husk [68], bone powder [69], coral fragments [70], lemna perpusilla torrey ash [71], waste shells of egg, golden apple snail, meretrix vensu [72], waste mud crab [73], oyster, mussel, turbonillastriatula, clam and cockle shells [74–77] respectively.

Flyash is one such source generated at 1200 – 1700 ^{o}C from the various inorganic and organic constituents of the feed coal. The bulk chemical composition of flyash on dry basis is: 50.2 - 59.7% SiO_2, 14.0 - 32.4% Al_2O_3, 2.7 - 14.4% Fe_2O_3, 0.5 - 1.2% Na_2O, 0.6 - 2.6% CaO, 0.1 - 2.1% MgO, 0.5 - 1.4% MnO 1.0 - 2.7% TiO_2 and 0.8 - 4.7% K_2O [51]. The presence of large amount of SiO_2 and Al_2O_3 makes this low-cost industrial waste, a potential catalyst with direct use or by modifications. Jain et al. [78] synthesized a solid base catalyst that can be reused four times using flyash chemically activated with NaOH and studied its activity on condensation of cyclohexanone and benzaldehyde. Kotwal et al. [79] reported the use of flyash loaded with KNO_3 (5 wt %) as catalyst for the transesterification of sunflower oil. At 15 wt % catalyst concentration a maximum oil conversion of 87.5% was obtained with methanol to oil molar ratio of 15:1 for 8 h at 170 ^{o}C and a decrease in catalytic activity was observed when the recovered catalyst was reused. The highest conversion of 87.5% was observed at a temperature of 200 ^{o}C at 20 wt % catalyst concentration when KNO_3 loaded African flyash was used [80]. At a reaction temperature of 160 ^{o}C, maximum oil conversion

of 86.1% was obtained. The catalytic activity shows that conversion increased from 52.2% to 86.1% with increase in the methanol to oil ratio from 6:1 to 15:1.

Scope for research

From the above literature, it is envisaged that development of a heterogeneous catalyst from industrial and household wastes would result in value addition to these materials and help in reduction of pollution as well. However, studies describing the use of modified flyash (by chemical treatment) for biodiesel synthesis were scant. Moreover, synthesis of a basic catalyst by addition of waste sources of calcium to flyash and its application on transesterification on mustard oil has not been reported yet. Thus, synthesis of catalyst from flyash by impregnating natural sources of calcium in order to improve its basic nature and to obtain similar properties to that of conventional catalyst could widen the scope for research in areas of catalysis. Further, for model prediction and process optimization, the use of response surface methodology (RSM) was preferred when compared to artificial neural network (ANN) and well known Taguchi models. The use of ANN requires a much greater number of experimental runs to develop an efficient model than RSM. Though ANN is superior to sum of least squares method (RSM), it does not have the ability of sensitivity analysis and optimization as it is a black box model that does not give any insight of transesterification reaction systems.

1.5.3 Synthesis of mesoporous materials from industrial wastes and its use as catalyst

Heterogeneous alkaline transesterification of triglycerides has emerged as an alternative to the conventional homogeneous system due to its high selectivity, easier

separation and fewer disposal problems. The growing environmental concerns and stringent legislations made the scientific community to develop catalysts that could enable its use in large scale industrial applications and help in subsiding pollution. Zeolites, aluminosilicate members of the family of microporous materials are basic solids and can act as supports for alkali metals and metal oxides [81]. The basicity of these materials can further be improved by occlusion of alkali metal oxide clusters by impregnated alkali metal salts [46, 82]**.** Zeolites occur naturally (analcime, chabazite, clinoptilolite, erionite, mordenite and phillipsite) and can be synthesized commercially in large scale by hydrothermal process (zeolites A, X, Y and ZSM-5) [83–86]. The principle raw materials used for the synthesis of these zeolites are silica and alumina. The preparations of zeolites from these chemical sources are expensive. Therefore, the possibility of the use of cheaper raw materials like clay minerals [87], oil shale ash [88], kaolinite [89], municipal solid wastes [90–93] and coal ashes [94–98] as starting materials for the synthesis of zeolite was successfully investigated.

Zeolite Y and X was synthesized from rice husk with alkali metal loading and was used as catalyst for transesterification of jatropha oil**.** Biodiesel yield of 73.4% and 95.2% was obtained at 65 ^{o}C in 3 h with methanol to oil molar ratio of 16:1 using 14 wt % K loaded zeolite Y and 16 wt % Na loaded zeolite X, respectively [47, 99]. Leclercq et al. [100] performed the transesterification of rapeseed oil using cesium-exchanged Na-X, mixed magnesium-aluminum oxides, magnesium oxide, and barium hydroxide for different methanol to oil ratios. Maximum conversion of 76% was obtained for Cs exchanged Na-X zeolite with methanol to oil molar ratio of 275 for 22 h of reaction and 20 wt % catalyst concentrations. The transesterification of palm oil to methyl ester was done in a packed-bed reactor using KOH/Na -Y as catalyst. It was found that KOH/Na-Y created strong basic sites,

and the agglomeration was greatly increased by increasing the potassium content. The highest yield of 92.1% was obtained for the 15 wt % K/Na-Y at reaction temperature of 60 ^{o}C for 7 h [101]. Kusuma et al. [102] studied the transesterification of palm oil using KOH modified natural zeolite at different concentrations (25, 50, 75 and 100 gL^{-1}) at zeolite to KOH solution weight ratio of 1:4. The maximum yield of biodiesel was obtained (95.1%) at 3 wt % catalyst loading. Use of microwave irradiation for the synthesis of Na-Y, KI and Na/ZSM-5 zeolites with different CaO loading was investigated by Wu et al. [103].

Scope for research

Use of coal flyash for zeolite synthesis could not only add value addition to waste but also helps in development of better technologies to promote its utilization. Comprehensive studies regarding the optimum parameters for zeolite synthesis, effect of flyash calcination temperatures, acid treatment, and variation of Si/Al ratio on type of zeolite product formed and the effect of these parameters on CEC and crystallinity of zeolitic materials has not been reported. Studies on the use of zeolite synthesized from flyash and its use on the transesterification by mustard oil has not been accounted yet. The use of alkali fusion prior to hydrothermal treatment was used when compared to conventional hydrothermal synthesis helps in dissolution of larger amounts of aluminosilicates in-turn enhancing hydrothermal conditions for zeolite synthesis.

1.5.4 Heterogeneous bi-functional catalyst for transesterification

In recent years, heterogeneous catalyst has been providing a sustainable and viable solution to glitches arising in diversified techno-economic straits of catalysis. Methods and technologies employed to develop these systems should be a motivation to address ecological and global distress associated with environment. In recent years, extensive research has been

carried out to develop such catalysts and their potential was explored in wide range of applications. Transesterification is one such area where the utilization of these catalysts could be play a major role for industrial level biodiesel production in near future. Though different types of catalysts such as NaOH, KOH, HCl and H_2SO_4 [104–106] are in use but, heterogeneous catalysis gained a lot of importance as they are easy to separate, requires mild conditions, can be regenerated and reused thus reducing the production cost [3]**.** The use of CaO from natural waste shells [107, 109]**,** Li modified rice husk [68]**,** calcined cement [110], zeolites from oil shale and bagasse flyash [88, 111] was investigated as heterogeneous catalyst in biodiesel production.

Hydrotalcites (HT) are layered anionic basic materials with *di* and *trivalent metal* ions commonly referred as layered double hydroxide (LDH). With variation in ratios of these *di* and *trivalent* metal ions, basicity of these materials can be altered. Deng et al. [112] synthesized micro sized mixed Mg/Al hydrotalcite with molar ratio of 3 and used it as catalyst for biodiesel production from Jatropha oil using sonication. A maximum biodiesel yield of 95.2% was obtained with methanol to oil molar ratio of 4 at 45 ^oC for 1.5 h, with 1 wt % catalyst concentration. Hydrotalcite with Mg: Al ratio of 2 was used as catalyst for transesterification of soybean oil by Gomes et al [113]**.** At 65 ^oC, 2.5 wt % of catalyst with methanol: oil molar ratio of 9:1 for 4 h of reaction, a biodiesel yield of 97.1% was obtained. Xie et al. [114] performed transesterification experiments of soybean oil using hydrotalcite with Mg/Al ratio of 3 at oil to methanol ratio of 15:1 for 9 h with 7.5 wt % catalyst concentration to obtain a conversion of 67%. Trakarnpruk et al. [115] prepared biodiesel from palm oil using 1.5% K loaded Mg-Al hydrotalcite with molar ratio 4. The yield of biodiesel was 86.6% with 30:1 methanol to oil molar ratio at 100 ^oC for 6 h and 7 wt % catalyst.

The catalytic activity of Quntinite-3T with Mg/Al ratio of 2:1 was studied for the transesterification of canola oil by Kondamudi et al [116]**.** The optimum conditions for biodiesel production were 10 wt % of the catalyst, methanol to oil molar ratio of 12:1, at 75 ^{o}C for 2 h. Zr incorporated Zn-Al hydrotalcite with molar ratios Zr/Zn/Al of 0.25/2.56/1 was used for transesterification of soybean oil in fixed bed reactor by Liu et al [117]**.** A biodiesel yield of 91.7% was obtained at 140 ^{o}C, 1.7 MPa, 1.0 h^{-1} and 1:1 volume ratio of methanol to soybean oil. Cantrellet al. [118] synthesized Mg-Al hydrotalcites with molar ratios varying from 1:1 to 4:1 and studied their activity in transesterification of glyceryl tributyrate. Biodiesel conversion of 74.8% was obtained at 60 ^{o}C for 3 h of reaction time. Navajas et al [30] studied the methanolysis of sunflower oil using Mg-Al hydrotalcite with molar ratios in the range of 0.5 - 2.3. At methanol/oil molar ratio of 12 and 2 wt % of catalyst, a conversion of 50% was obtained at 60 ^{o}C after 24 h.

Scope for research

In view of the above discussed literature, Mg-Al hydrotalcites have attracted much interest for their potential as heterogeneous catalysts for biodiesel production. For hydrotalcites, basicity can be influenced by varying the Mg/Al ratio (decrease or increase in the number of trivalent species Al^{3+}). Moreover, the complexity in their preparation and expensive nature of raw materials has limited their application for industrial scale operation. To the best of our knowledge, literature based on synthesis of flyash based hydrotalcites and its utilization as catalyst for biodiesel production has not been published yet. Further, use of flyash as raw material for hydrotalcite synthesis was not reported. Synthesis of flyash and flyash zeolite supported Mg-Al hydrotalcite using co-precipitation method could be novel.

Effective utilization of the available mineral composition in flyash may result in production of bifunctional solid base catalyst making flyash a value added industrial waste.

1.5.5 Physical properties, chemical composition and degradation kinetics of biodiesel

Biodiesel, has become a feasible substitute for petro-diesel due to its low exhaust emissions, higher flash point and inherent lubricity. However, high prices of their feedstock, its chemical composition, poor cold flow properties, low processing temperatures and inferior thermo-oxidative stability results in problems relating to their storage, injector plugging and formation of deposits on filter when use in diesel engine. Estimation of physical properties and chemical composition of biodiesel using standard test methods might help in answering the difficulties associated to their usage. In this context, use of thermo-analytical techniques like TGA (thermogravimetric analysis) and DSC (differential scanning calorimetry) has proven to be simple, effortless and time redeemable [119].

Jain et al [120] reported the effect of metal content on thermal and oxidative behavior of Jatropha biodiesel (JCB). Copper (Cu) showed strongest detrimental effect on both, oxidation and thermal stability. The values of activation energy and frequency factor for iron contaminated JCB is 54 KJ mol^{-1} and 125000 min^{-1}, respectively. Oliveira et al. [121] calculated the kinetic and thermodynamic parameters of volatilization of biodiesel from babassu, palm oil, and diesel by TGA. The order of activation energy was reported as diesel (E = 49.90 kJ mol^{-1}) < babassu biodiesel (76.3 kJ mol^{-1}) < palm biodiesel (E = 87 kJ mol^{-1}). Nautiyal et al [122] studied the single stage extraction transesterification process for biodiesel production from Spirulina platensis algae biomass. The optimum conditions for maximum

biodiesel yield (75%) were found to be 1.5 h duration for algae drying, 60% catalyst concentration, 1:4 algae biomass to methanol ratio, 450 rpm stirring intensity and 55 ^{o}C temperature. The values of rate constant and activation energy were found to be 0.001 min^{-1} and 145.18 KJ mol^{-1}, respectively. Cursaru et al [123] studied the oxidative behavior of methyl esters derived from sunflower, peanut, olive, grape and palm seeds. The decreasing order of oxidation stability of methyl esters were determined as olive (349 ^{o}C) < sunflower (345.6 ^{o}C) < grape (344.9 ^{o}C) < palm (333.6 ^{o}C) < peanut (329.9 ^{o}C). Conconi et al. [124] reported the activation energy of the thermal decomposition of farnesane (renewable diesel from sugar cane), biodiesel, fossil diesel and their blends using model free kinetic methods. The values of activation energy were evaluated as 82.2 ± 3.3 kJ mol^{-1}, 86.6 ± 8.4 kJ $mol^{-1}$and 96.6 ± 3.7 kJ mol^{-1}, for farnesane, diesel and biodiesel, respectively.

Zhao et al. [125] studied thermal stability, crystallization, oxidation, anti-oxidation, and moisture absorption, using TG, DSC, PDSC, and sorption analyzer of soybean biodiesel and compared them with reference to commercially available biodiesel. A total weight loss of 99% before 300 ^{o}C, indicating high purity of biodiesel. The preferable storage conditions were identified as humidity with less than 30% and 30 ^{o}C. Venu et al. [126] synthesized methyl esters from castor and waste cooking oils and studied their thermo-oxidative stabilities using TGA and DSC under nitrogen and oxygen at different heating rates. The presence of higher percentage of ricinoleic acid in the fatty acids composition, castor oil biodiesel exhibited higher thermal and oxidative stability. Lin et al. [127] performed thermal stressing experiments in batch reactors at 250 - 425 ^{o}C for 3-63 min to evaluate the influence of thermal decomposition on biodiesel viscosity and cold flow properties. The order of thermal degradation was found to be cis-trans isomerization > polymerization > pyrolysis, and

depends on thermal stressing temperature. Polymerization reactions resulted in increases in both viscosity and crystallization onset temperature.

Scope for research

Based on above literature it was evasive that, though there were numerous publication reporting the physical properties, thermo-oxidative behavior of biodiesel derived from various oils, there is no systematic study on thermal behaviours of biodiesel using thermal analysis techniques. Most of the literatures reported the use of Arrhenius equation for determination of activation energy but the use of model free iso-conversional methods were not reported. Further all the reported kinetic parameters reported were based on single heating rate which might result in incorrectness in the estimated data. The use of multiple heating rate would help in increasing the accuracy of the techniques and values estimated from the obtained data. The use of TGA and DSC would increase the efficiency in estimation of kinetic parameter and cold flow properties of synthesized biodiesel.

1.6 Aim and objectives of present research

Based on the state of the art presented in sections 1.5.1 to 1.5.5, the PhD thesis targets the fulfillment of the following major objectives.

1. Physico-chemical properties and thermal degradation studies of commercial oils in nitrogen atmosphere.
2. Utilization of flyash as heterogeneous catalyst for transesterification.
3. Selective preparation of zeolite X and A from flyash and its use as catalyst for biodiesel production.

4. Preparation and characterization of hydrotalcite with bifunctional properties from flyash for transesterification.
5. Thermal kinetics, physical properties and chemical composition of biodiesel: A comparative study.

1.7 Organization of the thesis

The PhD thesis is organized in eight chapters.

Chapter 1 addressed the state of the art, possible scope of research, objectives and organization of the thesis. **Chapter 2** presents the materials and the experimental methods used in this work. The purpose of this chapter is to provide background information on the raw materials used in the synthesis process and the experimental methods of the investigation. The fundamental techniques of characterization are also discussed in this chapter. **Chapter 3** discusses in detail the results and discussion in identification and characterization of raw materials (oils), their physico-chemical properties and degradation kinetics of edible and non-edible oils in nitrogen atmosphere using thermo-analytical techniques and standard test methods. **Chapter 4** provides useful information on their appropriate mineralogical and chemical composition of flyash and its use as starting material for synthesis of catalysts (flyash impregnated animal bone powder for transesterification. **Chapter 5** presents in detail the selective synthesis of zeolite X and A flyash to establish their potential for their use as heterogeneous catalyst for transesterification of mustard oil by controlling Si/Al ratio. The effect of temperature, cation exchange capacity and hydrothermal treatment on zeolite formation was discussed. **Chapter 6** elaborates the synthesis of hydrotalcites with bi-functional properties from flyash as starting material by controlling Mg/Al ratio for biodiesel production. The variation of basicity of catalyst with change in Mg/Al ratio along with their

characterization was presented **Chapter 7** it presents the estimation of physical properties and chemical composition of synthesized biodiesel to check its compatibility with commercial biodiesel and its degradation kinetics along with its activation energy and thermodynamic properties. **Chapter 8** presents various conclusions drawn from the research work. It also provides possible directions for future work.

Chapter 2

Experimental and Characterization

Materials;

Methods;

Characterization;

Synthesis.

In this chapter, details of the materials, sample preparation and experimental methods used in this work has been mentioned. This chapter consists of the three major parts which include (i) Section 2.1 describes the source of raw material and the list of chemicals used, (ii) Section 2.2 deals with experimental methods with detailed flow sheet for:

a. *Synthesis of flyash modified animal bone powder catalyst by wet impregnation method,*
b. *Selective preparation of zeolite X and A from flyash by alkali fusion prior to hydrothermal treatment,*
c. *Synthesis of hydrotalcite with bi-functional properties from flyash*
d. *Procedure for the optimization study of the transesterification of vegetable oils*

(iii) Section 2.3 explains the methods, fundamental techniques and the details of the equipment used for the characterization of synthesized heterogeneous catalyst and biodiesel.

2.1 Materials

Ten samples of commercial edible (sesame, palm, refined soybean, mustard and sunflower) and non-edible (neem, olive, mahua, castor and karanja) oils were purchased from several local retailers, waste animal bone (sheep) was obtained from slaughter house near IIT Guwahati, India. Coal flyash from boiler was collected from M/s SARACA laboratories limited, Andhra Pradesh, India. Aluminum nitrate ($Al(NO_3)_3 \cdot 9H_2O$, Fluka), hydrochloric acid (10%), sodium hydroxide (98%) and sodium aluminate (99.99%), sodium acetate, ammonium acetate, isopropyl alcohol, magnesium nitrate ($Mg(NO_3)_2 \cdot 6H_2O$) and sodium carbonate (Na_2CO_3) was obtained from Sigma-Aldrich Pvt. Ltd.

2.2 Experimental Methods

2.2.1 Synthesis of flyash impregnation animal bone powder catalyst

The flyash supported bone powder catalyst was prepared following wet impregnation method [44]. Flyash obtained was milled for 10 h using ball mill and dried in hot air oven at 100 ± 5 ^{o}C for 24 h. Animal bone powder (sheep) was prepared by crushing and boiling the bone for 4 h to remove tissue and fat, later dried and were calcined in a high-temperature muffle furnace at 900 ^{o}C for 2 h and Fig. 2.1 shows the process flow sheet. Three different types of catalysts were synthesized by mixing 10% (C10), 20% (C20) and 30% (C30) of calcined bone powder (CBP) in flyash. In order to prepare 5 g of 20 wt % catalyst, 1 g of CBP was added to 200 ml of water and this solution was then added to 4 g of pre-dried flyash and mixed vigorously under reflux for 4 h, at 70 ^{o}C and pH of 12. The solution was aged for 24 h; filtered, dried in hot air oven at 100 ± 5 ^{o}C for 24 h and was calcined at 900 ^{o}C for 2 h. The calcined powder was crushed and stored in desiccator for further use.

2.2.2 Selective preparation of zeolite X and A from flyash

Zeolite was synthesized from flyash by alkaline fusion prior to hydrothermal treatment [45]. The unburnt carbon along with other volatile materials present in flyash were removed by calcination at 900 (±10) °C for 2 h. Flyash sample was further treated with hydrochloric acid (10%) at 80 ^{o}C for 1 h to increase its activity in zeolite formation. A homogenous fusion mixture of flyash and NaOH was prepared by proper grinding and mixing in NaOH/flyash ratio of 1:1 to 1:2.5. The sample was heated in temperature range of 450 to 600 ^{o}C for about 1–2 h to study the effect of NaOH/flyash ratio, fusion temperature and time on the extent of zeolite formation.

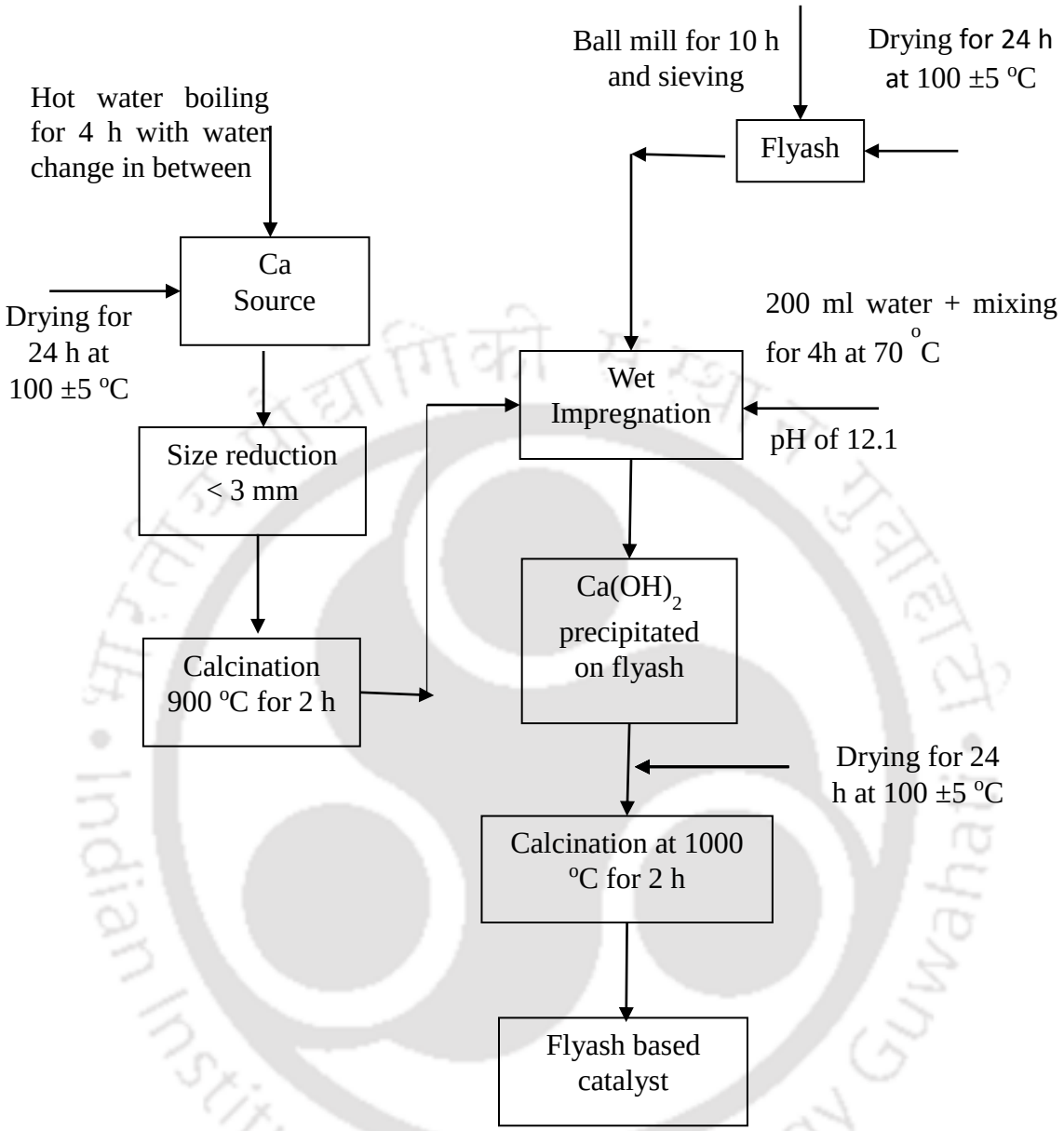

Fig. 2.1 Process flow sheet for synthesis of flyash impregnate animal bone powder catalyst

The resultant fused mass was cooled, milled and mixed thoroughly in de-ionized water in the ratio of 1:10 (flyash to water) with simultaneous addition of sodium aluminate (10-30 wt %) to control the Si/Al ratio and to study its effect on zeolite formation. The slurry was then subjected to aging for 12-16 h, allowed to crystallize between 90 to 120 °C for about 24 h to study the effect of hydrothermal temperature and time on zeolitization. The solid crystalline

product was recovered by filtration and washed thoroughly until the filtrate pH was around 10 and dried at 110 ^{o}C. The effect of calcination temperatures (800 to 1000 ^{o}C) and acid treatment of flyash on zeolite formation was also studied. The synthesized zeolite was modified by an ion exchange process using potassium acetate as a precursor. The dried zeolite was dispersed in 1.0 M solution of potassium acetate with powder to the solution ratio of 1:10 and heated at 60 ^{o}C for 24 h. The mixture was repeatedly washed with distilled water, dried in air at 110 ^{o}C and then calcined at 500 ^{o}C for 2 h to obtain the ion exchanged zeolite. Fig. 2.1 shows the process flow sheet for the synthesis of zeolite.

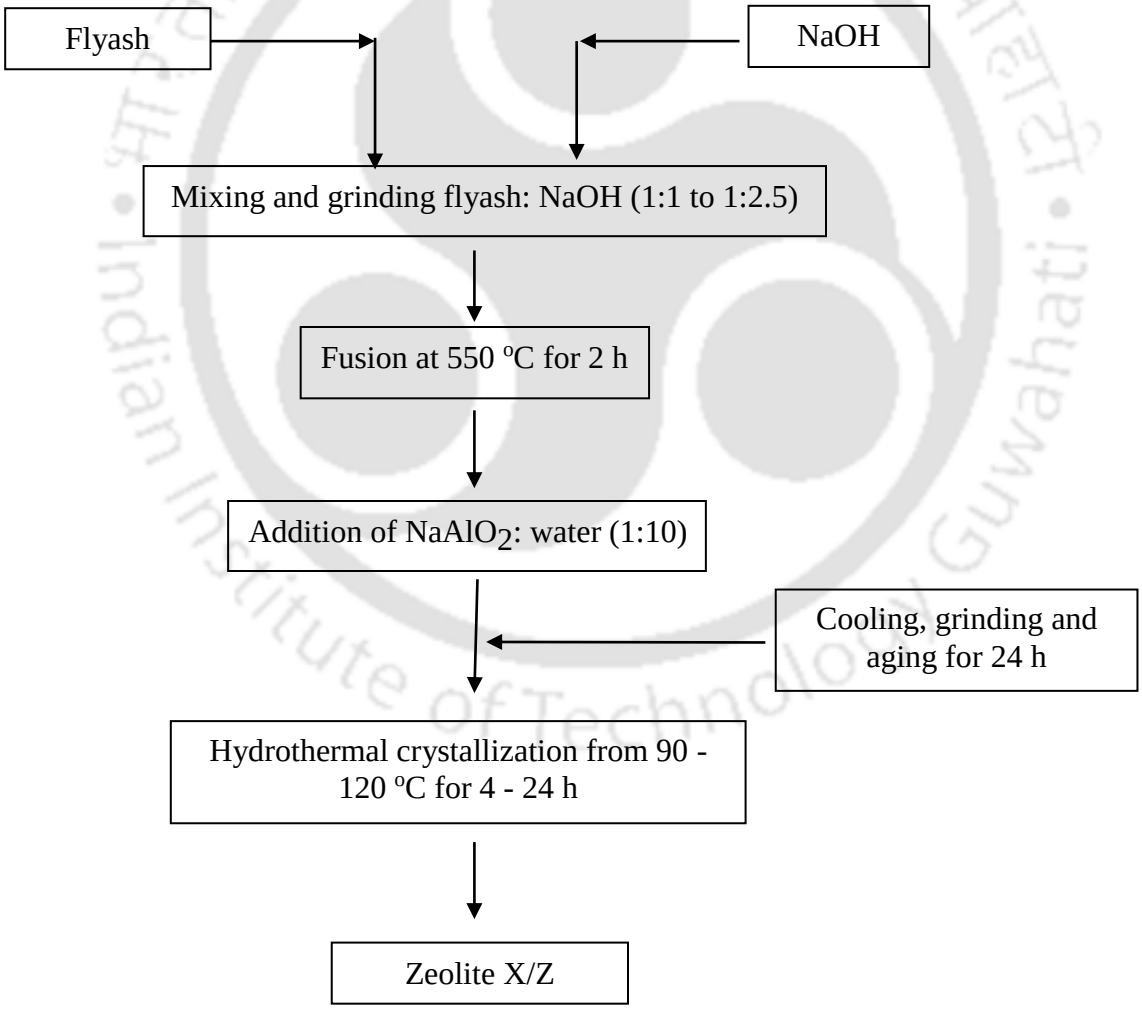

Fig. 2.2 Process flow sheet for synthesis of flyash based zeolite

2.2.3 Synthesis of hydrotalcite with bi-functional properties from flyash

Flyash zeolite was prepared by using alkali fusion method followed by hydrothermal treatment as per section 2.2.2**.** Mg-Al hydrotalcite (C-HT) was prepared using co-precipitating method [116] and Fig. 2.3 shows the detailed flow sheet**.** Flyash hydrotalcite (F-HT), flyash zeolite hydrotalcite (FZ-HT) was prepared by the method discussed below. Aqueous solution of (45 mL) of 0.1 mol $Mg(NO_3)_2 \cdot 6H_2O$, 0.05 mol $Al(NO_3)_3 \cdot 9H_2O$ and a second solution (70 mL) containing NaOH (0.35 mol) and Na_2CO_3 (0.09 mol) was added drop wise to required quantity of synthesized zeolite/flyash solution (flyash/zeolite: water as 1:10) in a 500 ml 3 neck round bottom flask while stirring at around 70 ^oC held at pH 10.

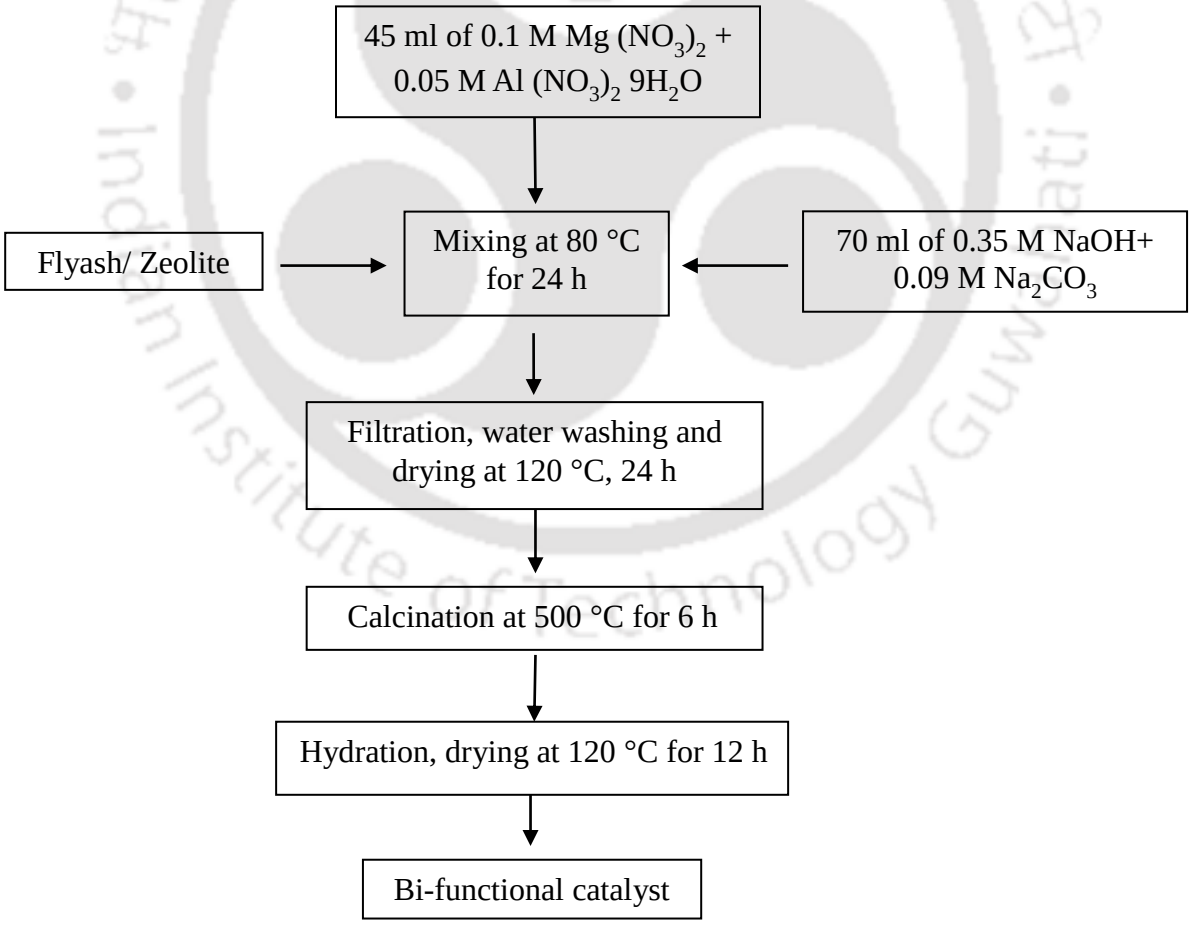

Fig. 2.3 Process flow sheet for the synthesis of flyash based bi-functional catalyst.

The mixture was stirred vigorously for 24 h, filtered, washed to remove occluded NaOH and was dried at 100± 5 ^{o}C. The resulting powder was calcined at 500 ^{o}C for 6 h to obtain the mixed metal oxide which is again hydrated with de-carbonated water and dried at 100± 5 ^{o}C.

2.2.4 Procedure for transesterification of vegetable oils

To study the catalytic activity, transesterification of refined mustard oil was carried out in a 500 ml three neck round bottom flask equipped with reflux condenser which was heated using oil bath provided with a PID temperature controller. A fixed quantity of refined mustard oil and prepared catalyst was mixed with methanol (alcohol/oil) at molar ratio of 3:1 to 18:1 and was stirred at 65 ^{o}C for 10 h. After carrying out the reaction, the mixture was cooled to room temperature, centrifuged at about 6000 rpm for 10 min. Ester was separated from catalyst, glycerol and unreacted methanol using a rotary evaporator. The final product was allowed to settle overnight to produce two phases: bio-diesel at the upper layer and glycerol at the bottom layer. The biodiesel yield (% FAME) was calculated from the ratio of the integrations of the ^{1}H-NMR signals of the methoxy protons (−CH_3O−) in the methyl ester at chemical shifts of 3.68 ppm (singlet peak) and methylene protons (− CH_2 −) of all triglycerides at chemical shifts of 2.30 ppm (triplet peak), according to the following formula:

$$\% \text{ FAME} = \frac{2\, A_{CH3}}{3\, A_{CH2}} \times 100$$

Where A_{CH3} is the integration value of the methoxy protons and A_{CH2} is the integration value of the methylene protons. The factors 3 and 2 are number of attached protons at methoxy and methylene carbons, respectively [70].

2.3 Fundamental techniques, methods and characterization of synthesized catalyst, oils and biodiesel.

2.3.1 Physical properties and fatty acid composition of oil samples

Physical and chemical properties of the raw materials such as pH, specific gravity, water content, viscosity, acid value (AV), calorific value, flash and fire point, cloud and pour point, refractive index and ash content were estimated using ASTM standards. The detailed description is given below.

pH

In chemistry, pH is defined as the negative log of the activity of the hydrogen ion in an aqueous solution. Solutions with a pH less than 7 are said to be acidic and solutions with a pH greater than 7 are basic or alkaline. Pure water has a pH of 7. The pH values of all the samples were measured by using pH Spear from Eutech instruments.

Specific gravity

Specific gravity is the ratio of the density of a liquid to the density of water. This property is important because it influences the efficiency of atomization of the fuel and it is a quality indicator for automotive, aviation and marine fuels, where it affects storage, handling and combustion properties [128]. The specific gravity of the oil sample was determined following the ASTM D1298.

Water content

Determination of water content in fuel oils is important because the presence of water can promote organic growth which results in blockage of automotive filter. Further, in transesterification, presence of water in raw material results in soap formation [129]. The

water content in oils and biodiesel samples was measured using Titrino 787 Karl Fischer from Metrohm by volumetric Karl Fischer technique.

Viscosity

Viscosity (μ) is the measure of resistance offered by fluid to flow and it increases when length of the fatty acid chain is increased. On the other hand, kinematic viscosity (v) is the ratio of viscosity to the fluid density (ratio of the viscous force to the inertial force). The major disadvantage of using neat vegetable oils as fuels in diesel engines is due to the high viscosity which results in poor atomization patterns and clogging of filters [130]. The viscosities of the samples were measured at 40 ^{o}C using Rehostress RS-1 Rheometer from Thermo Electron according to ASTM D 445.

Acid Value

Acid value is defined as the amount of potassium hydroxide (KOH) in milligrams required to neutralize one gram of chemical substance. It is the measure of free fatty acid in a mixture of compounds [131]. A known amount of sample dissolved in petroleum hydrocarbon and required quantities of rectified spirit was added and titrated with a solution of potassium hydroxide of known concentration with phenolphthalein indicator and is calculated by equation:

Acid value = (28.2 ×V× N / M)

where, V is the consumed volume of KOH (ml), N is the concentration of KOH (mol/l), and *m* is the mass of the tested sample (g). Acid value was determined as per ASTM D664-89.

Calorific value

Calorific (heating) value, is the amount of heat released during the combustion of one gram of fuel to produce CO_2 and H_2O at its initial temperature and pressure [132]. One gram

of sample was placed in the center of the crucible. Fuse wire was cut and threaded through the electrodes in v shape directly above the sample. One milliliter of distilled water was added to the bomb and the bomb was pressurized with pure oxygen and then placed in the calorimeter bucket which was filled with tap water at room temperature. The bomb was fired automatically after the jacket and bucket temperatures equilibrated to within acceptable accuracy of each other and the raise in temperature was recorded. Calorific value of samples were measured by Datacone oxygen bomb calorimeter using ASTM D 240-92.

Flash and fire point

Flash point is used generally as an indication of the fire and explosion potential of a product and indicates the hydrocarbon emissions of the source of oils in blend. It is the minimum temperature at which a product must be heated under prescribed conditions to release sufficient vapor to form a mixture with air that can be readily ignited [133]. Fire point is the temperature when the oil vapors can burn continuously for 5 seconds when tested in flash point apparatus and it occurs after the flash point, by 3 – 4 °C. Flash and fire points were obtained by using Cleveland open cup apparatus as per ASTM D 93-90.

Cloud and pour point

The temperature at which solidifiable compounds present in the sample begin to crystallize or separate from the solution under a method of prescribed chilling is called cloud point. It is a typical specification of middle distillate fuels [134]. The lowest temperature at which liquid ceases to flow under standardized test conditions is called pour point and is reported in 3 °C increments. For motor oils, a low pour point is very important to obtain proper start-up lubrication on cold days. Cloud and pour point determinations were performed according to ASTM D 2500, 97 using RW 2025 G JIEO Tech from Lab companion.

Refractive index

Refractive index (n), also called index of refraction, is the measure of the bending of a ray of light when passing from one medium into another. It is defined as the ratio of the velocity of light of a given wavelength in empty space divided by its velocity in a substance [135]. The refractive index was measured using ATAGO DR A1 refractometer from ABBE.

Ash content

The ash content is related to the amount of inorganic material in the fuel. It is the incombustible material which remains after the combustion, which mainly consists of the material such as vanadium, sulphur, silicon, aluminum, nickel, sodium, and iron content present in the fuel [136]. The maximum limit of ash content in the fuel is 0.2% m/m. Generally, fuel oils with low contents of ash, vanadium and sodium are preferable. These components tend to promote mechanical wear, high temperature corrosion and the formation of deposits in the turbocharger and on the exhaust valve. Ash content of the samples was determined by ASTM D 482-91.

Ultimate analysis

Ultimate analysis is used to determine the elemental composition of the oil sample including carbon, hydrogen, nitrogen, sulfur, and oxygen (by difference) and are expressed in percentage of the total mass of the original sample [137]. Ultimate analysis was performed using Elemental CHNS (carbon, hydrogen, nitrogen and sulfur) analyzer according to ASTM D5291-96.

TGA and DSC

TGA monitors the change in mass of a sample when heated caused due to the loss of water of crystallization, adsorbed surface species or decomposition of bulk phases via gas

production. DSC provides information about any exothermic or endothermic events occurring within the sample. Differences between the temperature of the sample and that of the inert reference material were measured during heating [138]. Thermogravimetric analysis (TGA) was done by using Mettler Toledo TGA/SDTA 851e with nitrogen as carrier gas at a constant flow rate of 45 ml min^{-1}. Suitable quantities of sample was heated from an initial temperature of 25–1000 ^{o}C at different heating rates of (10, 20, 30, 50 and 100 ^{o}C min^{-1}). A Mettler Toledo DSC-1 STAR^{e} with refrigerated cooling system operating within a temperature range from 25 to 450 ^{o}C was used to measure the heat requirement of the samples. The DSC was calibrated regularly with alumina as reference material. The obtained DSC curves give the heat flux (mW mg^{-1}) in function of the temperature or in function of the time (constant heating rate 10 ^{o}C min^{-1}).

^{1}H-NMR

^{1}H NMR analyses were performed at 25 ^{o}C on a Varian DRX – 400 spectrometer using 5 mm broadband probe head with a z-gradient [139]. The spectra were obtained at 400 MHz for ^{1}H, using dimethyl sulfoxide (DMSO) D6 as the solvent and trimethylsilane (TMS) as the internal standard. For each determination, 10 µL of the pure sample were dissolved in 40µL of DMSO.

GC-MS

Fatty acid composition and the average molecular mass of the oil samples were identified by Gas Chromatography-Mass Spectroscopy (GC-MS) [140]. The fatty acid compositions of these fats and oils was performed in Varian 450 Gas chromatography (GC) equipped with 240-IT mass spectrometer (MS) and VF-5 MS capillary column (30×0.25 mm; 0.25 µm film thickness). The oven temperature was held at 50 °C for 5 min and programmed

at 7 °C min^{-1} to 300 °C for 5 min. Other operating conditions were: Helium gas carrier at a flow rate of 1.0 mL min^{-1}. Injector and detector temperature were 250 °C and 280 °C respectively, with split ratio of 1:50. Mass spectra were taken at 70 eV mass ranges from m/z 40-400 amu.

2.3.2 Characterization of synthesized catalyst

BET

Surface area, pore size distribution was studied using nitrogen Brunauer-Emmett-Teller (N_2-BET) Beckmann-Coulter model SA 3100 surface area analyzer [141]. The catalyst samples (35 – 50 mg) were out gassed at 200 ºC for 1.5 h using nitrogen gas based on a 3 point procedure with 40 adsorption and 40 desorption points being measured. Pore diameters and volumes were calculated applying BJH method (mesoporous) to the desorption isotherm for relative pressures <0.02 and >0.35.

Degree of crystallinity and XRD

Percentage crystallinity of the samples was defined on the basis of the major (most intense) characteristic peaks by Topaz software using following formula:

$$\% \text{ Crystallinity} = \frac{\text{Sum of area of the crystalline phase}}{\text{Sum of the area of crystalline and amorphous phase}} \times 100$$

The mineral and amorphous phases in the catalyst samples were analyzed by XRD [142]. The samples (after being ground to a fine powder) were placed in a sample holder and the crystalline phases were characterized using a Bruker D-Advance X-ray diffractometer with Cu-K_α radiation of wavelength 1.54 Å with 2θ varying from 5 to 80 degrees. The phase identification was done with the help of JCPDS (Joint committee of powder diffraction standards) files for inorganic compounds.

XRF

The chemical composition of the raw materials and synthesized catalysts was determined using X-ray fluorescence (XRF) [143]. Analysis was performed for flyash and the synthesized catalyst for elemental composition using Philips PW 2404 wavelength dispersive spectrometer fitted with Rh tube. The samples were oven-dried at 50 ^{o}C for 12 h to reduce their water content prior to analysis.

H_2- TPR (Chemisorb)

Chemisorb is widely used to obtain a general feature of acidity/basicity of the catalyst. The acid/base strength can be evaluated by the maximum peak temperature (T_{max}) of desorption peak relating to the activation [144]. The TPR (temperature-programmed reduction) profiles of the samples were determined using Micromeristics - 2720. A bed of quartz wool was made and then required amount of catalyst (35 mg) was taken and outgassed at 150 ^{o}C for 1h. Then the reduction of catalyst was done in a flow of 10% H_2/Ar in 30 ml up to 850 ^{o}C to determine the reduction temperatures.

FTIR

Various characteristic functional groups were identified by using SIMADZU CORP Fourier Transform Infrared spectroscopy (FTIR). On interaction of an infrared light with materials, chemical bond will stretch, contract and absorb infrared radiation in a specific wave length range regardless structure of the rest of the molecules. The FTIR spectra were collected in the range of 450 – 4000 cm^{-1} region with 8 cm^{-1} resolution.

Basicity

The method of titration was used to determine the acidity/basicity of the catalysts. In general, the basicity of a base was to report the acidity of the conjugate acid and vice versa for

the acidity [145]. For basicity, the basic catalyst was mixed with a known concentration of HCl which neutralize HCl by an equivalent amount to its basicity. As a result, the original concentration of HCl will be reduced. The resultant concentration of HCl was determined by titration with NaOH, and finally, the adsorbed amount of HCl on the catalyst was reported. The final concentration of HCl was determined by titration (neutralization) with 1N NaOH using phenolphthalein indicator; the adsorbed amount of HCl on the catalyst could, thus, be determined.

Raman

The Raman spectra were obtained using a Horiba Jobin Vyon, Model Lab Ram HR, which includes a monochromator, a filter system and a charged-coupled device (CCD) as the detector [146]. Raman spectra were excited on a Spectra-Physics model 127 He/Ne laser (633 nm) and recorded in the range of 400–1500 cm^{-1}. Data analysis, such as baseline adjustment, smoothing and normalizing as well as interpretation, was performed using the Spectracalc software package GRAMS (Galactic Industries Corporation, NH, USA) and Microsoft EXCEL.

LPSA

The measurement of particle size distribution in the range 0.02 to 2000 micron was performed in Malvern Master Sizer 2000 Laser Particle Size Analyzer (LPSA). About 10 mg of sample dispersed in water was sonicated for 10 min and was analyzed for their particle size distribution.

CEC

The cation exchange capacity (CEC) of the materials was determined by ammonium acetate method [147]. 1g of sample is taken, 9 ml 1M sodium acetate was added and was

shaken for 10 minutes. The mixture was then centrifuged to separate the supernatant and is discarded. The above two steps are repeated 2 more times (totally 3 times it is mixed with sodium acetate). The above process is meant to saturate any vacant cationic spots in the sample with Na+ ions. Similarly, the above steps are repeated 3 times with IPA (instead of sodium acetate). This Step ensures that all free (floating, unbonded) ions surrounding the particles get washed out. Then 9 ml ammonium acetate is added and is shake for 10 minutes. Then the solution is centrifuged and the supernatant was collected in a 50 ml bottle. This is done two more times and around 27 ml of supernatant is collected. The metal concentration (Na, Ca, Mg, and K) in the solution was determined by using Perkin Elmer A Analyst 200 Atomic Adsorption Spectroscopy (AAS). CEC of individual cations can be calculated from the formula:

$$\text{CEC (meq/100g)} = \frac{(\text{Concentration of cation (meq/l)} \times \text{Volume of extract (ml)} \times 100)}{\text{Sample wt (g)} \times 1000}$$

Morphology and EDX

Field emission scanning electron microscopy (FESEM) images were recorded on Sigma/Zeiss FESEM operating at 10 kV. Samples were mounted on aluminium stubs using adhesive carbon tape and gold coated to reduce charging. Scanning electron microscopy images were taken by using LEO (LEO-1430 VP) microscope having an acceleration voltage of 15 kV, equipped with a 6587 EDX scanning spectrometry detector.

Chapter 3

Physico-Chemical Properties and Thermal Degradation Studies of Commercial Oils in Nitrogen Atmosphere

Commercial oils;
Thermogravimetric analysis;
Iso-conversional method;
Activation energy;
Flash point.

Work Published:

Volli V, Purkait MK. Physico-chemical properties and thermal degradation studies of commercial oils in nitrogen atmosphere. Fuel 2014;117:1010–9.

The current study deals with the thermal degradation behavior of commercial oils along with the determination of activation energy using model-free iso-conversional methods. Four degradation models including modified Coats and Redfern, Friedman, Kissinger and Flynn–Wall–Ozawa methods were used. These methods calculate the reaction activation energy (E_a) without making any modelistic assumptions and hence accurate results were obtained. Physical properties such as moisture content, viscosity, specific gravity, acid value, calorific value, refractive index, ash content, flash, fire, pour and cloud points were also determined. The chemical composition and thermal properties were investigated by using Fourier transform infrared spectroscopic (FTIR), differential scanning calorimetric (DSC), proton nuclear magnetic resonance (^1H NMR) and ultimate analysis. Results are reported in the subsequent sections of this chapter

3.1 Kinetic modeling consideration

Non-isothermal kinetic study of carbonaceous materials is an extremely composite task because of the presence of numerous complex components and their parallel and consecutive reactions [148]. The decomposition rate during thermal treatment can be represented by the following equation:

$$\frac{dX}{dt} = k * f(X)^n \quad (3.1)$$

Where, $f(X) = (1 - X)$, X is the extent of conversion, t is the time, K is the specific rate constant and n is the order of reaction. The extent of conversion can be represented as follows:

$$X = \frac{(W_0 - W_t)}{(W_0 - W_\infty)} \quad (3.2)$$

Where, W_0 is the initial weight, W_t is the weight after time, t and W_∞ is the weight after pyrolysis. The temperature dependence of the rate constant is given by Arrhenius equation:

$$k = A\, e^{(-Ea/RT)} \tag{3.3}$$

Where, A is the frequency factor, E_a is the activation energy, T is the temperature and R is the universal gas constant. To simplify the calculations, the order of reaction (n) is assumed as unity. For constant heating rate (β), a linear relation between time and temperature can be written as

$$T = To + \beta t \tag{3.4}$$

Now, substituting Eq. (3.3) and (3.4) in (3.1) and rearranging, the expression becomes:

$$\frac{dX}{(1-X)} = \frac{A}{\beta}\, e^{(-Ea/RT)}\, dT \tag{3.5}$$

The above equation can be used to evaluate E and A at constant heating rate using TG data. Unfortunately, the right hand side of Eq. (3.5) has no definite integral which makes it difficult to find the exact solution. Therefore, several methods were developed to estimate the value of E_a and A.

3.1.1 Friedman method

Friedman method [149, 150] is the first and the more general iso-conversional method of kinetic analysis. Combining Eq. (3.1) and (3.3) we get

$$\frac{dX}{dt} = Ae^{(-E_a/RT)} f(X)^n \tag{3.6}$$

Taking natural logarithm on both sides, Eq. (3.6) became

$$\ln\left(\frac{dX}{dt}\right) = -\frac{E_a}{RT} + \ln(Af(X)^n) \tag{3.7}$$

A plot of $\ln\left(\frac{dX}{dt}\right)$ versus 1/T gives the slope equal to $-E_a/R$ and an intercept of $\ln(Af(X)^n)$. In his original analysis, Friedman considered that there was a single n^{th} order reaction which indicates that at each level of conversion, the value of $-E_a/R$ is same and a plot of $\ln(Af(X)^n)$ versus $\ln(X)$ would be linear with a slope of n and an intercept of ln(A). But the value of E_a/R is not same for all levels of conversion for complex materials, and the plot of $\ln(A\, f(X)^n)$ versus $\ln(X)$ is rarely linear.

3.1.2 Coats-Redfern (modified) method

The aspects of the Friedman and Coats-Redfern analyses [151, 152] can be combined for analyzing data at multiple constant heating rates. The general integrated solutions for first order reaction may be written as [153]

$$X = e^{-\int_0^t k(T)dt} \tag{3.8}$$

The most common solution for kinetic integral, assuming an Arrhenius dependence for $k(T)$ is given by the following equation:

$$\int_0^t k(T)dt = \left(\frac{ART^2}{\beta E_a}\right)\left(\left(1-\frac{2RT}{E_a}\right)+\cdots\right)e^{(-E_a/RT)} \tag{3.9}$$

The $2RT/E_a$ term is small relative to 1 and substituting Eq. (3.9) in Eq. (3.8) we get

$$X = e^{-\left(1-\frac{2RT}{E_a}\right)\left(\frac{ART^2}{\beta E_a}\right)e^{(-E_a/RT)}} \tag{3.10}$$

Taking natural logarithm and rearranging Eq. (3.10), the following equation is obtained

$$\ln\left(\ln\left(\frac{X}{T^2}\right)\right) = -\frac{E_a}{RT} + \ln\left(\frac{-AR\,(1-2RT/E_a)}{\beta E_a}\right) \tag{3.11}$$

Rearranging the above equation we get

$$\ln\left(\frac{\beta}{T^2}\right) = \ln\left(\frac{-AR(1-2RT/E_a)}{E_a \ln(X)}\right) - \frac{E_a}{RT} \quad (3.12)$$

At different heating rates (β), the left-hand side is plotted against $1/T$ giving a series of straight lines one for each conversion level [151]. The slope of each line gives E_a/R, which may be substituted into the intercept to obtain frequency factor (A).

3.1.3 Kissinger method

The generalized form of Arrhenius rate equation [154] is given by Eq. (3.13)

$$\frac{dX}{dt} = A\, f(X)\, e^{\frac{-E_a}{RT}} \quad (3.13)$$

When the above equation is differentiated by parts, Eq. (3.14) may be obtained

$$\frac{d(dX/dt)}{dt} = A\, e^{\frac{-E_a}{RT}} \frac{d(f(X))}{dt} + Af(X) \frac{d(e^{\left(-\frac{E_a}{RT}\right)})}{dt} \quad (3.14)$$

Where, $\frac{d\left(e^{\left(-\frac{Ea}{RT}\right)}\right)}{dt} = \frac{E_a \beta}{RT^2}\, e^{\left(-\frac{E_a}{RT}\right)}$ (3.15)

And at the maximum of the reaction exothermic peak, $T = T_m$, $\frac{d(dX/dt)}{dt} = 0$ and Eq. (3.15) becomes;

$$0 = \frac{d(f(X))}{dt} + f(X) \frac{\beta\, E_a}{RT_m^2} \quad (3.16)$$

If $f'(X) = \frac{d(f(X))}{dX}$ then $\frac{d(f(X))}{dt} = f'\left(\frac{dX}{dt}\right)$ and substituting in Eq. (3.16) we get

$$0 = A\, e^{\frac{-E_a}{RT}} f'(X) + \frac{\beta\, E_a}{RT_m^2} \quad (3.17)$$

Solving for $\frac{\beta}{T_m^2}$ and taking natural logarithm, we get

$$\ln\left(\frac{\beta}{T_m^2}\right) = \ln\frac{AR}{E_a} + \ln\left(-f'(X)\right) - \frac{E_a}{RT_m} \quad (3.18)$$

Assuming first order reaction, then $f' = -1$, $\ln\left(-f'(X)\right) = 0$ and Eq. (21) simplifies to

$$\ln\left(\frac{\beta}{T_m^2}\right) = \ln\left(\frac{AR}{E_a}\right) - \frac{E_a}{RT_m} \quad (3.19)$$

The above equation (Eq. 3.19) is called Kissinger equation. When temperature reaches its maximum value, the effect of heating rates on the peak temperature is followed by Eq. (3.19). A graph of $\frac{1}{T_m}$ versus $\ln\left(\frac{\beta}{T_m^2}\right)$ was plotted. Regression analysis with least square fitting method was used to find the equation of the straight line and the values of E_a is evaluated.

3.1.4 Flynn–Wall–Ozawa (FWO) analysis

Flynn and Wall [155] and Ozawa [156] proposed this method (FWO) using TG/DSC data to determine kinetic parameters of reactions. This method is based on the Doyle approximation [157] for heterogeneous chemical reactions:

$$\ln\beta = \ln\frac{AE_a}{Rf(X)} - 5.331 - 1.052\left(\frac{E_a}{RT}\right) \quad (3.20)$$

Activation energy (E_a) was determined from the slope of the linear equation by plotting ln β against 1/T at particular conversion.

3.2 Determination of various physico-chemical properties

All the samples, edible (sesame, palm, refined soybean, mustard and sunflower) and non-edible (mahua, neem, olive, castor and karanja oils) oils were analyzed for their physical properties and reported in Table 3.1. The pH of edible oils was in the range of 4.07 to 4.84 and for non-edible oils it varied from 3.73 to 4.46. The water content of all the samples was ranging

from 0.01 to 0.06%. Specific gravity of all the oils was in the range of 0.904 to 0.932 gm cc^{-1}. In general, specific gravity of oils decreases with decrease in molecular weight and increases with unsaturation. Viscosity is a measure of intermolecular friction in a fluid and hence of its resistance to flow. Commercial oils behave as ideal Newtonian liquids and their viscosity of oils decreases exponentially with increasing temperature [158]. Viscosity of edible oils varied from 31.61 to 52.61 cP and it was in the range of .30.8 to 55.32 cP for non-edible oils.

One of the most important physico-chemical properties for ensuring safe storage of flammable materials is flash and fire point [159]. Flash points of all the edible oils were in the range of 320 to 335 ^{o}C and non-edible oils had slightly lower flash points when compared to edible oils and they were in the range of 240 to 300 ^{o}C. Fire point for the rest of the oils except for karanja and neem was in the range of 334 to 355 ^{o}C. Measure of cold flow properties of oils such as cloud and pour points play a prominent role in their usage as fuel in diesel engines. Cloud point is the temperature at which crystallization begins and the pour point is the temperature at which fuel ceases to flow [160]. Cloud point of refined edible oils was much higher than unrefined oils. Refined sunflower, mustard and soybean oils had cloud point of -4, -4 and -3 ^{o}C, respectively. Cloud point of sesame oil was 10 ^{o}C to that of palm oil was 22 ^{o}C. Non-edible oils had cloud point ranging from 1 to 20 ^{o}C. Neem and karanja oils have high cloud points of 17 and 20 ^{o}C, respectively. Pour point of non-edible oils is very high and they are in the range of 9 to -8 ^{o}C. In general, oils with low cold flow properties are preferred so that fuel can be transported easily without getting clogged through flow lines, pumps and feeds to fuel chambers during low temperatures. The presence of free fatty acid (FFA) content in the samples was measured by calculating its acid value (% of FFA is almost half the AV).

Table 3.1 Physical properties and ultimate analysis of various oils.

*Physical properties	Edible oils					Non-edible oils					Diesel	Standards
	Sesame	Palm	Soybean	Mustard	Sunflower	Neem	Olive	Mahua	Castor	Karanja		ASTM
pH	4.77	4.84	4.07	4.71	4.27	3.73	3.83	4.46	4.24	4.38	5.6	--
Water content (% vol)	0.01	0.03	0.01	0.02	0.01	0.08	0.02	0.02	0.01	0.06	0.05	D 1796-94
Specific Gravity ($gmcc^{-1}$)	0.916	0.904	0.912	0.918	0.923	0.928	0.904	0.906	0.932	0.917	0.84	D 1298-85
Viscosity @ 40 ^oC(cP)	35.56	45.1	31.61	52.61	33.01	38.52	47.4	43.9	30.8	55.32	2.7	D 445
Flash Point (^oC)	323	326	334	321	324	246	292	314	296	253	60	D 93-90
Fire Point (^oC)	342	340	347	355	353	263	331	345	334	265	65	D 93-90
Pour Point (^oC)	-1	10	--	--	--	9	-7	-8	-8	7	-35	D 97-93
Cloud Point (^oC)	12	22	-4	-4	-3	17	1	1	2	20	-20	D 2500-91
Acid value(mg KOH g^{-1})	2.115	1.41	0.564	1.41	0.987	14.1	4.23	19.74	2.82	18.33	0.062	D 664-89
Refractive index	1.460	1.462	1.471	1.468	1.472	1.464	1.464	1.471	1.475	1.476	1.454	--
Calorific value(MJ Kg^{-1})	38.6	37.6	38.3	36.9	37.8	40.4	39.5	36.7	41.2	36.8	45.2	D 240-92
Ash content (%wt)	<0.02	<0.01	<0.01	<0.03	<0.01	<0.04	<0.04	<0.04	<0.03	<0.05	0.01	D 482-91
Ultimate analysis												D5291- 96
C (wt %)	56.16	60.11	62.42	61.24	64.42	59.71	61.97	48.45	63.98	41.28	85.72	
H (wt %)	3.51	6.12	4.24	4.4	6.25	3.48	5.94	5.04	4.04	5.68	13.2	
N (wt %)	6.21	5.13	4.05	4.12	3.48	5.5	3.58	2.54	6.8	3.81	0.18	
S (wt %)	2.38	0.12	0.27	1.34	0.2	0.19	0.3	0.56	0.23	0.18	0.05	
O (wt %)	31.74	28.52	29.02	28.9	25.65	31.12	28.21	43.41	24.95	49.05	0.85	
H/C molar ratio	0.75	1.22	0.82	0.86	1.16	0.70	1.15	1.25	0.76	1.65	1.85	
O/C molar ratio	0.42	0.36	0.35	0.35	0.30	0.39	0.34	0.67	0.29	0.89	0.01	

*Experiments were done three times and the average value was reported

All the edible oils had low acid values ranging from 0.564 to 2.11 mg KOH g^{-1}. The FFA content of non-edible oils is usually high when compared to edible oils. Refractive index of the samples was in the range of 1.462 to 1.476 [161]. All the raw materials had a calorific value ranging from 36.8 to 41.2 MJ Kg^{-1}. Ash content of the samples was in the range of 0.01 to 0.05 weight percent. Ultimate analysis of the samples revealed higher sulfur content in mustard and sesame oil. Karanja and mahua oils had higher oxygen content and lower carbon content as the calorific value is low when compared to other samples. Combustion energies of all the fossil fuels can be estimated from the bond energies. The amount of energy released is dependent on the oxidation state of the carbons which is related to the hydrogen (H)/ carbon (C) ratio. At higher H/C ratio (lower oxidation state) more energy is liberated during the oxidation reaction. Thus, more energy released during combustion at greater H/C ratio. H/C molar ratio is high for palm, sunflower, mahua, olive and karanja oils. From the above it can be inferred that edible and non-edible oils cannot be used as fuel in the present form. Modifications to the physical properties of these oils by reducing the viscosity, increasing the cold flow properties and calorific value could make these oils as an alternate source of fuel.

The presence of functional groups in the raw materials was analyzed by using FTIR and the bands are listed in Table 3.2. All the samples had common bands at around 3008, 2920, 2858, 1747, 1463, 1377, 1165 and 723 cm^{-1} which can be attributed to -OH stretching, -CH- asymmetric stretching of alkenes and aromatics, -CH- symmetric stretching of alkanes, -C=O stretching of esters, -C=C- stretch of alkenes, -C-O- stretch of ethers, -C-O deformation, -CH- deformation of methyl group, respectively. Furthermore, small band in the range of 1652 cm^{-1} was observed in mustard, soybean, karanja, neem, mahua, castor and olive oils which was due to $-NH_2$ stretching vibrations. Bands between 1000 to 1260 cm^{-1} was observed

Table 3.2 FTIR spectra of various oils.

Functional group	Wave number (cm^{-1})									
	Edible oils				Non-edible oils					
	Sesame	Palm	Soybean	Mustard	Sunflower	Neem	Olive	Mahua	Castor	Karanja
-OH- Stretching	3008.9	3007.1	3008.9	3007.1	3008.9	3007.1	3005.8	3007.1	3007.1	3007.5
-CH- Asymmetric stretching	--	2929.8	2929.8	2922.1	2926.1	2924.5	2924.3	2933.7	--	2924.2
-CH- Symmetric stretching	2854.6	2856.5	2852.1	2852.7	2854.6	2852.3	2853.4	2852.8	2852.7	2852.3
-C=O- Stretching	1755.9	1747.5	1747.5	1747.5	1747.5	1747.4	1748.5	1751.5	1745.6	1743.3
-NH_2 Stretching	--	--	1654.9	1652.1	--	1654.2	1651.1	1651.6	1652.4	1654.3
-C=C- Stretching	1463.9	1463.9	1463.9	1463.9	1463.9	1463.3	1463.2	1463.1	1463.1	--
-C-O- Stretching	--	1377.1	--	1377.1	1377.1	1377.1	1377.3	1375.2	1375	1374.4
-C-O- Deforming	1165.4	1165.1	1166.9 to 1097.4	1166.9 to 1097.4	1166.3 to 1097.4	--	1165.1 to 1095.7	1163.2 to 1097.6	1165 to 1097.4	1166.1 to 1097.3
-CH- Deformation	721.3	723.5	723.3	721.3	723.3	721.3	723.3	732.2	725.2	723.3

in mustard, palm sunflower, karanja and olive shows the presence of -C–O- deformation bonds [44, 162].

All the samples were analyzed by ^{1}H-NMR spectroscopy and the hydrogen distribution is listed in Table 3.3**.** The spectra can be divided into three main regions viz; aromatic, olefinic and aliphatic resonances that occur in the chemical shift regions of 9–6, 6–4 and 3–0.5 ppm, respectively [163,164]. From Table 3.3 it is very clear that all the oils (except olive and karanja) do not contain any aromatics. The majority of the characteristic peaks are in the range of 4.5 to 3.3 ppm having composition of hydroxyl groups or ring-join methylene (Ar–CH_2– Ar) group. Dominance of protons at a chemical shift of 3.3 to 2.0 ppm was observed in sesame, olive and mahua oils. β-CH_3, -$CH_2$and γ-CH- protons were present as the second major composition in mustard, palm, neem and castor oils. Protons of paraffinic γ -CH_3 were present in sesame, olive and mahua oils.

3.3. Thermogravimetric analysis

Fig. 3.1 shows the TG curves of mustard, soybean, olive and karanja oils at five different heating rates of 10, 20, 30, 50 and 100 °C min^{-1} from ambient temperature (25 ^{o}C) to 600 °C. All the TGA profile shows similar trends and a plateau can be observed between 300 to 350 °C for mustard and soybean oils and 230 to 330 °C for olive and karanja oils indicating their thermal stability. The onset temperature (T_{onset}) is used to indicate the resistance of the oils to thermal degradation. This was determined by extrapolating the horizontal baseline at 1% degradation. The intercept of this line with the tangent to the downward portion of the weight curve was the T_{onset} [60]. The TGA curve becomes almost flat when the sample was completely burnt. Offset temperature (T_{offset}) was calculated from the intercept of the extrapolation on the same line and the tangent to the downward portion.

Table 3.3 ^{1}H-NMR results for various oils.

*Type of hydrogen	Chemical Shift (ppm)	Edible oils (%)					Non-edible oils (%)				
		Sesame	Palm	Soybean	Mustard	Sunflower	Neem	Olive	Mahua	Castor	Karanja
Aromatics	6.5 - 9	--	--	--	--	--	--	1.72	--	--	4.26
Phenolic (OH) or olefinic proton	6.5 – 5.0	--	2.91	23.98	5.64	--	2.38	1.82	3.85	3.69	7.16
Hydroxyl groups or ring-join methylene ($Ar–CH_2–Ar$)	4.5 – 3.3	--	51.92	61.03	42.26	99.46	44.94	3.74	7.21	51.33	61.25
CH_3 CH_2 and CH to an aromatic ring	3.3 – 2.0	79.82	--	9.73	20.16	0.54	6.74	45.07	40.15	9.40	3.48
CH_2 and CH $_\beta$ to an aromatic ring	2.0 – 1.6	2.84	7.65	5.26	4.89	--	3.7	2.08	6.59	3.66	8.14
β-CH_3, CH_2 and CH $_\gamma$ to an aromatic ring	1.6 – 1.0	7.05	32.14	--	23.51	--	33.52	24.2	2.49	24.50	11.1
CH_3 $_\gamma$ or further from paraffinic	1.0 – 0.5	10.29	5.38	--	3.54	--	8.72	21.37	39.71	7.41	4.61

*Experiments were done three times and the average value was reported

Table 3.4 shows the temperatures of the start (T_{onset}), finish (T_{offset}) of the main mass loss and the temperatures of maximum rate of mass loss of of all samples at different heating rates. The onset temperatures of all the samples increased with increase in heating rate. This is due to the fact that low heating rates favors the early decomposition of poly and mono unsaturated fatty acids resulting in increasing the onset temperature and activation energy thereon.

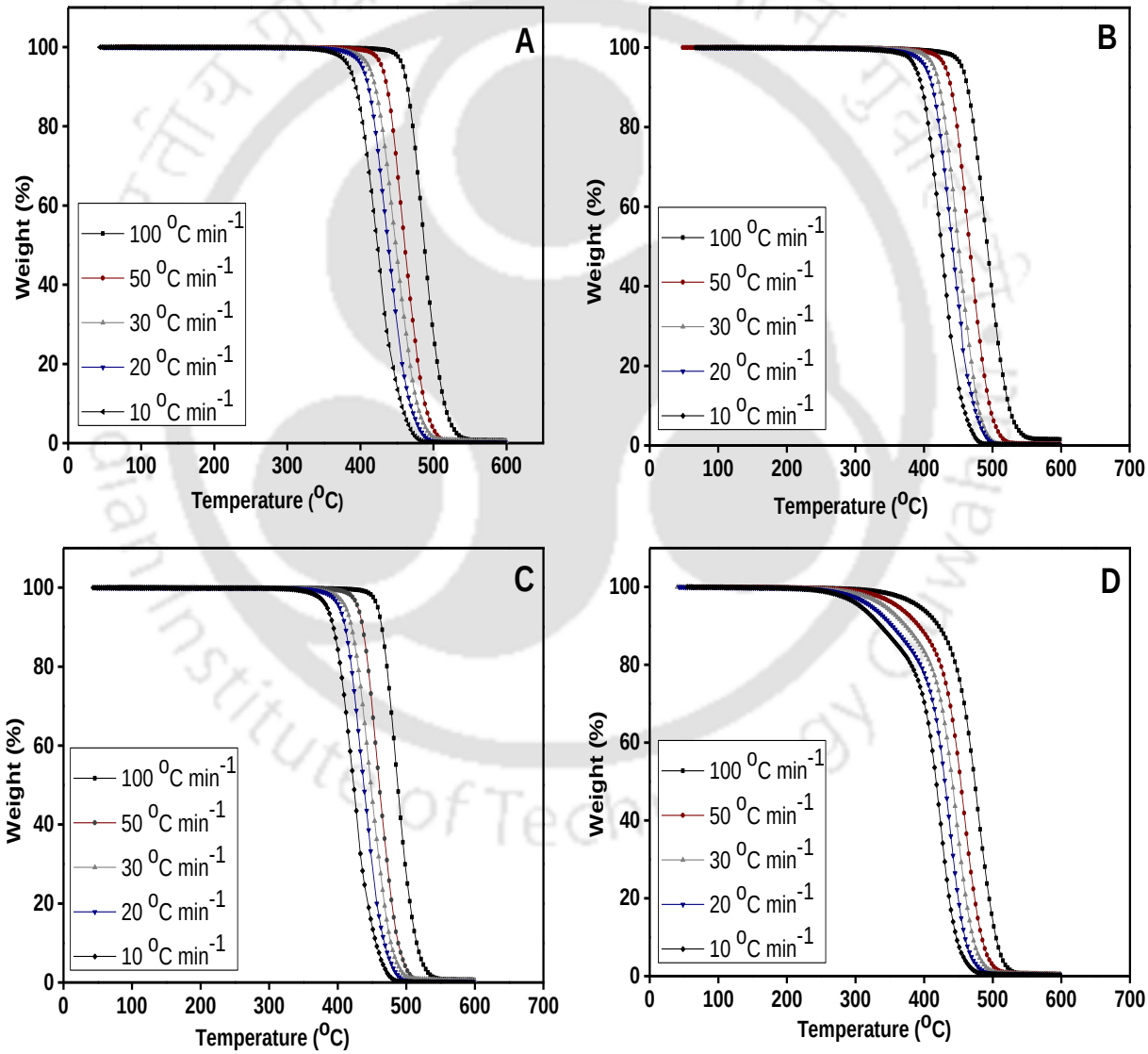

Fig. 3.1 TGA curve for various oils at heating rate of 10, 20, 30, 50 and 100 °C min^{-1}. (A) soybean, (B) mustard, (C) olive and (D) karanja oils.

Table 3.4 Onset, offset and peak temperatures of soybean, mustard, karanja and olive oils.

Heating rate (^oC min^{-1})	Soybean oil (^oC)			Mustard oil (^oC)			Karanja oil (^oC)			Olive oil (^oC)		
	T_{onset}	T_{peak}	T_{offset}	T_{onset}	T_{peak}	T_{offset}	T_{onset}	T_{peak}	T_{offset}	T_{onset}	T_{peak}	T_{offset}
100	411	475	548	395	491	553	288	478	541	375	485	535
50	375	455	521	371	465	525	261	458	518	351	461	511
30	340	443	509	361	451	505	238	445	510	340	449	504
20	328	433	499	346	441	499	220	435	499	325	439	492
10	307	415	490	334	425	484	202	418	481	316	424	484

*Experiments were done three times and the average value was reported with error of ± 3 ^oC

T_{onset} for soybean oil increased from 307 to 411 ^{o}C, for mustard oil increased from 334 to 395 ^{o}C, for karanja oil increased from 202 to 288 ^{o}C and for olive oil increased from 316 to 375 ^{o}C with the increase in heating rate from 10 – 100 ^{o}C min^{-1}. The region where the major weight loss occurred was from 307 to 548 ^{o}C for soybean oil, mustard oil was from 334 to 553 ^{o}C, karanja oil was from 202 to 541 ^{o}C and olive was from 316 to 535 ^{o}C with no residues remaining after 550 ^{o}C. Thermal decomposition of these oils in nitrogen environment might be for polyunsaturated, monounsaturated and saturated fatty acids [53, 55].

Fig. 3.2 shows the DTG plots of mustard, soybean, olive and karanja oils. The nature of a TG curve with the corresponding DTG peaks gives a clear indication of the number of stages of the thermal degradation. The DTG plots show the appearance of a single peak for all the oils. The DTG peaks differed in their position and height, because the heating rate acted as a significant factor on thermal decomposition. With increasing the heating rate from 10 to 100 °C min^{-1}, the thermal decomposition rate increased, shifting the DTG curves towards a higher temperature zone as well as shifting the temperatures corresponding to the maximum loss of mass peaks towards higher values. The shifting of DTG curves to higher temperature zone was because of faster release of volatiles materials.

Fig. 3.3 shows the DSC plots of all the samples. This analytical technique is used to measure variation in enthalpy due to changes in the physical and chemical properties of oil as a function of temperature or time. In typical experiment of DSC, changes in the sample that are associated with absorption or evolution of heat cause a change in the differential heat flow which is then recorded as a peak. The area under the peak is directly proportional to enthalpy change and its direction indicates whether the thermal event is endothermic or exothermic [59, 165].

The DSC thermograms began with an endothermic region and no exothermic event was seen (the sign of the heat flow changing from negative to positive) before 352 ^{o}C for soybean oil, 194 ^{o}C for sesame oil, 158 ^{o}C for sunflower oil, 172 ^{o}C for olive oil and 217 ^{o}C for mahua oil. Karanja and mustard oils did not show any exothermic event.

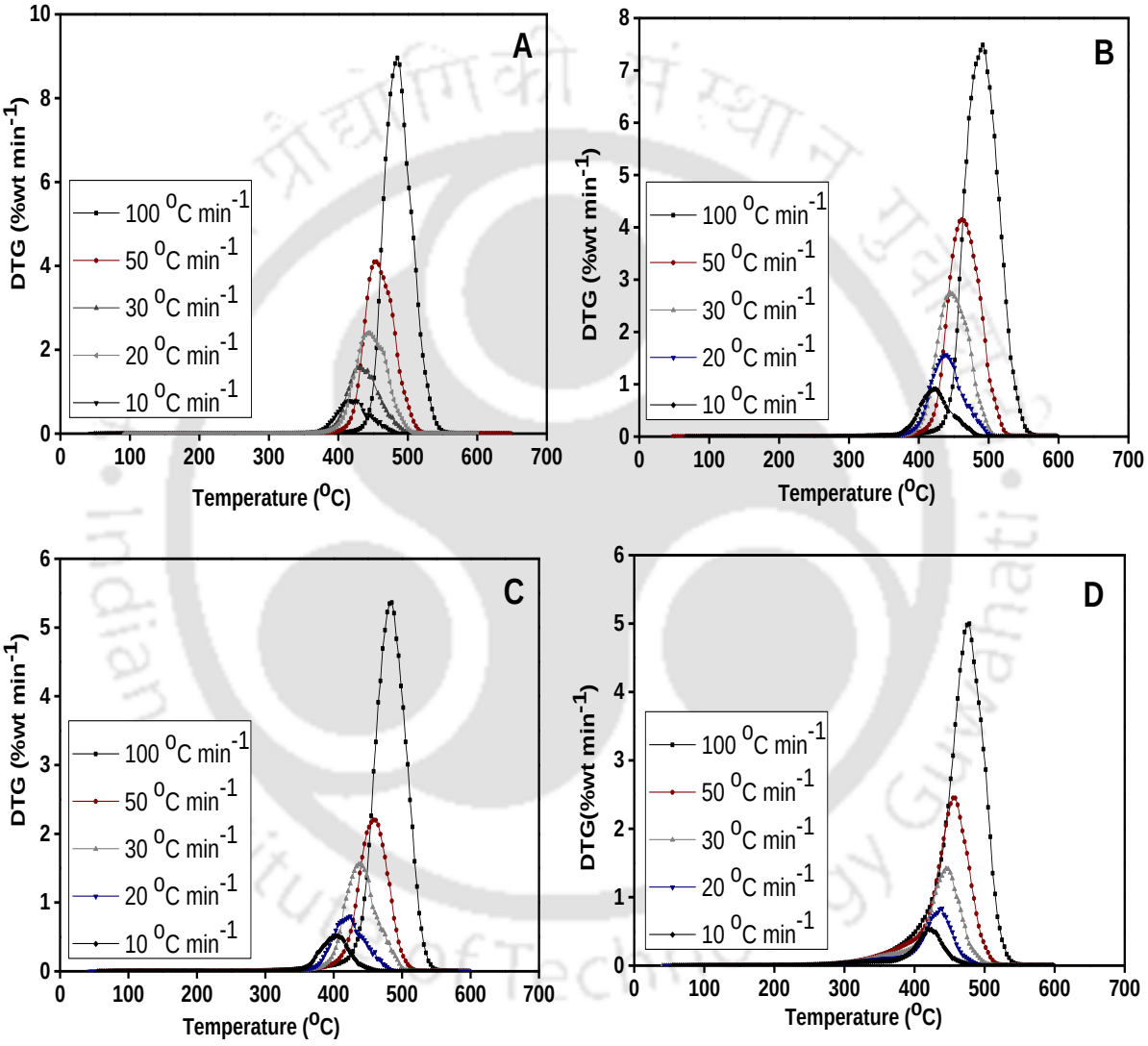

Fig. 3.2 DTG curves of various oils at heating rate of 10, 20, 30, 50 and 100 ^{o}C min^{-1}. (A) soybean, (B) mustard, (C) olive and (D) karanja oils.

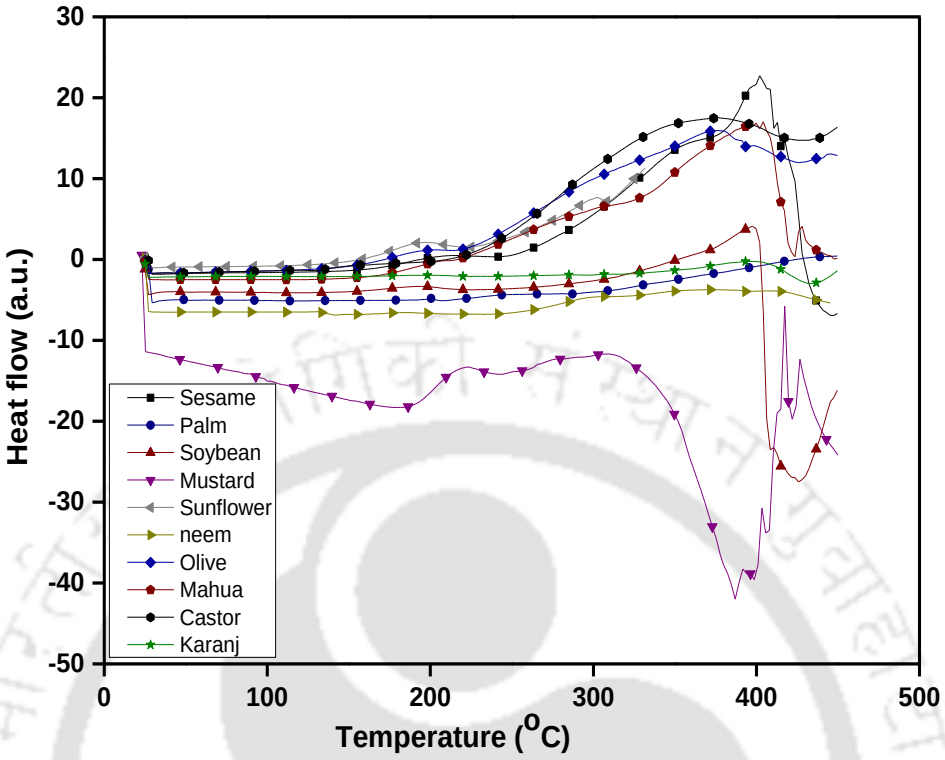

Fig. 3.3 DSC plots of sesame, palm, soybean, mustard, sunflower, neem, olive, mahua, castor and karanja oils.

3.4. Kinetic study

Activation energy (E_a) of four commercial oils (soybean, mustard, olive and karanja) in single step decomposition were determined using Friedman,modified Coats - Redfern, Kissinger and Flynn - Wall - Ozawa models in the conversion range of 0.2<X<0.9.The selection of this typical conversion range was to get accurate kinetic data and the activation energy there on. Initial thermal degradation (conversion upto 0.2) might involve multiple reactions whereas at the conversion beyond 0.9, insignificant amount of residue increased the experimental measurement errors. Figs. 3.4 (A, B and C) depict the fitting results obtained from Friedman plot of mustard oil, F-W-O plot of karanja oil and modified Coats-Redfern plot of soybean oil, respectively. It can be observed from these figures that the fitted lines are

parallel indicating activation energy at different conversion following a single mechanism or unification of multiple reaction mechanisms.

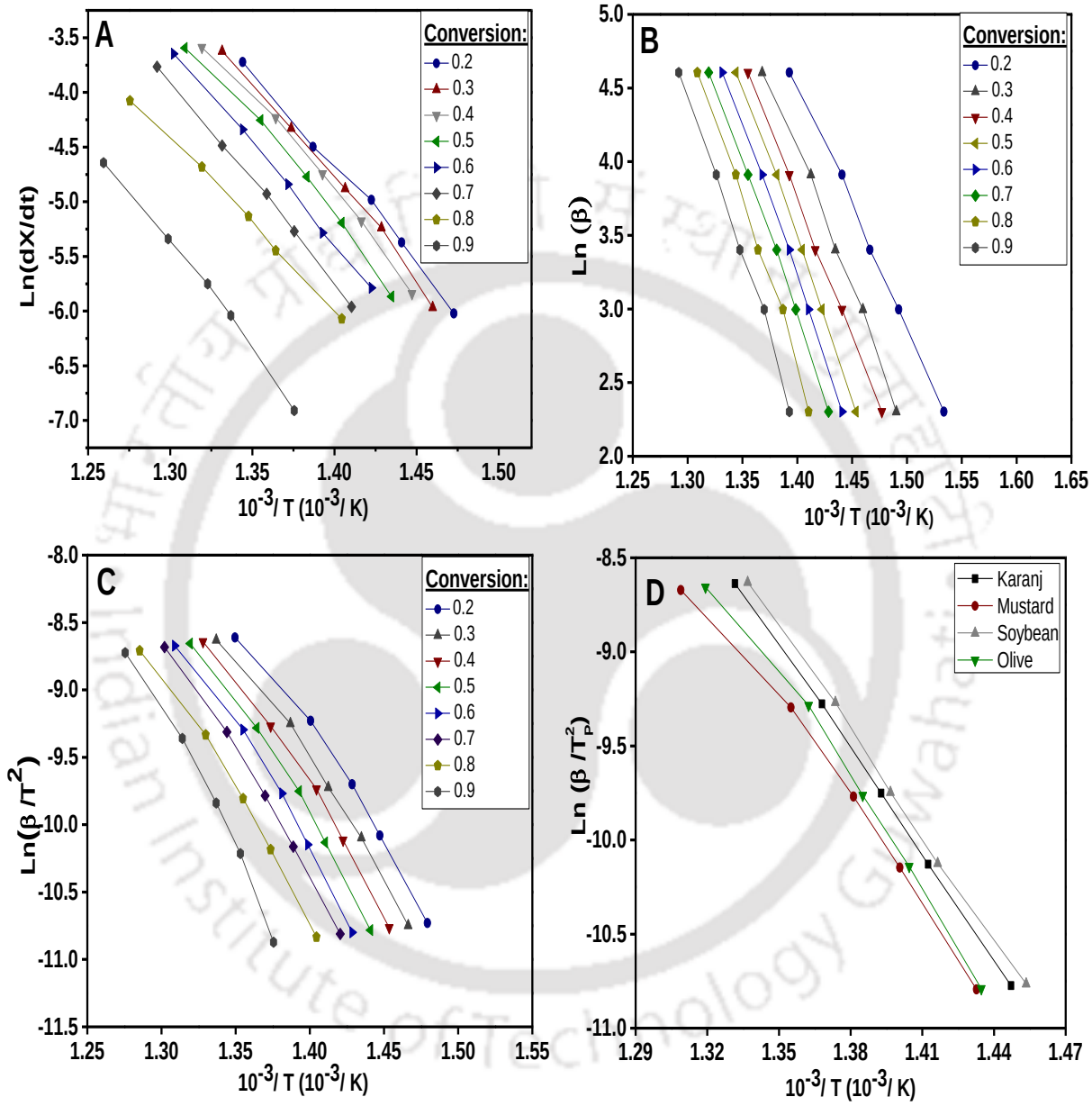

Fig. 3.4 Iso-conversional plot of (A) Friedman method (mustard oil), (B) F-W-O method (karanja oil), (C) modified Coats-Redfern method (soybean oil) at varying degree of conversion and (D) Kissinger plot of soybean, mustard, olive and karanja oils.

Table 3.5 Calculated values of activation energy using different models.

Raw material	Method	E_a^*/ R^2	Conversion (X)								Average
			0.2	**0.3**	**0.4**	**0.5**	**0.6**	**0.7**	**0.8**	**0.9**	
Soybean	Friedman	E_a	157.1	159.7	165.1	159.3	168.4	171.9	166.2	158.2	160.2
		R^2	0.99	0.99	0.99	0.98	0.98	0.99	0.99	0.98	0.99
	FWO	E_a	139.9	135.7	141.7	149.7	151.7	156.9	149.4	179.4	150.5
		R^2	0.98	0.98	0.98	0.98	0.98	0.98	0.98	0.98	0.98
	Coats - Redfern	E_a	135.4	135.8	137.6	144.4	147.4	149.6	148.5	173.7	146.6
		R^2	0.98	0.98	0.98	0.98	0.98	0.99	0.99	0.99	0.98
Mustard	Friedman	E_a	145.4	148.9	145.8	149.6	149.4	153.1	129.6	160.9	147.8
		R^2	0.99	0.99	0.99	0.99	0.99	0.99	0.99	0.99	0.99
	FWO	E_a	138.8	139.4	140.8	143.4	149.8	154.5	142.8	159.7	146.1
		R^2	0.99	0.99	0.99	0.99	0.99	0.99	0.99	0.99	0.99
	Coats - Redfern	E_a	134.2	134.7	136.1	138.7	145.3	150.2	143.6	154.1	142.1
		R^2	0.98	0.99	0.99	0.98	0.99	0.99	0.99	0.99	0.99
Olive	Friedman	E_a	129.5	139.7	148.4	146.4	149.1	157.1	156.6	161.6	148.5
		R^2	0.99	0.99	0.99	0.99	0.98	0.98	0.99	0.99	0.99
	FWO	E_a	124.9	131.4	136.9	146.1	148	153.8	165.0	157.3	145.4
		R^2	0.99	0.99	0.98	0.99	0.99	0.98	0.99	0.99	0.99
	Coats - Redfern	E_a	119.5	126.1	134.3	145.3	150.2	151.8	160.7	152.5	142.5
		R^2	0.99	0.99	0.99	0.99	0.99	0.99	0.99	0.99	0.99
Karanja	Friedman	E_a	164.4	164.3	157.4	159.4	161.9	160.4	158.1	159.5	160.7
		R^2	0.99	0.99	0.99	0.99	0.99	0.99	0.99	0.99	0.99
	FWO	E_a	130.3	148.4	149.2	167.1	166.4	165.8	176.6	177.3	160.1
		R^2	0.99	0.99	0.99	0.99	0.99	0.99	0.99	0.99	0.99
	Coats - Redfern	E_a	125.7	144.5	145.2	163.9	163.1	162.3	173.6	174.1	156.5
		R^2	0.99	0.99	0.99	0.99	0.99	0.99	0.99	0.99	0.99

*E_a in KJ mole $^{-1}$

Activation energies (E_a) for all the oils within the conversion range of $0.2<X<0.9$ were calculated from the slops of above figures using the aforesaid methods and are summarized in Table 3.5. From the table it may be found that the activation energy (E_a) for edible oils was in the range of 129.6 – 179.4 KJ mole^{-1} with varying conversion ($0.2<X<0.9$). The average value was observed as 160.2, 150.5 and 146.6 KJ mole^{-1} for soybean oil and 147.8, 146.1 and 142.1 KJ mole^{-1} for mustard oil for Friedman, FWO and modified Coats-Redfern methods, respectively. It may be seen from the figure that FWO and Friedman method fitted well for (within 1% error) for mustard oil. On the other hand for soybean oil both FWO and modified Coats-Redfern methods fitted well within an error of 2%. Similarly, for non-edible oils, with varying conversion, the activation energy was calculated as 119.5 – 177.3 KJ mole^{-1} (Table 3.5). For olive oil, the average values of E_a was 148.5, 145.4 and 142.5 KJ mole^{-1} and that of for karanja oil was 160.7, 160.2 and 156.5 KJ mole^{-1} for Friedman, FWO and modified Coats-Redfern methods, respectively. For both olive and karanja oils, Friedman and FWO methods had the best fit (with regression coefficient of 0.99).

Fig. 3.4 D shows the linear plots of ln (β/T_p^2) against $1/T_p$ for soybean, mustard, olive and karanja oils and the values of activation energy were calculated as 142.9, 148.3, 142.7 and 153.9 KJ mole^{-1}. It was also envisaged that the activation energy depends on heating rate and it increase when the heating rate is increased. From the results as above it is clear that the obtained values of activation energy (E_a) by Kissinger method are slightly lower than that obtained from Friedman, FWO and modified Coats and Redfern methods. When all the above methods are compared, it is observed that the activation energy varied from 141.9 – 148.3 KJ mole^{-1} for mustard oil, 142.9 – 160.2 KJ mole^{-1} for soybean oil, 141.9 – 148.2 KJ mole^{-1} for olive oil and 153.9 – 160.7 KJ mole^{-1} for karanja oil. The average value of activation energy

considering all the above four methods was determined as 145.9, 150.6, 144.4 and 157.4 KJ $mole^{-1}$ for mustard, soybean, olive and karanja oils, respectively. The obtained values were in the range of literature value [53]. Sanjiv et al. [53] reported that the activation energy of soybean oil varied from 155.6 to 196 KJ $mole^{-1}$ during thermal decomposition in presence of air. Variation of activation energy was reported in the range of 158 - 278 KJ $mole^{-1}$ during thermal degradation of olive oils in air atmosphere [55]. From the present investigation it may be concluded that the activation energy calculated in nitrogen atmosphere was quite less than that of in thermal oxidation. Thermal degradation data of mustard and karanja oil obtained from this studies increases the novelty of the work. More over the results obtained from this work provides the new kinetic data during thermal degradation in presence of nitrogen atmosphere.

Chapter 4

Utilization of Flyash as Heterogeneous Catalyst for Transesterification

Flyash;
Biodiesel;
Wet-impregnation method;
Response surface methodology.

Work under review:

Volli V, Purkait MK. Utilization of flyash as heterogeneous catalyst for transesterification. J Ind & Eng Chem.

A novel, low cost and highly effective heterogeneous base catalyst from flyash and a natural source of calcium (bone powder) was developed and characterized. Different catalysts was synthesized by varying calcined animal bone powder loading (10, 20 and 30 wt %) in flyash described in section 2.2.1 and its catalytic activity was studied by transesterification of mustard oil. A three level 3 factor central composite design in RSM was used for model prediction. Details of characterization results are reported below.

4.1 Characterization of flyash and flyash based catalyst

4.1.1 Compositional study

Flyash is formed during the combustion of pulverized coal in coal-fired power stations which has a significant influence on its bulk chemical composition. The principle components of flyash are silica, alumina, ferrous oxide and calcium oxide with varying amounts of carbon. From XRF analysis, the order of bulk chemical composition of flyash was found to be SiO_2 (56.6) > Al_2O_3 (23.2) > CaO (7.9) > Fe_2O_3 (5.8) > MgO (1.5) > K_2O (1.4) > TiO_2 (1.3) > SO_3 (0.5) > P_2O_5 (0.3) > Na_2O (0.2) > SrO (0.06) > MnO (0.05) by wt %. The trace element content in flyash was determined using AAS and was found to be chromium (Cr) 0.001 ppm, nickel (Ni) 0.002 ppm, arsenic (As) 0.002 ppm and zinc (Zn) 0.07 ppm. Ultimate analysis of flyash showed the presence of carbon (C), hydrogen (H), nitrogen (N), sulfur (S) and oxygen (O) as 62.6, 1.24, 10.32, 2.72 and 23.05 wt %, respectively. The loss of ignition (LOI) of flyash was found to be around 1%. The LOI of Indian based flyash is in the range of 0.5 to 5%. From the above it is clear that the flyash used in the experiments is of class 'F' and based on chemical composition it can be classified as Calsialic ($SiO_2 + Al_2O_3 + K_2O + TiO_2 + P_2O_5$ < 89%, $CaO + MgO + SO_3 + Na_2O + MnO$ < 11.5%, Fe_2O_3 < 11.5%) flyash [166]. The

elemental composition of calcined animal bone powder and flyash based catalysts is shown in Table 4.1. The synthesis procedure of the catalyst was described in section 2.2.1. From the table it is clear that with increase of CBP loading in flyash, a clear increase in the concentration of calcium, magnesium and phosphorus which play a major role in the basic nature of the catalyst can be observed.

Table 4.1 Elemental composition, BET surface area and basicity of calcined bone powder, C30, C20 and C10 flyash based catalyst.

Characteristic	Calcined bone powder (wt %)	Catalyst (wt %)		
		C30	C20	C10
O	47.15	39.7	33.0	49.0
Al	0.21	1.8	11.5	7.9
Si	0.39	5.0	16.2	25.1
Ca	29.79	39.7	31.7	9.5
Mg	0.48	4.0	1.0	0.9
Fe	--	1.4	1.3	1.5
P	9.2	8.5	5.3	3.1
K	5.22	0.4	0.5	0.7
Na	--	0.2	0.2	0.3
Surface area (m^2gm^{-1})	100	11.3	7.1	4.2
Basicity (mmole of HCl gm^{-1})	27.2	17.4	8.7	3.1

4.1.2 Basicity

The basicity of CBP and synthesized catalyst was determined by the method described in section 2.3.2, the analysis was performed in triplicate and mean of values is reported in Table 4.1. The basicity of calcined bone powder was found to be 27.2 mmoles of HCl g^{-1}. The

basicity of the synthesized catalyst was found to be increased with increase in the concentration of CBP. Basicity was determined as 17.4, 8.7 and 3.1 for C30, C20 and C10 respectively. Singh et al. [145] reported the similar kind of observation for MgO, ZnO, and Pb_3O_4 as 46.05, 32.3 and 14.5 mmoles of HCl g^{-1}.

4.1.3 Surface area analysis

The BET surface area of flyash, CBP, C30, C20 and C10 was found to be 1.7, 100, 11.3, 7.1 and 4.2 m^2 g^{-1}. Surface area of CBP was close to the reported value (110 m^2 g^{-1}) [167]. The total pore volume of 0.037, 0.14, 0.098, 0.085 and 0.075 ml g^{-1} for flyash, CBP, C30, C20 and C10, respectively, suggest that the catalyst synthesized was mesoporous in nature. Increase in surface area with increase in the concentration of CBP could result in high catalytic activity. The type III isotherm convex to the axis was observed from the nitrogen adsorption-desorption isotherms. The increase in surface area of catalyst could be due to increase in crystal growth of calcium oxide with increase in bone powder loading [76].

4.1.4 Thermal degradation analysis

The thermal degradation of flyash, bone powder and flyash based catalyst was studied by using TGA from ambient temperature to 1200 ^oC at a heating rate of 10 ^oC min^{-1} and shown in Fig. 4.1(A). From the figure it is clear that flyash was thermally stable up to around 515 ^oC with a slight weight loss at less than 150 ^oC due to loss of water vapor from the surface of alumina silicates. The major weight loss which was due to thermal decomposition of $CaCO_3$ to CaO and CO_2 was in the temperature range of 510 to 840 ^oC. The maximum rate of weight loss occurred at the temperatures of 693 ^oC for flyash and 843 ^oC for bone powder. The total weight loss of 6.2%, 9.1%, 5.8%, 4.7% and 1.1% was observed for flyash, bone powder, C30, C20 and C10, respectively.

4.1.5 Particle size distribution

The particle size distribution (PSD) of flyash, CBP, C30, C20 and C10 is represented in Fig. 4.1(B). The PSD of flyash was in the range of 10 µm to 100 µm with mean particle size of 14 µm, the smallest particles approximately 0.4 µm, and the largest particles approximately 22 µm. The PSD of CBP was in the range of 0.2 µm to 60 µm with smallest and the largest particles at 0.24 µm and 0.7 µm. The PSD range of flyash based catalyst was 10 to 110 µm with the smallest particle ranging from 0.2 µm to 22 µm.

4.1.6 FTIR analysis

The FTIR spectra of flyash, CBP, C30, C20 and C10 catalyst is shown in Fig. 4.1(C). The FTIR spectra of flyash shows a broad band at 1053 cm^{-1} depicts the presence of Al, Si asymmetric stretching vibrations. Peak appearing at 1380 -1400 cm^{-1} shows the presence of potassium (weak aliphatic bonds). The FTIR spectra of the calcined bone powder exhibited only the characteristic peaks of hydroxyapatite. The peaks around 1047 to 1095 cm^{-1} correspond to asymmetric stretching vibrations of P–O bonds. The bands around 570 to 632 cm^{-1} correspond to the vibrations of O–P–O bonds in calcium phosphate. The FTIR spectra of flyash based catalyst (C10, C20, and C30) shows both the characteristic peaks of flyash and calcined bone powder. With increase in the concentration of CBP, appearance of band at 570 to 632 cm^{-1} can be observed.

4.1.7 XRD

The powder XRD patterns and mineral composition of flyash, calcined bone powder and flyash based catalyst (C10, C20, and C30) are presented in Fig. 4.1(D). From the XRD pattern of flyash, it was found that the predominant phases were quartz (SiO_2) with major peak at 20.86, 26.9, 36.5 and 50.32 degrees 2θ and less intense peaks of mullite ($3Al_2O_3$.

SiO_2) at 39.4 degrees 2θ and magnetite. The main component of animal bone is calcium phosphate and after calcination it transforms to hydroxyapatite. The flyash based catalysts (C10, C20 and C30) exhibited both the characteristic peaks of quartz, mullite and hydroxyapatite as well.

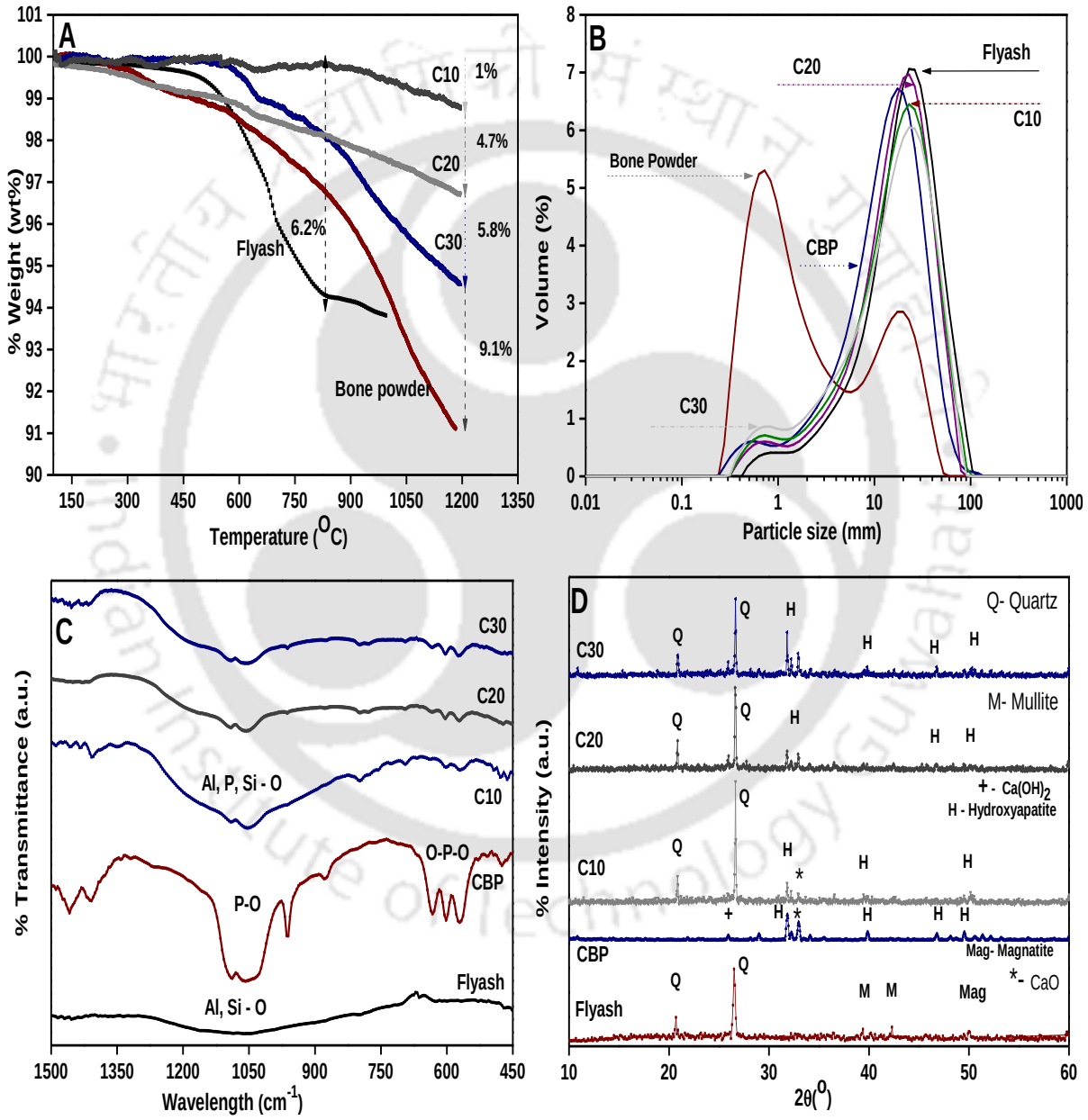

Fig. 4.1 Spectra for (A) TGA, (B) particle size distribution, (C) FTIR, and (D) XRD of flyash, bone powder, CBP, C10, C20 and C30 catalyst.

A clear increase in the intensity at 31.8, 32.2, 32.9, 40.4, 50.5 and 51.3 degrees 2θ was observed with increase in catalyst loading. This suggests that a good dispersion of bone powder occurred under the activation condition. Occlusion of calcium metal clusters enhances the basicity of the flyash by increasing the negative charge of the framework oxygen atoms. The supported species typically introduced through wet impregnation of a solution containing the solvated precursor into the pores and calcination decomposes the occluded compounds thus creating the supported alkali metal oxides [168].

4.1.8 Surface morphology

The surface morphology of flyash, CBP and flyash based catalysts is shown in Fig. 4.2 (A, B, C, D and E). Flyash (A) particles are primarily spherical in nature and from the above it is clear that the flyash used in the present study are Cenospheres, irregularly shaped carbon particles, mineral aggregates and agglomerated particles. The CBP (B) sample appeared like a mass of aggregates. Flyash based catalysts (C, D and E) show porous nature with high surface roughness.

Table 4.2 Levels of the transesterification condition variables.

Factors	Coding	Units	Level		
			-1	0	1
Bone powder concentration	A	wt %	10	20	30
Catalyst concentration	B	wt %	5	7.5	10
Methanol to oil molar ratio	C	mol/mol	5.5	7.25	9

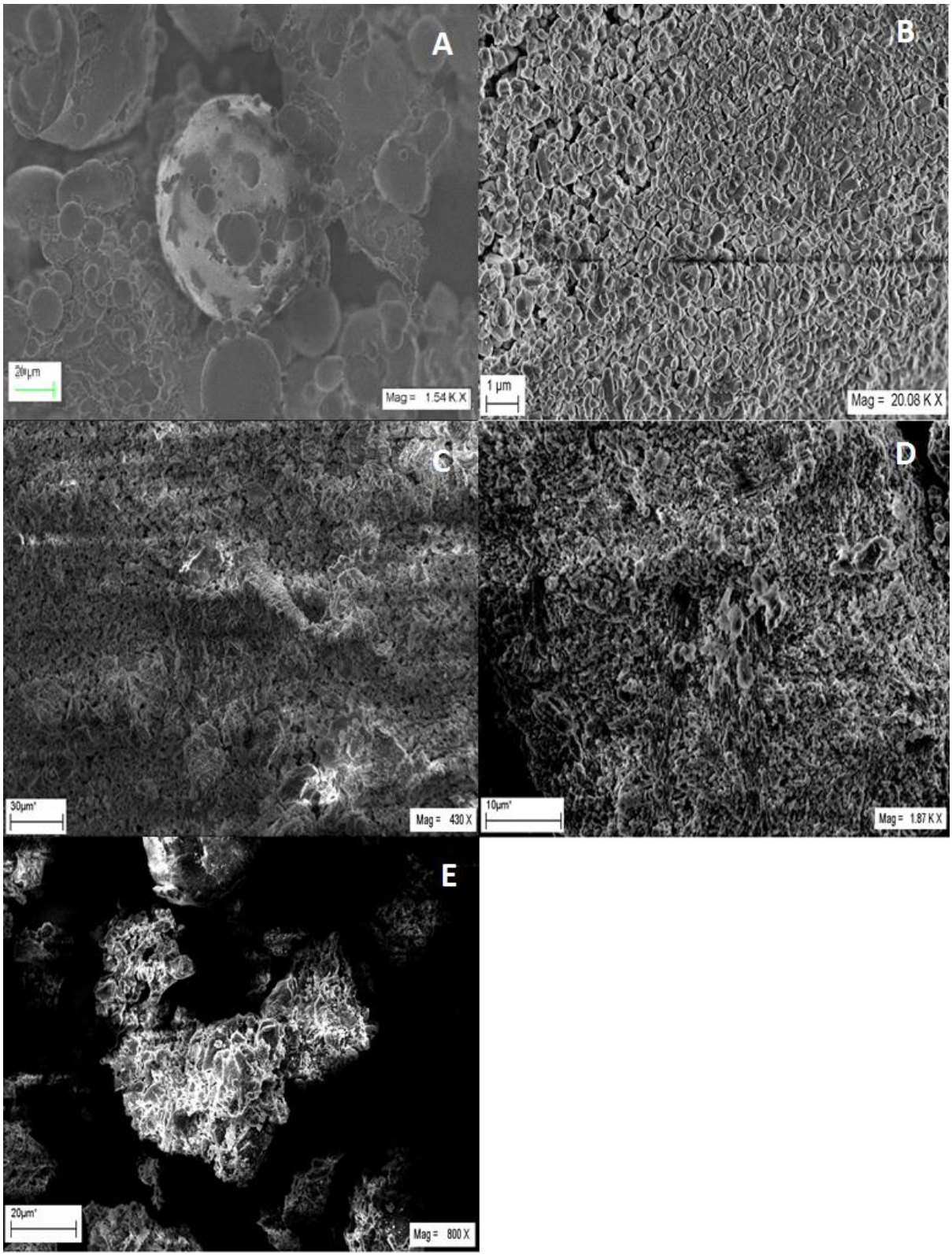

Fig. 4.2 SEM images of (A) flyash, (B) CBP, (C) C10, (D) C20 and (E) C30 catalyst.

4.2 Statistical analysis

The optimization of process parameters for biodiesel synthesis was done by RSM using design expert software (Trail version 7.0.0, StatEase, Inc., USA). A three level central composite design (CCD) with three factors was applied to evaluate the effect of variables such as CBP loading (A), catalyst concentration (B) and methanol / oil molar ratio (C) with % yield as the response of the experimental design. Preliminary studies were undertaken for 8 - 12 h to determine the range of these variables and the selected range is shown in Table 4.2. The total number of design experiments was calculated by using the formula: $2^K + 2K + 6$ where K is the number of variables (factors). The complete design matrix of experiments in terms of coded values is presented along with results in Table 4.3. The model equation (4.1) was used to predict the optimum value to explain the interaction between the factors.

$$Y = a_0 + \sum_{i=1}^{k} a_i x_i + \sum_{i=1}^{k} a_{ii} x_i^2 + \sum_{i=1}^{k} \sum_{j=i+1}^{k} a_{ij} x_i x_j + \varepsilon \quad (4.1)$$

Where, a_0 is defined as the constant, a_i is the linear coefficient, a_{ii} is the quadratic coefficient and a_{ij} is the interaction coefficient. x_i and x_j are the levels of independent variable (factors). K is number of tested factor, ε is error and Y is the predicted response value. The quality of the polynomial fit was studied by determination coefficients (R^2) and (R^2_{adj}) calculated by using equation (25) and (26), respectively [169].

$$R^2 = 1 - \frac{SS_{residual}}{SS_{model} - SS_{residual}} \quad (4.2)$$

$$R^2_{Adj} = 1 - \frac{SS_{residual}/DF_{residual}}{(SS_{model} + SS_{residual})/(DF_{model} + DF_{residual})} \quad (4.3)$$

Where DF is the degrees of freedom which is the number of model terms including the intercept minus one and SS is the sum of squares which is sum of the squared differences

between the average values for the blocks and the overall mean. The overall trend is more concerned than the accuracy of individual data points because, the software used in this study also requires repetitions made at the center point of the process variables. Response surface and counter plots were developed using the equation obtained from regression analysis of experimental data.

4.2.1 Statistical data analysis and optimal process parameters

A three level 3 factor central composite design for response surface optimization was developed and validated to study the effect of process parameters (CBP loading, catalyst concentration and methanol to oil molar ratio) which corresponds to maximum biodiesel yield. The total number of model experiments for the current study was 20. Of these, 14 experiments and 6 imitation tests at design center where experiments were conducted randomly to estimate the error. Though 20 experiments were considered for RSM calculations, a total of 15 experimental trails were represented in Table 4.3 for easier interpretation. RSM software has suggested two factor interaction (2FI) model with significant mode terms as A, B, AB and BC. The model equation which shows the realtionship between process variables and biodiesel yield in terms of coded factors was as follows:

Yield = 83.04 – 2.5 A – 1.12 B + 0.66 C – 5.41 AB + 0.65 AC – 1.66 BC

In terms actual factors:

Yield = 40.92 + 1.10 A + 6.63 B + 2.84 C – 0.21 AB + 0.03 AC – 0.38 BC

Positive sign in front of the terms indicate synergistic effect where as negative sign indicate antagonist effect [20]. C and AC were found to be insignificant model terms and can manually be removed from the model to improve the regression model and optimization

results. However, individual model term C cannot be removed as it is required to support the model hierarchy [170].

The analysis of variance (ANOVA) of response surface model determines the effect of individual model terms and their interactions along with significance and fitness of the 2FI model (Table 4.4). The Model F-value of 43.01 with p-value >0.0001 implies that the model is significant at 95.2% confidence level. The p-value (probability of error value) gives the significance of each model coefficient, which also indicates the interaction effect of each cross product. Smaller the p-value (<0.05), stronger will be the significance of the corresponding coefficient. Values between 0.05 and 0.1 indicate the model terms as marginally significant [171].

Coefficient of the variation (CV) is the ratio of standard deviation to mean and is expressed in percent (%). A low value of coefficient of the variation (CV, 1.4%), indicates a high degree of accuracy and a good agreement with the experimental values. The residual sum of squares is split into two portions, one is called pure error which is based on replicate measurement and the other is called lack of fit which is based on model performance. The lack of fit test indicates the significance of replicates error in corresponding to model dependent error. The lack of fit F-value of 1.91 implies the lack of fit is not significant relative to the pure error indicating that the model satisfactorily fitted to experimental data [172].

The quality of model fit was evaluated by the coefficient of determinination (R^2) and the value was found to be 0.95. The R^2 value is always between 0 and 1 and its magnitude indicates the aptness of the model. The value of R^2_{Adj} was found to be 0.93 which is the measure of the amount of variation around the mean, adjusted for the number of terms in the

model and its value decreases as the number of terms in the model increases. Predicted R-squared is the measure of the amount of the variation in new data explained by the model and its value was 0.83 and is in reasonable agreement with R^2_{Adj}.

Table 4.3 Experimental design matrix and results.

Run	Type	Factors			Response
		A: CBP loading	B: Catalyst concentration	C: Methanol to oil molar ratio	Yield (%)
1	Fact	1	1	1	72.2
2	Axial	0	-1	0	84.6
3	Axial	0	0	-1	81.6
4	Fact	1	1	-1	73.5
5	Fact	1	-1	1	89.8
6	Axial	0	0	1	83.1
7	Center	0	0	0	84.2
8	Fact	-1	-1	1	82.3
9	Axial	-1	0	0	87.7
10	Axial	0	1	0	81.4
11	Fact	-1	1	-1	90.4
12	Fact	-1	1	1	88.2
13	Fact	1	-1	-1	82.6
14	Axial	1	0	0	80.7
15	Fact	-1	-1	-1	79.6

The predicted R-squared and the adjusted R-squared should be within 0.20 of each other. Otherwise, there may be a problem with either the data or the model. Adequate

precision (25.2) compares the range of the predicted values at the design points to the average prediction error. Ratios greater than 4 indicate the adequacy of the model [171]. Fig. 4.3 shows that the values of the response predicted from the empherical model was in agreemnent (regression coefficient is close to 1) with the observed values. The above model proved to be an appropriate representation of the real relationship between the factors. Similar kind of model (2FI) was predicted and validated by Chakraborty et al [44].

Table 4.4 Analysis of variance (ANOVA) for response surface model.

Source	**Sum of squares**	**DF**	**Mean square**	**F value**	**p-value (Prob> F)**
Model	368.1	6	61.4	43.0	< 0.0001
A	85.4	1	85.4	59.9	< 0.0001
B	17.0	1	17.0	11.9	0.0043
C	5.9	1	5.9	4.1	0.0630
AB	234.3	1	234.3	164.2	< 0.0001
AC	3.4	1	3.4	2.4	0.1470
BC	22.1	1	22.1	15.5	0.0017
Residual	18.5	13	1.4		
Lack of Fit	14.0	8	1.7	1.9	0.2469
Pure Error	4.6	5	0.9		
Cor.total[a]	386.7	19			
Std. dev.[b]	1.2		R-squared	0.952	
Mean	83.0		Adj R-square[d]	0.930	
C.V[c]	1.4%		Pred R-square[e]	0.830	
			Adeq Precision[f]	25.243	

[a] Corrected total; [b] Standard of deviation; [c] Coefficient of variation;
[d] Adjusted R^2; [e] Predicted R^2; [f] Adequate precision.

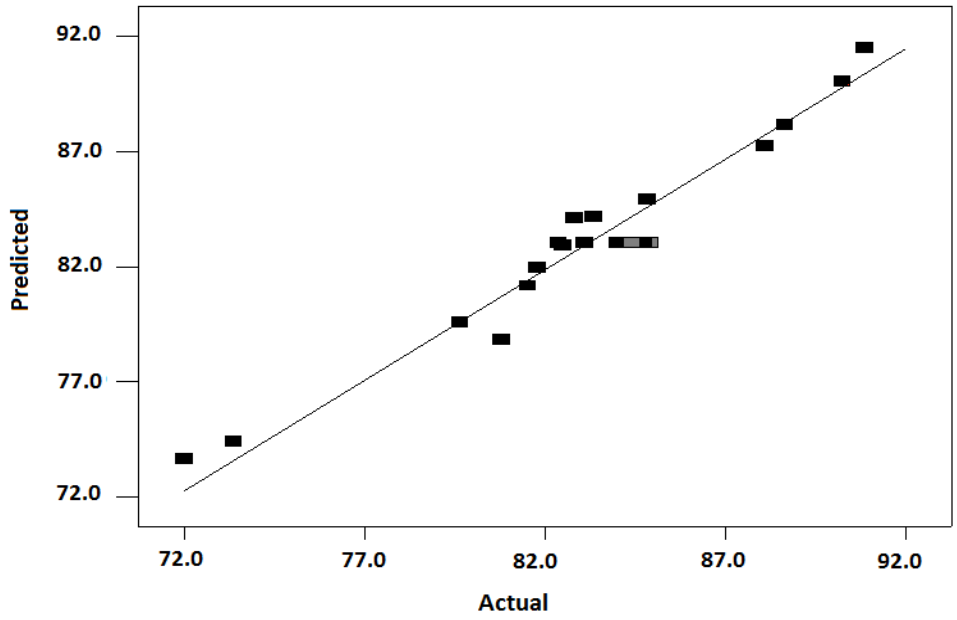

Fig. 4.3 Graphical comparison between actual and predicted data.

Table 4.5 Comparative study of the optimum conditions for biodiesel synthesis from mustard oil with different catalysts.

Oil source	Author	Catalyst	Optimum conditions				Conversion (%)
			Time (h)	Temp (ºC)	Alcohol: oil molar ratio	Catalyst (wt %)	
Mustard oil	Ashri et al. [173]	KOH	0.7	60	6:1	1	99.7
	Singh et al. [174]	KOH	1	60	5:1	1	83.2
	Bouaid et al. [175]	KOH	--	25	6:1	1.5	98
	Zapata et al. [176]	NaOH	2	55	6:1	1	91.1
	Jham et al. [177]	NaOH	1.5	60	6:1	0.5	92
	Jazie et al. [178]	Egg shells	3	60	9:1	3	90
	Chakraborty et al. [66]	Duck egg shells	4	70	3:1	3.82	91
	Present work	Flyash bone powder	6	65	5.5:1	9.6	90.4

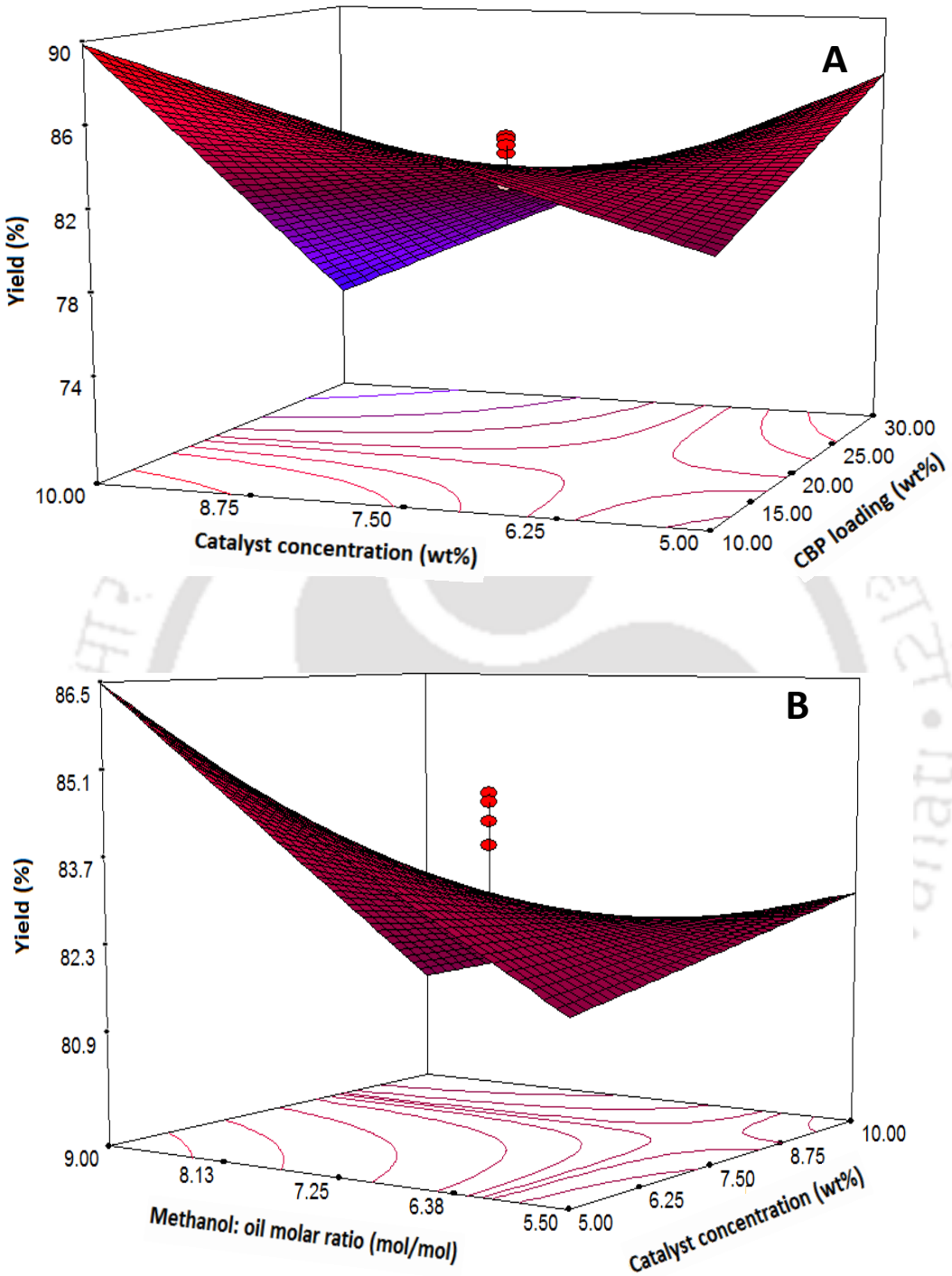

Fig.4.4 3D surface plots of yield (A) effect of CBP loading and catalyst concentration at optimum value of methanol to oil molar ratio, (B) effect of methanol to oil ratio and catalyst concentration at optimum values of bone powder concentration.

The interactions of bone powder loading and catalyst concentration at the optimum value of methanol to oil molar ratio corresponding to biodiesel yield over 6 hours of reaction time is depicted in Fig. 4.4(A). From the figure it is clear that at lower catalyst concentration with increase in bone powder loading the yield of biodiesel increased. This may be due to major resistance offered by surface reaction kinetics at low bone powder loading as the rate of transesterification reaction is proportional to the available concentration on catalyst surface as increase in catalyst concentration would increase biodiesel yield. A decrease in yield was observed at maximum catalyst concentrations with increase in bone powder loading. Low mixing intensities or poor dispersion of reactant phases at high bone powder loading, with increase in catalyst concentration resulting in mass transfer as the major controlling resistance resulting in a reduced biodiesel yield [44, 73].

Fig. 4.4(B) indicates the trends of the effect of catalyst concentration and methanol to oil molar ratio on biodiesel yield at optimim bone powder loading. At lower methanol to oil ratio, with increase in catalyst concentrations yield of biodiesel increased. A similar pattern was observed with simultaneous increase in both methanol to oil ratio and catalyst concentration. At low catalyst concentration, with increase in methanol to oil ratio increased biodiesel yield and this can be attributed as surface kinetics controlling instead of diffusion controlled owing to proper dispersion of catalyst into reactant phases [44, 179].

The optimum conditions for the synthesis of biodiesel by the model equation from design expert software was : bone powder loading (A) of 10%, catalyst concentration (B) 9.6% and methanol to oil molar ratio (C) of 5.5:1 that corresponds to a maximim yield of 90.4%. In order to verify the prediction of the model, experiments at the optimim reaction conditions were conducted in triplicate and the average yield was found to be 87.6%. About

2.8% error was found between experimental and therotical value predicted from RSM. A comparative study of the optimum conditions for biodiesel synthesis from mustard oil with different catalysts is shown in Table 4.5. It is clear from the table that that the prepared flyash based catalyst used in this study provided satisfactory performance with respect to conventional catalyst.

4.3 Catalyst reusability studies

The reusability of the catalyst was studied by performing the transesterification reaction at different cycles. After transesterification, the catalyst was separated from reaction mixture, washed with acetone, methanol and was dried overnight at 110 ^{o}C. At the given optimum conditions as explained in section 3.2, 7 successive runs was performed and the yield was found to be 88.4%, 87.9%. 86.7%, 86.1%, 85.8%, 83.2% and 80.3%. For the first five experimental runs, a marginal decrease in the yield was observed. But the yield of biodiesel decreased by 5.2% and 8.1% after 6 and 7 cycles of reaction. This could be due to blockage of the active sites or hydration of catalyst resulting in the formation of calcium hydroxide that was confirmed from the XRD analysis. From the above it can be conclude that the catalyst can be reused for 5 times without any reduction in its activity. Further activation of catalyst is suggested after 5 successive run.

Chapter 5

Selective Preparation of Zeolite X and A from Flyash and its use as Catalyst for Biodiesel Production

Flyash zeolite;
Alkaline fusion;
Cation exchange capacity;
Transesterification.

Work Published:

Volli V, Purkait MK. Selective preparation of zeolite X and A from flyash and its use as catalyst for biodiesel production. J Haz Mat. 2015;297:101-111.

Bhandari R, **Volli V**, Purkait MK. Preparation and characterization of flyash based mesoporous catalyst for transesterification of soybean oil. J Env Chem Eng. 2015;3:906-914

The main objective of the present study is the selective production of zeolite X and A from flyash. The effect of synthesis condition like NaOH/flyash ratio, temperatures (fusion, calcination and hydrothermal), time (fusion and crystallization) and addition of aluminum source on the formation of final product was studied. Further, effect of acid treatment of flyash on zeolites formation was also studied. The procedure for the production of zeolite was explained in section 2.2.2 and the synthesized zeolite was characterized by XRD, XRF, FESEM, BET, FTIR and CEC. Zeolite X thus obtained was ion-exchanged with potassium source and was used as a catalyst for biodiesel production. Details of results are reported in this chapter.

5.1 Zeolite synthesis and its parametric study

Numerous experiments were performed using different flyash/NaOH ratio, hydrothermal, fusion and flyash calcination temperatures, fusion and crystallization time to determine the optimal conditions for the synthesis of pure zeolites based on degree of crystallinity and CEC of the synthesized product. The Si/Al ratio was strictly controlled by the addition of sodium aluminate (10, 20 and 30%) for avoiding the formation of other zeolitic phase or mixture of them. The effect of variables are discussed in the subsequent sections.

5.1.1 Effect of flyash/NaOH ratio

The XRD pattern of original flyash mainly represents the presence of crystalline quartz (SiO_2) and mullite ($3Al_2O_3{\cdot}2SiO_2$). Besides some crystalline phases (quartz, mullite, hematite etc), ash is primarily composed of amorphous material. The phases in flyash were quartz (SiO_2) with major peaks at 20.86 and 26.65 degrees 2θ (d spacing d_{hkl} of 4.2745 and 3.3508 Å). Less intense peaks were also identified as mullite at 16.42 and 40.82 degrees 2θ (d

spacing d_{hkl} of 5.399 and 2.208 Å) and hematite [180, 181]. The hump at 18 to 35 degree 2θ represents the presence of amorphous glassy phase in flyash.

Zeolite formation in terms of crystallinity and CEC was examined as a function of NaOH concentration. The sodium hydroxide added to flyash not only works as an activator, but also adjusts the sodium content in the starting material. The glass phase on the surface of flyash particles easily dissolves into the alkaline source. Sodium ions are known to stabilize the sub-building units (specially six member ring) of zeolite frameworks and usually are required for zeolite synthesis under hydrothermal conditions. Insufficient concentration of alkali might lead to minimal extraction of alumino-silicates from flyash which adversely affects the crystallization process [91].

The effect of flyash/NaOH (1:1 to 1:2.5) ratio on zeolite formation was studied and XRD patterns were shown in Fig. 5.1(A). At flyash/NaOH ratio of 1, mixture of zeolite X and A was formed. The crystallinity increased with the increase in flyash/NaOH ratio upto 1:1.5. The same was slightly decreased at the ratio of 1:2 with the formation of single phase zeolite X and then decreased rapidly due to the formation of hydroxysodalite (HS) at ratio of 1:2.5. The change in the type of zeolite product could be due to increase in supersaturation with increase in NaOH concentration [182]**.** According to Ostwald's rule of successive transformation, the higher the supersaturation, better the condition to nucleate metastable phases, such as zeolite X, which later recrystallizes and is replaced by highly stable zeolite HS [183]**.** Thus the optimum value of flyash/NaOH ratio was found to be 1:1.2.

5.1.2 Effect of time

The effect of fusion and crystallization time on the formation of resultant zeolites was shown in Fig. 5.1(B) and (C), respectively. Homogeneous fusion mixture of flyash and NaOH

was heated at 550 ^{o}C for 0.5, 1 and 2 hours to study its effect on zeolitization. It was observed that fusion time of 30 min shows no peaks. However, after 1 h zeolite X peaks appears, with a maximum crystallinity occurring after 2 h. From the above it is clear that a fusion time of 1hour is required for the formation of zeolite X. It can be seen from the XRD pattern (Fig. 5.1(C)) that the minimum time required for the complete formation of zeolite is 12 hours. No product was obtained at crystallization time of 4 and 8 hours.

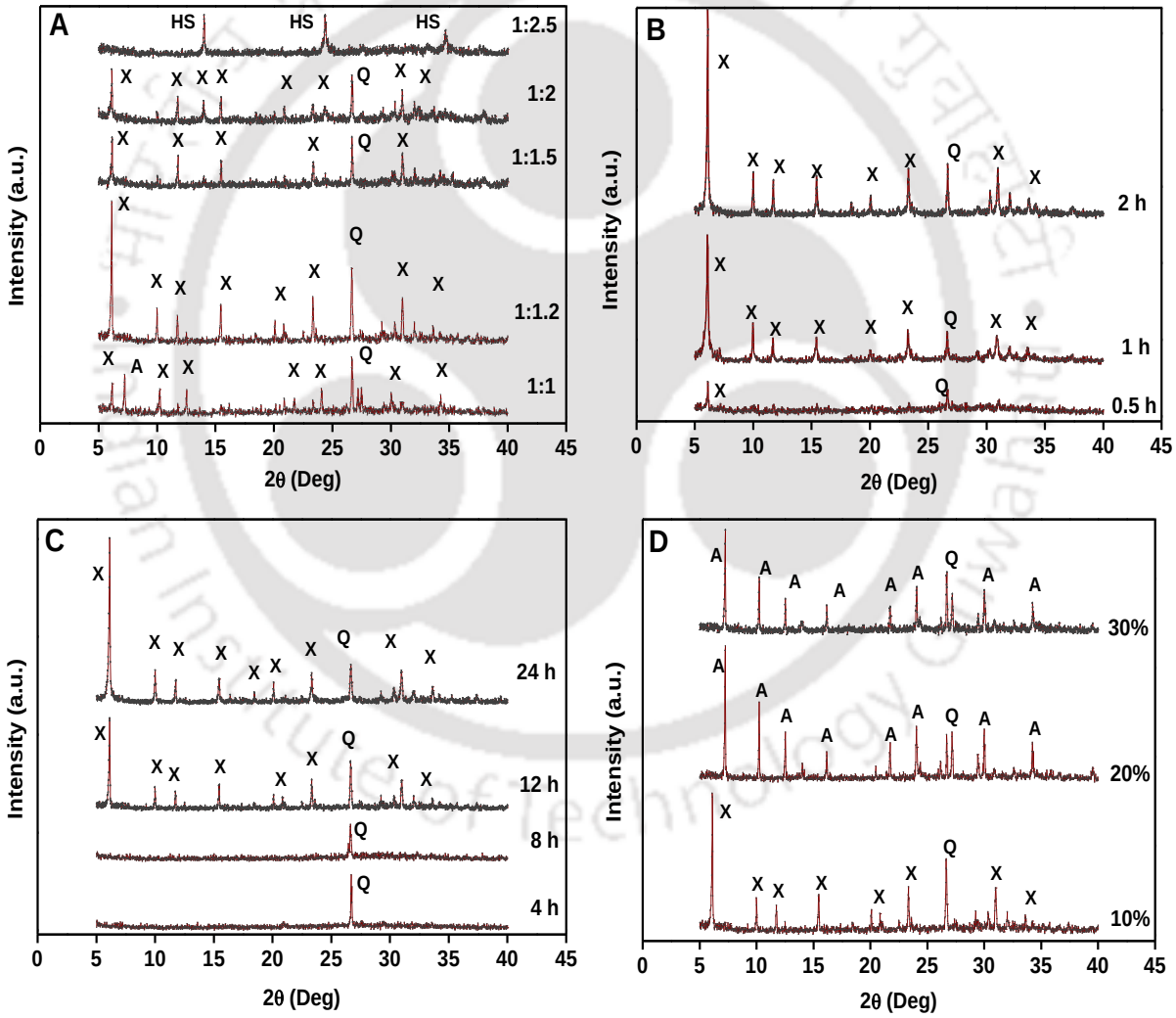

Fig. 5.1 XRD patterns showing the effect of (A) flyash/NaOH ratio, (B) fusion time, (C) crystallization time and (D) sodium aluminate addition on zeolite formation.

5.1.3 Effect of sodium aluminate

The effect of Si/Al ratio, by the addition of sodium aluminate (10-30 wt %) on the type of zeolite formation was studied and Fig. 5.1(D) shows the XRD patterns. Addition of 10% of sodium aluminate resulted in the formation of highly crystalline zeolite X with Si/Al ratio of 1.94. With further increase in amount from 20 to 30%, zeolite A (LTA) was formed with Si/Al ratio of 1.67 and 1.48, respectively. For the flyash used in the present study, it is clear that at Si/Al ratio < 1.8 would result in the formation of zeolite A and Si/Al ratio > 1.8 would result in the formation of zeolite X.

5.1.4 Effect of temperature

The effect of fusion, crystallization and flyash calcination temperatures for a mixture of flyash/ NaOH of 1:1.2 on zeolite formation was studied and the XRD patterns are shown in Fig. 5.2 (A), (B) and (C) respectively. It can be seen from the XRD plot (Fig. 2(A)) that the fusion temperatures of 450 ^{o}C did not result in the formation of single phase zeolite. The minimum fusion temperature required for the complete formation of single phase zeolite is 500 ^{o}C. However, maximum crystallinity of zeolite was obtained at fusion temperature of 550 ^{o}C. Further increase in temperature to 600 ^{o}C did not affect the crystallinity of the material.

From the Fig. 5.2(B) it can be observed that 90 ^{o}C temperature resulted the formation of mixture of zeolite X and A during hydrothermal process. Highly crystalline single phase zeolite X was formed as the temperature was increased from 100 to 120 ^{o}C. The minimum temperature required for the complete crystallization of zeolite was 110 ^{o}C. Above this temperature no significant change in the crystallinity of the product was observed. The formation of zeolite A along with zeolite X was explained by Catalfamo et al. [184]. At the

initial stages of zeolite formation, rate of dissolution of alumina is faster than that of silica and with increase in temperature, dissolution of silica increases. At 90 ^{o}C, Si/Al ratio is low

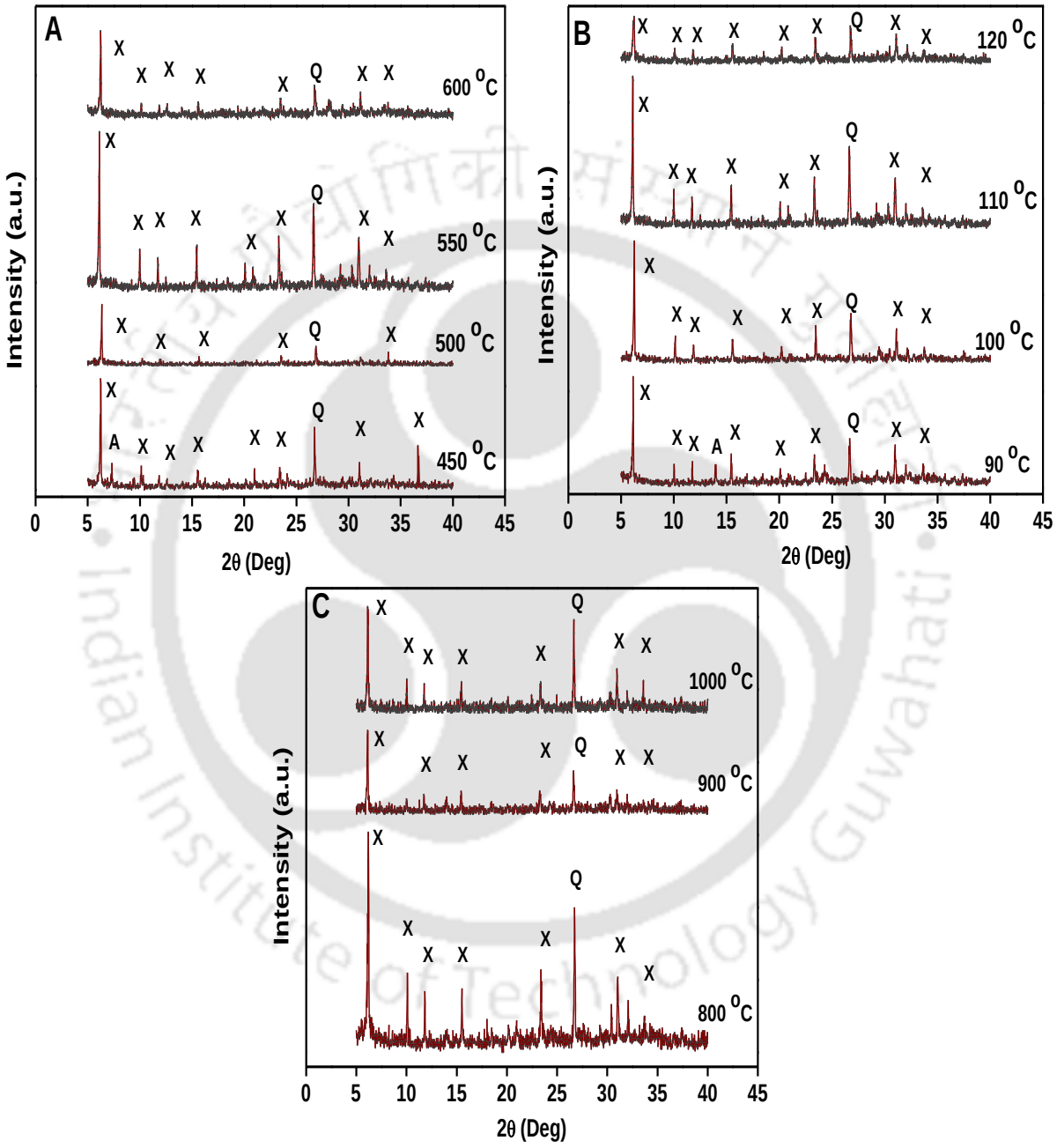

Fig. 5.2 XRD patterns showing the effect of temperature (A) fusion, (B) crystallization, and (C) flyash calcination on zeolite formation.

enough to promote the formation of zeolite A and it can be assumed that at higher temperatures dissolution of silicon increase. Change in Si/Al ratio favors the formation of zeolite X. Most of the literatures indicated that fusion temperature above 500 ^{o}C favors the formation of single phase zeolite. On the contrary Rungsuk et al. [147] reported that fusion temperature at 450 ^{o}C resulted in the formation of zeolite X**.**

The flyash used in the present study was calcined at 800 ^{o}C, 900 ^{o}C and 1000 ^{o}C to study the effect of calcination temperature on zeolite formation (Fig. 5.2(C)). From the figure it is clear that single phase zeolite X was formed at above calcination temperatures. Calcination of flyash at 800 ^{o}C resulted in the formation of highly crystalline zeolite X. It may be envisaged that the optimum value of temperature for fusion, crystallization and calcination are 550 ^{o}C, 110 ^{o}C and 800 ^{o}C, respectively.

5.2 Characterization of modified flyash and synthesized zeolite X and A

5.2.1 Cation exchange capacity (CEC)

The effect of flyash to NaOH ratio, fusion and crystallization time and $NaAlO_2$addition on CEC values of the synthesized zeolite was presented in Figs. 5.3(A, B, C and D), respectively. From Fig. 5.3(A) it is clear that with increase in NaOH concentration in flyash, CEC value increased and was maximum (168.2 meq/100g) at flyash to NaOH ratio of 1:1.2. This was due to the increase of degree of zeolitization with higher NaOH content in the reaction. With further increase in NaOH concentration, CEC values decreased and the product transformed from zeolite X to hydroxysodalite (HS) which was in agreement with the literature [90, 147]. With increase in fusion time from 0.5 to 2 h, CEC value was also increased from 82.6 to 192.3 meq/100 g as shown in Fig. 5.3(B). The effect of crystallization

time on CEC is represented in Fig. 5.3(C). CEC values were found to be increasing with reaction time and reached a maximum value at 12h and decreased thereafter. With an addition of sodium aluminate from 10 to 30%, CEC values increased from 168.2 to 723.4 meq/100 g (Fig. 5.3(D)). It may also be seen that CEC value was initially increased and then decreased with increase in fusion and hydrothermal temperatures.

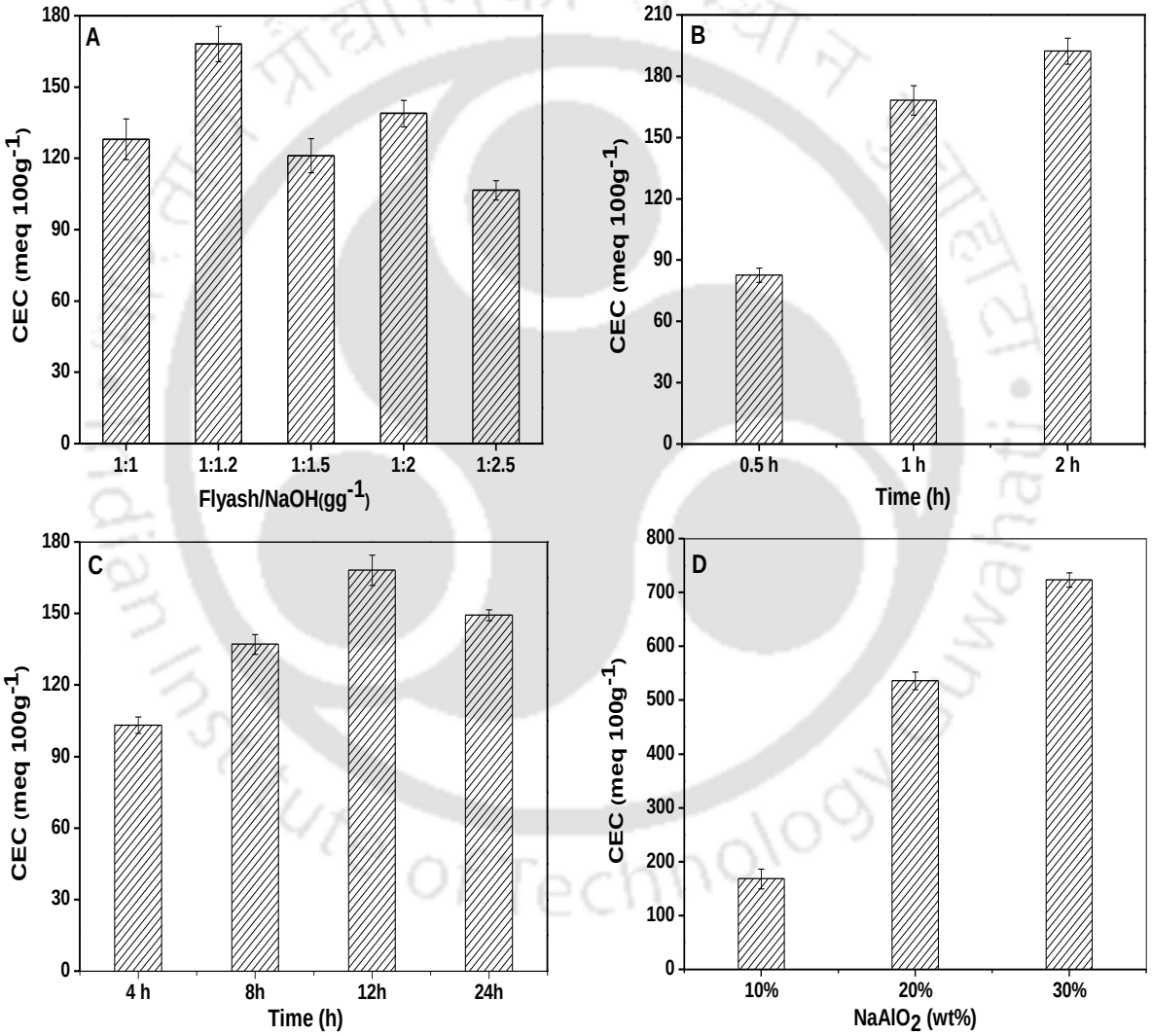

Fig. 5.3 Effect of (A) flyash/NaOH ratio, (B) fusion time, (C) crystallization time, and (D) $NaAlO_2$ addition on CEC

The CEC value was maximum at fusion and hydrothermal temperatures of 550 ^{o}C and 110 ^{o}C, respectively (Fig. 5.4(A and B)). Zeolite X (CZ-X) was synthesized from flyash calcined at different temperatures (800 to 1000 ^{o}C) and its effect on CEC was shown in Fig. 5.4(C). It was found that with increase in calcination temperatures, CEC value decreases. The CEC value of the synthesized uncalcined zeolite X with Si/Al ratio of 1.94 was found to be 168.2 meq/100g. The CEC value increased to 276.5 meq/100g when uncalcined zeolite X was ion-exchanged with potassium. At Si/Al ratio of 2.19, acid treated zeolite X had a CEC of 352.7 meq/100g and the corresponding ion-exchanged zeolite had CEC of 380.6 meq/100g. Zeolite A at Si/Al of 1.67 had the highest CEC of 536.3 meq/100g. Zeolite A is known to be an excellent cation exchanger owing to the higher proportion of aluminum in its framework which dictates the highest CEC.

The chemical composition of flyash, modified flyash and product was analyzed by XRF analysis and the results are tabulated in Table 5.1. From the above it is clear that flyash used in this study accounts for more than 60 to 80% of the glass phase (SiO_2 + Al_2O_3 + Fe_2O_3) and can be classified as class F (according to the ASTM standard C618). The average SiO_2/Al_2O_3 weight ratio of the flyash and acid treated flyash used in this study was found to be 2.44 and 2.75, respectively. Upon acid treatment, the calcium oxide content decreased from 7.93 wt % in the raw flyash to 1.57 wt % causing an increased portion of all other oxides, especially SiO_2. The decreased CaO content in the HCl treated flyash was due to the neutralization between HCl and CaO causing dissolution of CaO [185]. The acid treatment helped to dealuminate the flyash and remove iron to a certain extent, thereby increasing the activity, thermal stability and acidity of the zeolite, all aiming for better catalytic applications [186].

Table 5.1 Chemical composition of flyash, acid treated flyash, UZ-X, CZ-X, AZ-X and zeolite A

Component	Flyash		Zeolite			
	Raw	Acid treated	UZ - X	CZ - X	AZ- X	Zeolite-A
CaO	7.93	1.57	3.52	4.49	0.36	3.49
Fe_2O_3	5.89	2.41	5.02	3.51	2.21	5.71
K_2O	1.39	0.82	0.69	0.75	1.29	0.65
MnO	0.05	0.04	0.04	0.05	0.03	0.04
P_2O_5	0.27	0.17	0.05	0.07	0.09	0.04
SO_3	0.53	0.01	0.02	0.01	0.01	0.02
SrO	0.06	0.02	0.08	0.08	0.07	0.08
TiO_2	1.35	1.1	1.05	1.21	1.25	1.07
Al_2O_3	23.21	22.88	18.64	22.64	21.74	23.09
MgO	1.53	0.10	0.40	0.59	0.55	0.19
SiO_2	56.61	62.94	36.12	44.34	47.63	38.55
Na_2O	0.28	0.58	32.48	18.21	18.48	26.12
SiO_2 / Al_2O_4	2.44	2.75	1.94	1.96	2.19	1.67

The formation of a particular zeolite species depends on the Si/Al ratio in the raw material. Change of this ratio may result in a change of the final structure obtained and may also lead to the crystallization of unwanted phases [187]. The synthesized uncalcined, calcined, acid treated zeolite X and A had Si/Al ratio of 1.94, 1.96, 2.19 and 1.67 respectively.

It was observed that lower Si/Al ratios favors formation of zeolite A and Si/Al ratio of 2 results in the formation of zeolite X. Zeolite synthesized from acid treated flyash had lower CaO content.

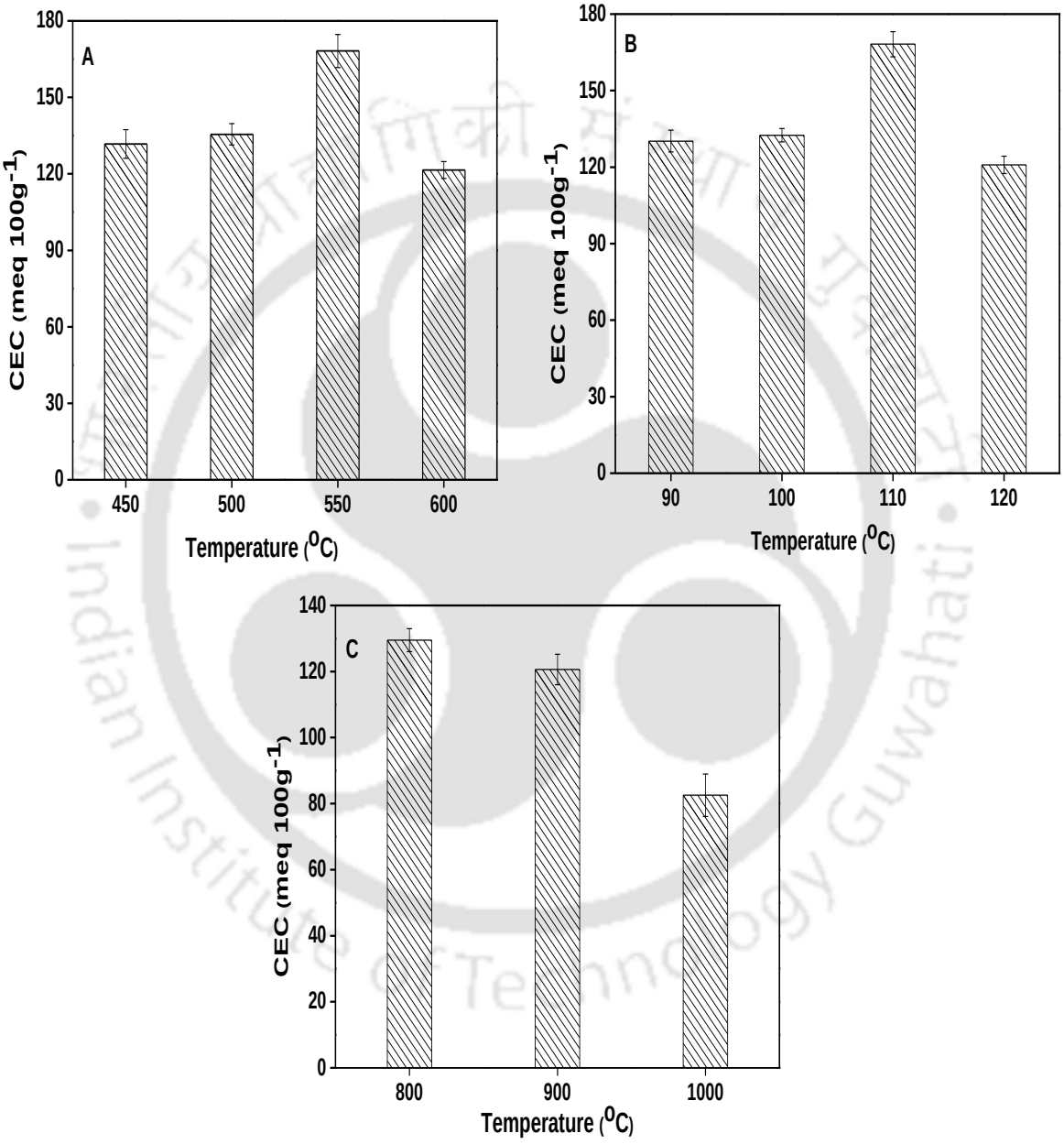

Fig. 5.4 Effect of CEC on (A) fusion, (B) crystallization, and (C) flyash calcination temperatures on zeolite formation.

5.2.2 Surface area and pore analysis by nitrogen adsorption measurements

The BET surface area of flyash, UZ-X, AZ-X and zeolite A was determined to be 1.7, 164.9, 167.4 and 24.1 m^2/g with total pore volume of 0.03, 0.24,0.25, and 0.11 cc/g respectively. Zeolite X obtained from coal flyash has much higher specific surface area than zeolite A and flyash. The surface area of ion-exchanged UZ-KX and AZ-KX were found to be 323.7and 334.7 m^2g^{-1} with total pore volume 0.29, 0.312, cc g^{-1} and shown in Fig. 5.5(A). According to IUPAC classification all the samples showed type II isotherm. In the case of isotherm of zeolite A and zeolite X (type II isotherms), it can be observed that adsorption increases more at relatively low pressure than in original flyash sample. This proves that samples contain certain number of micropores in relation to original flyash. Hysteresis loops for zeolites can be classified similarly to flyash as H3, which indicates uniform size slit pores in parallel plates.

5.2.3 Structural analysis of the synthesized zeolites

The IR spectra of uncalcined zeolite X (UZ-X), uncalcined zeolite KX (UZ-KX), acid treated zeolite X (AZ-X), acid treated zeolite K-X (AZ-KX) and zeolite A was illustrated in Fig. 5.5(B). The characteristic IR vibration band at 1467 cm^{-1} represents asymmetric stretching of Si/Al – O. The main asymmetric stretching of Si – O – Si was at 982 cm^{-1}. Symmetric stretching of Si – O – Si occurs at 756 and 675 cm^{-1}. The band at 560 cm^{-1} is associated with the double 6 rings that connect the sodalite cages.

5.2.4 TPR studies of zeolite

The reduction profiles of UZ-X, UZ-KX, AZ-X and AZ-KX zeolite was given in Fig. 5.5(C). From the figure it is clear that the reduction of uncalcined X zeolite started at a

temperature of 378 ^{o}C. A clear shift in the value to about 467 ^{o}C was observed for ion-exchanged uncalcined KX zeolite. Acid treated X and KX zeolite had almost the same reduction temperature of uncalcined KX zeolite. Shift in the temperatures at 680 ^{o}C to 750 ^{o}C was observed when acid treated zeolite X was ion-exchanged with KX.

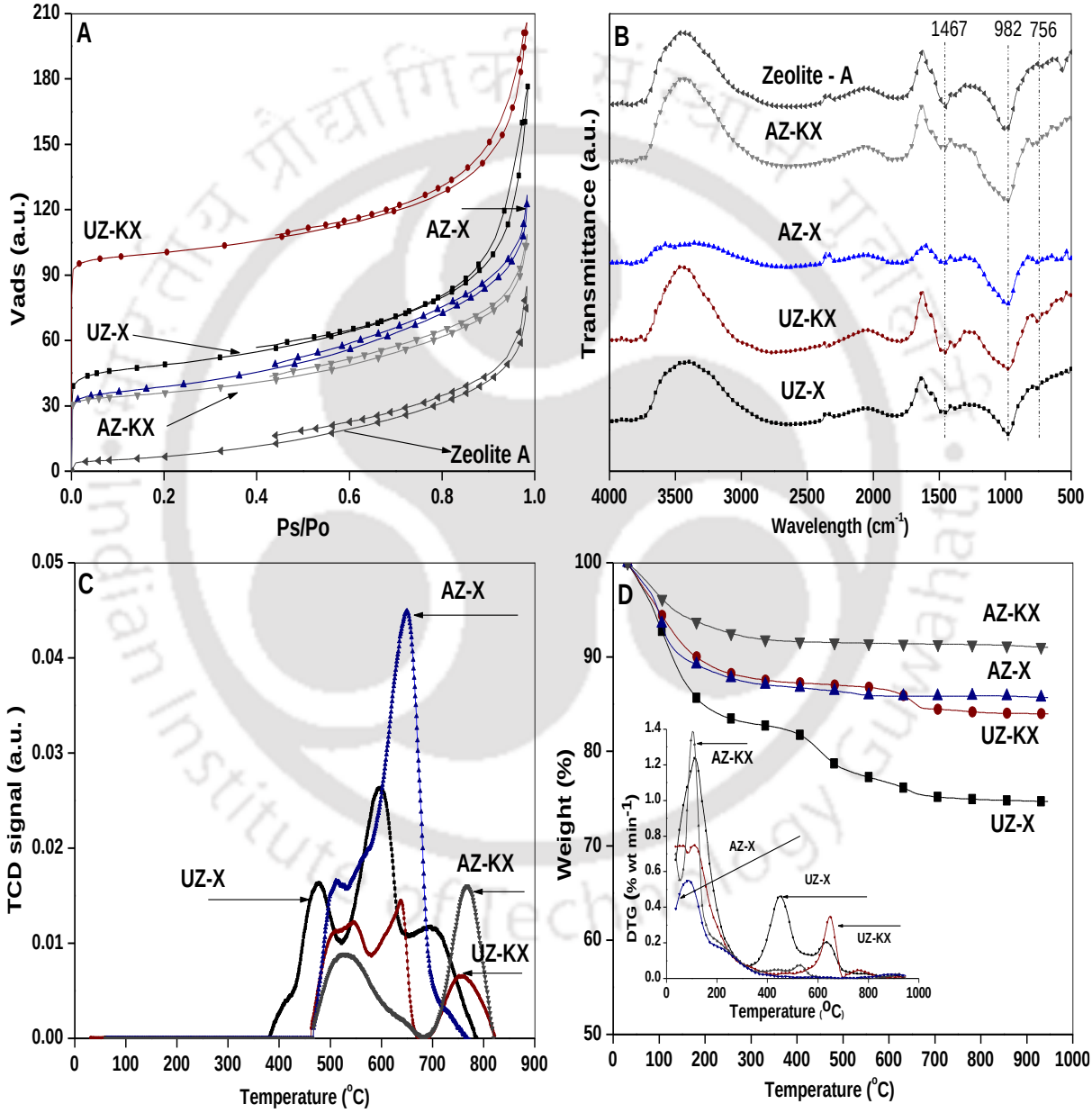

Fig. 5.5 (A)Nitrogen adsorption–desorption isotherms, (B) FTIR spectra, (C) TPR, (D)TGA and DTG curves of UZ-X,UZ-KX, AZ-X, AZ-KX and zeolite A.

5.2.5 TGA analysis

The thermal stability of the synthesized zeolite was determined through weight loss at 950 ^{o}C and shown in Fig. 5.5(D) for TGA and DTG curves. A weight loss of 26%, 17%, 15% and 9% was observed for UZ-X, UZ-KX, AZ-X and AZ-KX zeolites, respectively. Initial weight loss was due to the removal of physisorbed and occluded water within 95 to 110 ^{o}C. A major decomposition of material was observed at 453 ^{o}C with partial weight loss at 636 ^{o}C for UZ-X. Ion exchange of zeolite resulted in shift of temperature of this major degradation to 647 ^{o}C. A partial weight loss was observed at 531 ^{o}C after which the degradation curve becomes almost flat for acid treated zeolite. No further weight loss was observed with increase in temperature indicating complete destruction of crystalline lattice of zeolite [97].

5.2.6 Morphological analysis

The surface morphology of flyash is shown in Fig. 6(A). Flyash particles are primarily spherical in shape with a relatively smooth surface texture and a wide particle size range. In some cases smaller particles are attached to the surface of larger particles, serving as substrates. The spherical particles are either solid or hollow (Cenospheres).The FESEM images of UZ- X **(B)**, AZ- X **(C)** and AZ- KX **(D)** revealed the typical octahedral crystals of zeolite X. The structure of ion-exchanged zeolite remained same and similar kind of observation was reported by Babajide et al. [45]. The FESEM image of the surface of the synthesized zeolites revealed a clear transformation of the spherical particles of the flyash **(A)** into cubic crystalline structures which is a characteristic of zeolite A **(E)**. However, these cubes had smooth edges and were covered with unconverted amorphous materials.

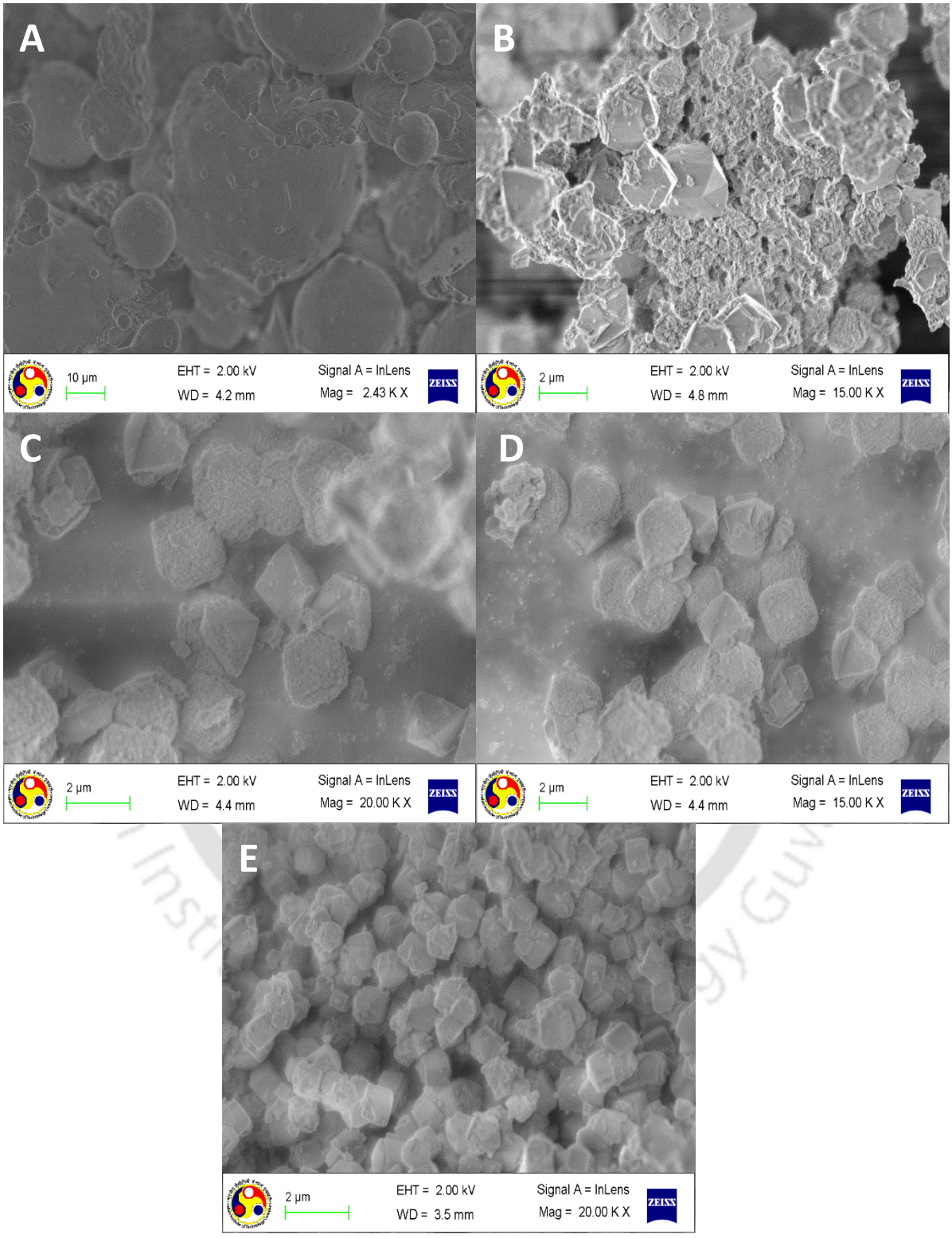

Fig. 5.6 Surface morphology of (A) flyash, (B) UZ -X, (C) AZ-X, (D) AZ-KX and (E) zeolite A.

5.3 Catalytic activity in transesterification process

The catalysts UZ-X, UZ-KX, AZ-X and AZ-KX were selected for transesterification of mustard oil because of their high surface area when compared to zeolite A. Samples were collected after 1 h interval using catalyst load of 3 wt %, methanol/oil molar ratio of 6:1 and reaction temperature of 65 ^{o}C with all experiments done in triplicate. The order of conversion after 7 h of reaction was AZ-KX (72.2%) <UZ-KX (65.7%) < AZ-X (53.7%) < UZ-X (41.9 %). Interestingly, acid treated ion-exchanged zeolite showed more conversion compared to other zeolites (Fig. 5.7(A)). This could be due to the increase in base strength of ion-exchanged zeolite when modified with materials containing more electropositive nature (K^{+}) from parent zeolites [45, 188].

Based on conversion, zeolite AZ-KX was considered further to optimize methanol/oil molar ratio keeping other reaction conditions constant. As per stoichiometry, 3 moles of methanol is required for every mole of oil but commonly excess methanol is used inorder to shift reaction equilibrium towards biodiesel formation. From Fig. 5.7(B) it is clear that when methanol/oil molar ratio was increased from 6:1 to 18:1, a maximum conversion of 79.8% was obtained at methanol/oil molar ratio of 12:1, beyond which addition of methanol did not show any significant increase in conversion. The presence of excess methanol helps in dissolution of glycerol which would constrain the reaction of methanol in oil as well increasing the difficulty in separating biodiesel [103]. A methanol/oil molar ratio of 12:1 was found to be optimum for the present study.

The effect of catalyst concentration (3, 5, 7 and 10 wt %) on conversions of biodiesel was shown in Fig. 5.7(C). From the figure it is clear that with increase in catalyst concentration (5 wt %), biodiesel conversion increased to 84.6% and remained almost same

with further increase in catalyst concentration which could be due to mixing (mass transfer) resistance concerning solid catalyst, oil and product. At low catalyst concentrations, deficient amounts of catalyst might have resulted in lower conversions [12]. The yields were in agreement with the literature explained in Table 5.2.

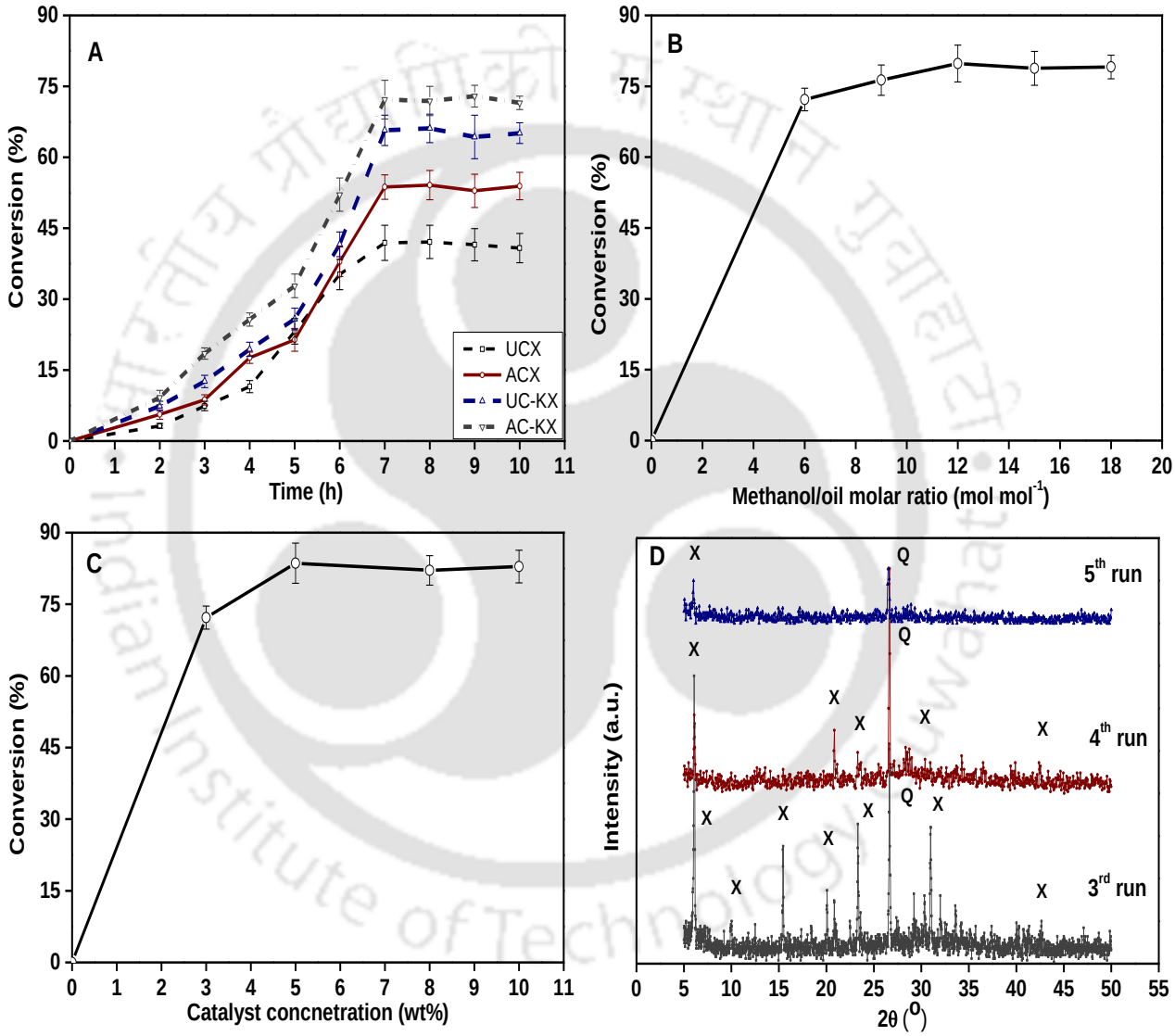

Fig. 5.7 Effect of (A) time, (B) methanol: oil molar ratio, (C) catalyst concentration on biodiesel conversion and (D) XRD spectra for catalyst reusability studies.

.

Table 5.2 Comparison of % yield of methyl ester with some reported zeolite based catalysts.

Author	Raw material	Oil	Time (h)	Temperature (ºC)	Catalyst con. (wt %)	Meth/oil molar ratio (wt %/wt %)	Conversion (%)
Present study	Flyash zeolite - X	Mustard	7	65	5	12:1	84.6
Singh et al. [189]	(TPA) suppoterd MCM-48	Jatropha	16	65	6	8:1	93
Sanchez et al.[190]	K, Ca, Na, Li, Ba - γAl_2O_3	Soybean	4	60	6	7.28:1	90
Suppes et al. [46]	Na-X, ETS-10 zeolite and metal catalysts.	Soybean	24	120, 150	0.03g	6:1	90
Feyzi et al. [191]	Strontium nano catalysts supported on the ZSM-5	Sunflower	4	60	3	9:1	87.7
Shu et al. [192]	La/zeolite beta	Soybean	4	60	0.011(mass ratio)	14.5:1	48.9
Intarapong et al. [101]	KOH/Na-Y zeolite	Palm	7	60	15	--	92.1
SathyaSelvabala et al.[193]	Phosphoric acid modified β-zeolite	Tamanu	1	60	1	9:1	93

5.4 Catalyst reusability studies

The spent catalyst was separated from the reaction mixture by centrifugation, washed with methanol and filtered to remove impurities (if any). It was then calcined at 300 ^{o}C for two h and was used for next run. In reusability studies, transesterification was carried out at optimum conditions (reaction time: 7 h, catalyst loading: 5 wt % and methanol/oil molar ratio: 12:1). For the first 3 runs, a small decrease in conversions 82.8%, 80.4% and 78.1%, respectively was observed. The blockage of active sites by adsorption of intermediates and products could be the possible reason. With further use of catalyst for 4th and 5th runs resulted in the significant deactivation of the catalyst that can be confirmed from XRD patterns Fig. 5.7(D). In spite of its heterogeneity, the above catalyst can be reused upto three times with a marginal decrease in its activity for transesterification.

Chapter 6

Preparation and Characterization of Hydrotalcite with Bifunctional Properties from Flyash for Transesterification.

Flyash hydrotalcite;
Transesterification;
Basicity;
Mg: Al ratio.

Work under review:

Volli V, Purkait MK. Preparation and characterization of hydrotalcite with bifunctional properties from flyash and use as heterogeneous catalyst. Clean Technol Environ Policy

In this study, flyash and flyash zeolite based Mg-Al hydrotalcite with different Mg/Al ratios were synthesized (explained is section 2.2.3) and their activity was estimated in transesterification of mustard oil with methanol. The synthesized catalyst was characterized (i.e. morphology, physico-chemical and phase identification) by using FESEM, FTIR, XRD, BET, XRF, TGA and TPR. Effects of the catalyst loading, molar ratio of methanol to oil, and reaction time on the catalyst activity were investigated to optimize transesterification conditions. All the results are reported in the subsequent sections of this chapter.

6.1 Characterization of synthesized catalyst

6.1.1 Compositional and structural analysis

The chemical composition of the synthesized catalyst was analyzed in order to assess the effective incorporation of Mg and Al in the synthesized hydrotalcite. The Mg/Al weight ratio of flyash and flyash zeolite was 0.07 and 0.02 as shown in Table 6.1. The synthesized catalyst C-HT, FZ-HT and F-HT had Mg/Al ratio of 2.3, 1.75 and 1.3, respectively, showing a significant increase in Mg/Al ratio in the product. This could be due to the higher pH used in the synthesis of the catalyst. The solubility of $Mg(OH)_2$ increases when compared to $Al(OH)_3$ resulting in greater incorporation of Mg in hydrotalcite layers [118].

The XRD pattern of the synthesized catalysts is shown in Fig. 6.1(A) and is found to be consistent with hydrotalcite materials. A series of reflections at 11.8°, 23.4°, 35.8°, 39.6°, 47.1°, 61.18° and 62.48° 2θ were observed for C-HT. The calcination of C-HT at 500 °C resulted in the appearance of peaks at 42.9° and 62.3° corresponds to MgO (periclase) and a broad peak at 35.1° represents the presence of amorphous alumina [115]. This could be due to destruction in lamellar structure of hydrotalcite. The catalysts F-HT and FZ-HT attained the

similar structure as C-HT and is evident from Fig 6.1(A). Similar peaks at 11.8°, 23.4°, 35.8° and 39.6° was observed in both F-HT and FZ-HT which corresponds to (0 0 3), (0 0 6), (0 1 2) and (0 1 5), respectively [194, 195]. When calcined C-HT was re-hydrated, the catalyst attained the similar structure confirming the recovery of original lamellar structure [116].

Table 6.1 Mineral composition of flyash, flyash zeolite, FZ-HT, C-HT and F-HT

Component	Flyash		Catalyst		
	Raw	Zeolite	FZ-HT	C-HT	F-HT
Al_2O_3	23.21	23.13	23.71	25.70	23.11
MgO	1.53	0.50	41.46	57.56	30.02
SiO_2	56.61	36.12	35.84	--	43.09
Na_2O	0.28	22.71	17.28	4.40	6.20
Fe_2O_3	5.89	2.4	2.09	--	5.4
CaO	7.93	0.69	0.23	--	0.38
MnO	0.05	0.04	0.03	--	0.03
P_2O_5	0.27	0.05	0.13	--	0.03
Mg/Al	0.07	0.02	1.75	2.38	1.30

6.1.2 FTIR and basicity

To assess the presence of both Bronsted and Lewis acid sites in the synthesized catalyst, the samples were saturated with pyridine vapor for 2 h, vacuum dried at 200 °C for 1 h to remove the excess pyridine and the analyzed FTIR spectra is shown in Fig. 6.1(B). A broad band at 3455 cm^{-1} represents the presence of -OH stretching vibrations (water) bonded to octahedral layers [114]. The presence of Bronsted acid sites was observed at 1620 cm^{-1} which could be due to Mg-OH-Al bonds. A sharp peak at 1455 cm^{-1} represents the presence of Al-OH group confirming the presence of Lewis acid site in the catalysts. Peak at 1360 cm^{-1}

represents the presence of carbonates in the materials. The bands at 763 and 672 cm^{-1} represents Mg-OH translation mode [113, 195].

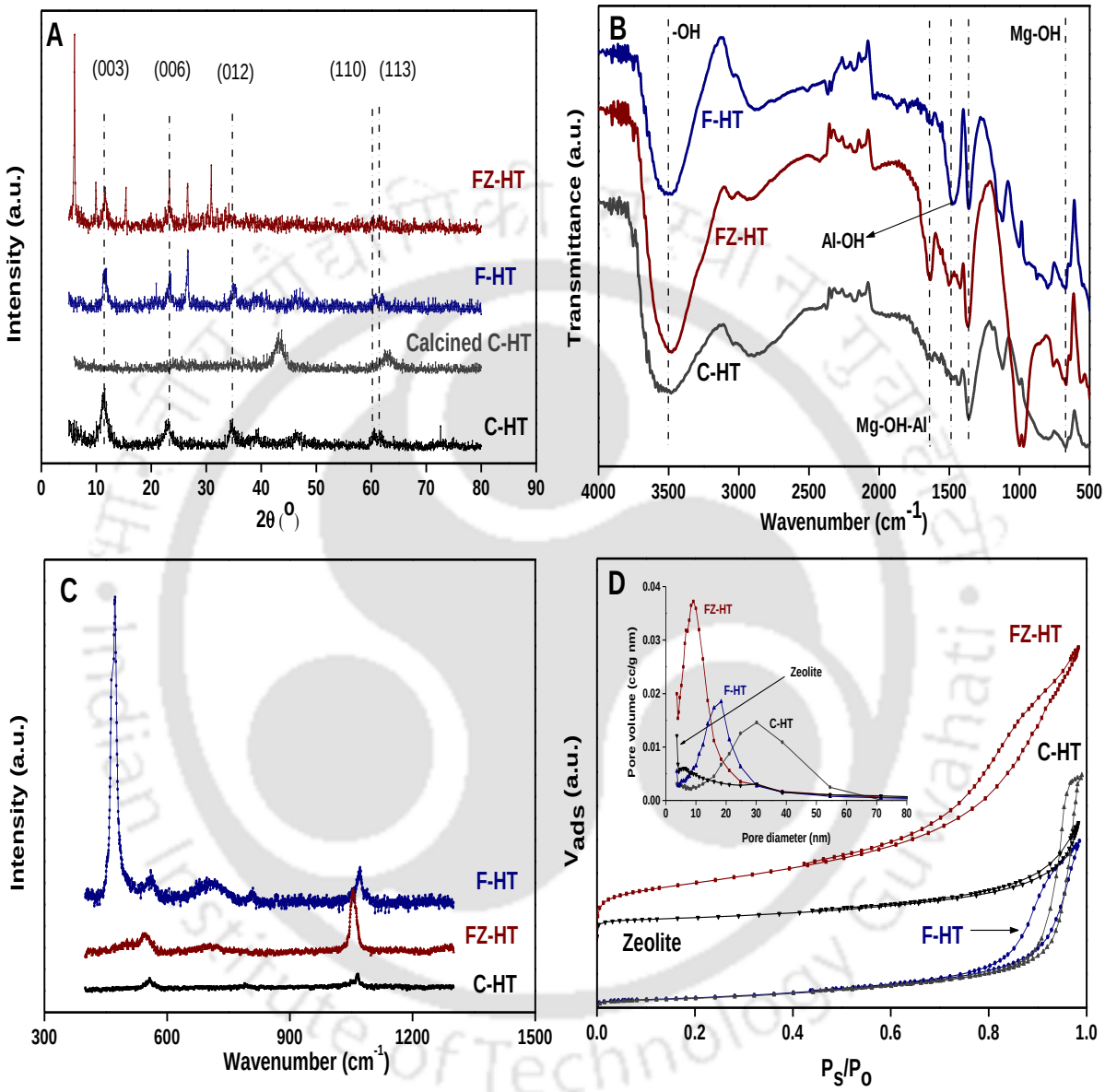

Fig. 6.1 (A) XRD patterns, (B) FTIR, (C) Raman spectra and (D) Nitrogen adsorption–desorption isotherms of C-HT, F-HT FZ-HT and Zeolite.

The basicity of catalyst depicts the acidity of the conjugate acid and was determined by titration method [145]. Basicity of zeolite used in the present study was 17.1 mmol of HCl g^{-1}. The synthesized hydrotalcites FZ-HT, C-HT and F-HT had the basicity of 36.6, 28.8 and

12.4 mmol of HCl g^{-1}. The increase in basicity of the catalyst was due to increase in MgO and Na_2O concentration in the synthesized catalyst. In general, calcined hydrotalcite consists surface sites of low (OH^- groups), medium (Mg-O pairs), and strong (O^{2-} anions) which is responsible for their basicity [196]. Singh et al. [145] reported the similar kind of observation for MgO, ZnO, and Pb_3O_4 *as 46.05, 32.3 and 14.5* mmoles of HCl g^{-1}. The presence of both acidic and basic properties makes the above synthesized catalyst bifunctional.

6.1.3 Raman analysis

The synthesized catalysts were further characterized by Raman spectroscopy and are shown in Fig. 6.1(C). Presence of Mg-OH and Al-OH translations were observed at 472 and 534 cm^{-1}, respectively in all the catalysts. A band at 1058 cm^{-1} represents the presence of $(MgAl)_3$-OH deformation in FZ-HT. Band at 1075 cm^{-1} signifies the formation of spinel $MgAl_2O_4$. Presence of a broad band at 716 cm^{-1} represents in-plane bending of carbonate ions [30,197]. Kloprogge et al [198] reported that bands at 1052 and 553 cm^{-1} represents M-OH translation and deformation mode of hydroxide layers and due to reorganization of interlayer staking they decrease intensely when heated.

6.1.4 Surface area analysis

Flyash and flyash zeolite (mesoporous) used in the present study had a surface area of 1.7 and 323.2 m^2 g^{-1} representing type III and type II isotherms with total pore volume of 0.037 and 0.29 cc g^{-1}, respectively. The nitrogen adsorption-desorption isotherms of the synthesized catalysts represents type IV isotherm with H1 hysteresis loop which is a characteristic of mesoporous materials with well-defined cylindrical pore channels as shown in Fig. 6.1(D). The surface area of 32.9, 39.6 and 476.6 m^2 g^{-1} with total pore volume 0.33,

0.27 and 0.61 cc g^{-1} was obtained for C-HT, F-HT and FZ-HT. The BJH pore size distribution was in the range of 10 - 60 nm indicate that the synthesized catalyst is mesoporous.

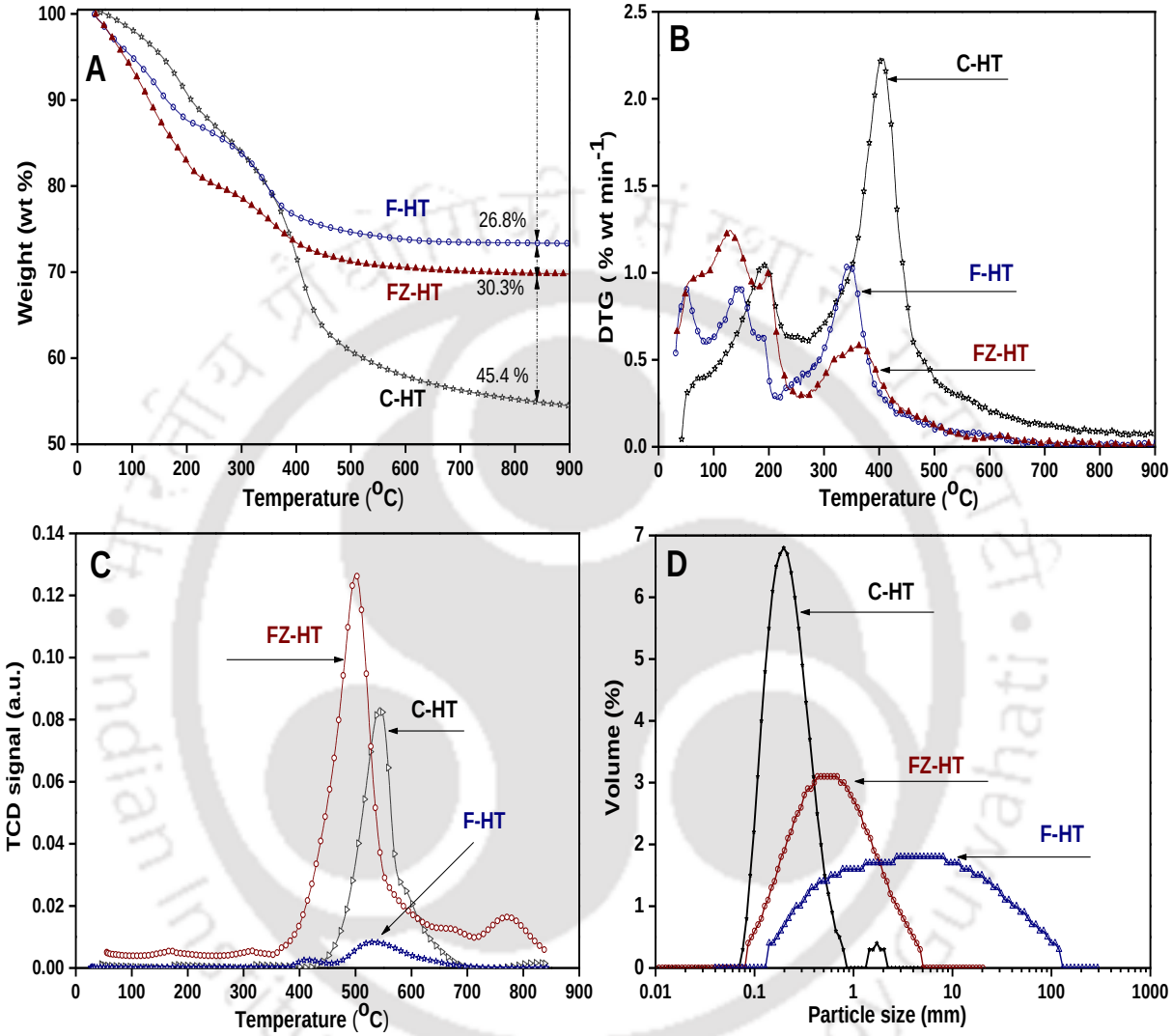

Fig. 6.2 (A) TGA (B) DTG, (C) H2-TPR curves and (D) particle size distribution of C-HT, F-HT and FZ-HT.

A significant increase in surface area and total pore volume was observed in the conversion of flyash and flyash zeolite to F-HT and FZ-HT. This could be due to the fact that, the collapse and elimination of interlayer CO_3^{2-} ions after calcination results in the transformation of hydrotalcite to mixed oxides with three-dimensional texture and porous channels [199].

6.1.5 Thermal stability

The thermogravimetric (TGA) and derivative mass loss (DTG) curves of the synthesized catalysts before calcination was shown in Fig. 6.2 (A, B), respectively. Two major mass loss steps corresponding to two major peaks in DTG curves with a total mass loss of 45.4, 26.8 and 30.3 wt % was observed for C-HT, F-HT and FZ-HT, respectively. The first sharp peaks at 190, 143 and 127 ^{o}C was observed over a temperature range of 25 to 265 ^{o}C for C-HT, F-HT and FZ-HT, respectively with an average mass loss of 12.3 wt % in the first stage. This could be due to loss of inter layer water [200]. The second stage of decomposition which could be attributed to dehydroxylation and decarboxynation (loss of interlayer anions), occurred over a temperature range of 270 to 650 ^{o}C. Sharp peaks at 404, 338 and 364 ^{o}C with mass loss of 31, 12 and 13 wt % was observed in the second stage for C-HT, F-HT and FZ-HT, respectively [201, 202].

6.1.6 Chemisorption

The reducibility of the synthesized catalyst was measured using H_2 -TPR as shown in Fig. 6.2(C). From the figure it is clear that reduction of C-HT and F-HT occurred over a temperature range of 418 to 665 ^{o}C with maximum reduction temperatures at 529 and 544 ^{o}C, respectively. FZ-HT had slightly lower reduction temperature range between 343 to 710 ^{o}C with maximum reduction temperature at 505 ^{o}C showing that it reduces more readily when compared to F-HT and C-HT. Hosoglu et al [203] studied the reduction profiles of calcined hydrotalcite and reported the range of temperature reduction as 300 to 450 ^{o}C.

6.1.7 Particle size distribution

The particle size distribution (PSD) and average particle size of the synthesized catalyst was shown in Fig. 6.2(D). PSD for C-HT and FZ-HT was in the range of 0.07 to 4

μm with average particle size of 0.35 and 0.93 μm, respectively. The PSD for F-HT was found to be slightly higher when compared to C-HT and FZ-HT which is in the range of 0.2 to 110 μm with average particle size at 6 μm. The PSD of flyash used in the present study was in the range of 10 to 100 μm with average particle size at 14 μm. Xu et al. [204] reported that the particle size of Mg/Al hydrotalcite 0.04 to 0.4 μm with average particle size of 0.47 μm. Oh et al. [205] synthesized Mg/Al hydrotalcite with range of particle size as 0.9 to 4.5 μm.

6.1.8 Surface morphology

The surface morphology of synthesized catalysts, flyash and flyash zeolite is shown in Fig. 6.3. The flyash (A) used in the present study were Cenospheres or in some cases smaller particles attached to the surface of larger particles. Flyash zeolite (B) were octahedral crystals covered with unconverted amorphous materials. The synthesized hydrotalcite C-HT (E) has platelet like morphology. The formation of platelet like structure of hydrotalcite on surface of flyash and flyash zeolite particles was observed for F-HT (C) and FZ-HT (D).

6.2 Catalytic activity

The transesterification of mustard oil was carried out using the synthesized catalyst to study their catalytic activity. All the experiments were performed at 65 ^{o}C with methanol to oil molar ratio varying from 3:1 to 18:1 at 5 wt % catalyst concentration for 8 h to estimate the minimum time required to achieve maximum biodiesel conversion.

The effect of reaction time on conversion of biodiesel for C-HT, F-HT and FZ-HT was shown in Fig. 6.4(A). From the figure it is clear that conversion of mustard oil to biodiesel increased gradually up to 6 h and reached plateau thereafter for all the catalysts. With further increase in time, no significant increase in biodiesel conversion was observed.

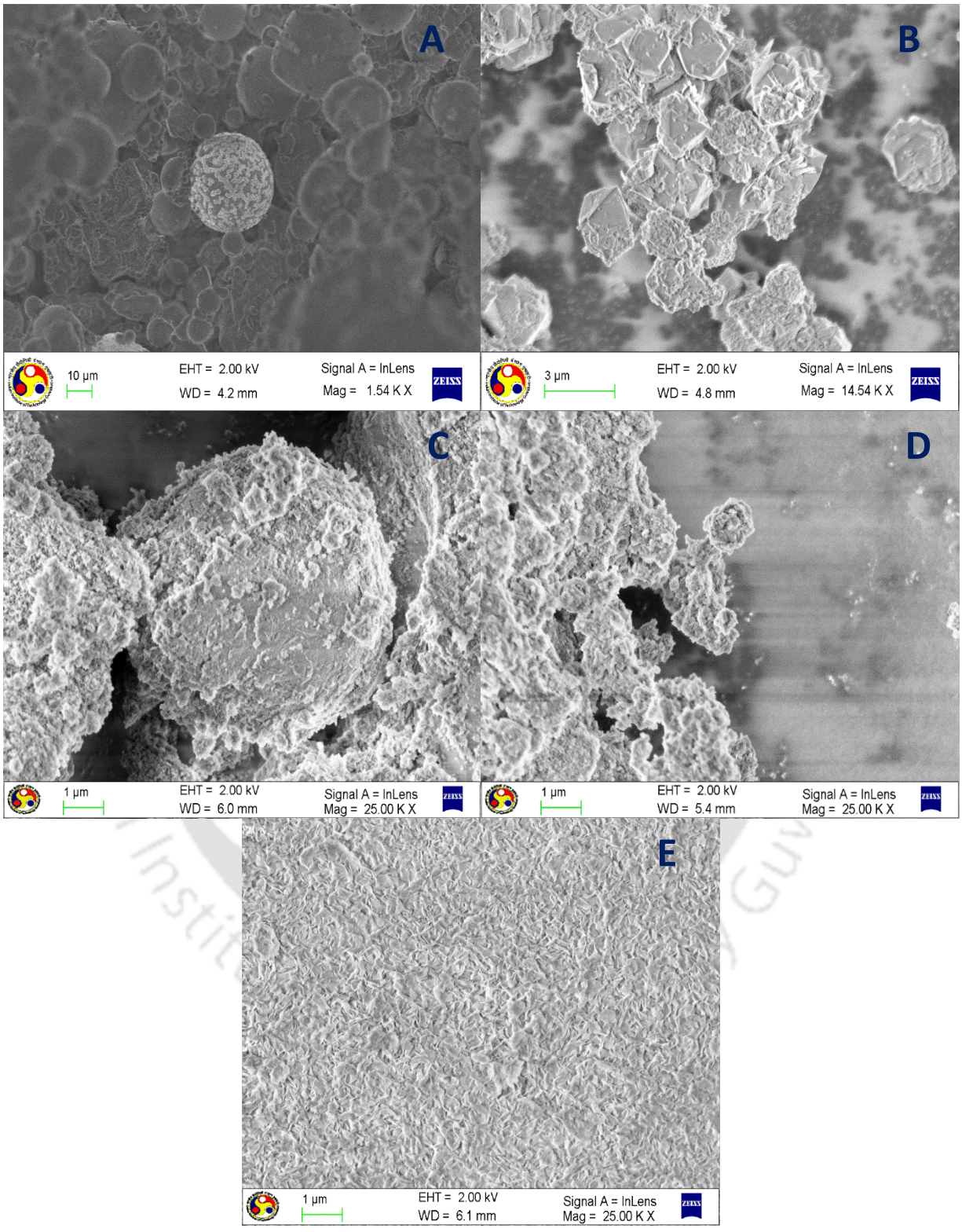

Fig. 6.3 Surface morphology of (A) flyash, (B) flyash zeolite, (C) F-HT, (D) FZ-HT and (E) C-HT

The order of conversion for 6 h of reaction was FZ-HT (86.4%), C-HT (81.2%) and F-HT (64.8%). Catalyst FZ- HT achieved higher conversion when compared to C-HT and F-HT. Thus 6 h was considered as optimum reaction time for biodiesel conversion.

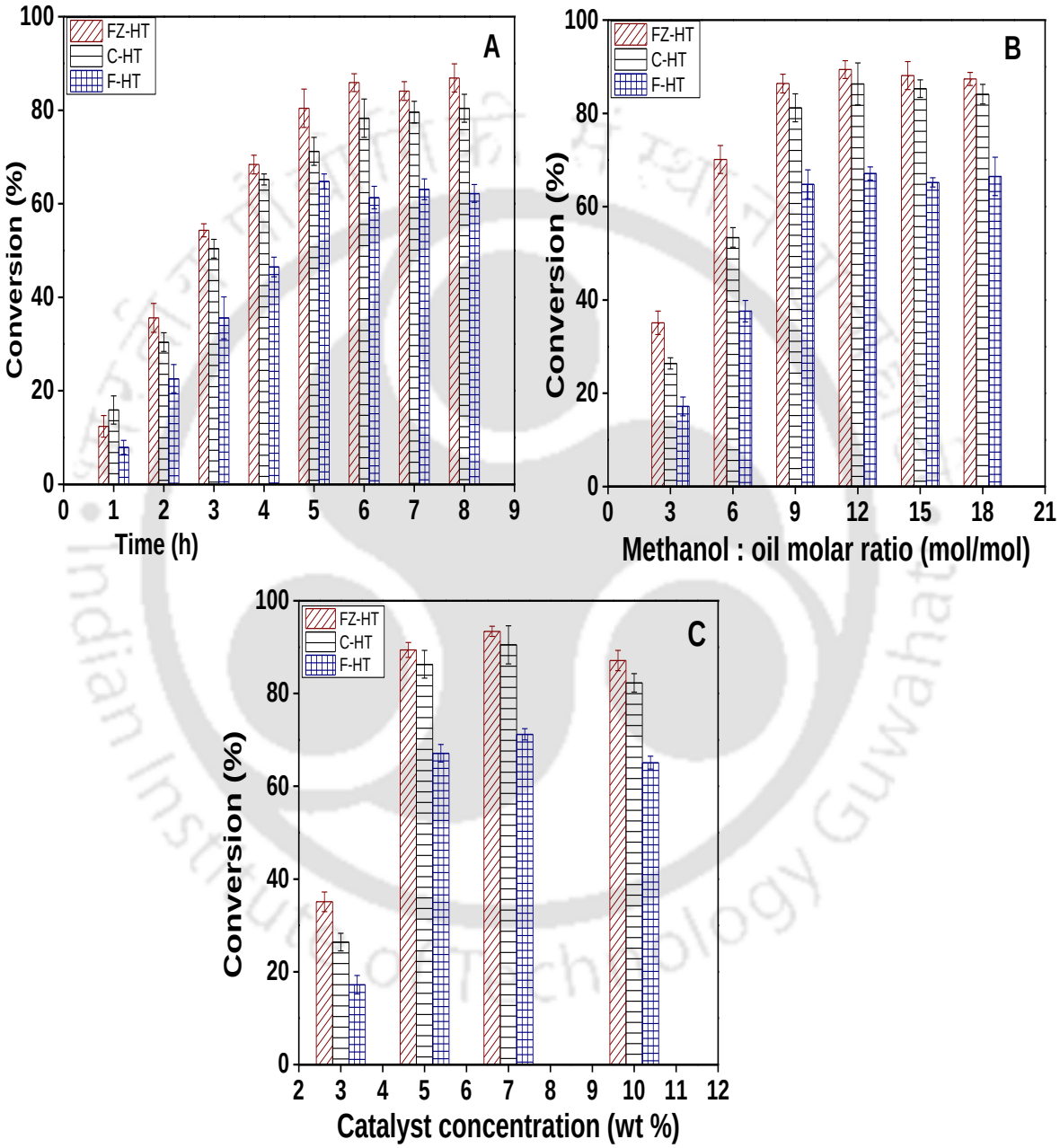

Fig. 6.4 Plots showing the effect of (A) time, (B) methanol: oil molar ratio and (C) catalyst concentration on FZ-HT, C-HT and F-HT.

Table 6.2 Comparison of present study with literature.

Catalyst	Ratio (Mg/Al)	Oil	Optimum Conditions				Conversion (%)	Author
			Time (h)	Temp. (°C)	Methanol /oil (wt %/wt %)	Cat. Con (wt %)		
Mg-Al HT	3:01	Jatropha	1.5	45	4:1	1	95.2	Deng et al. [112]
Mg-Al HT	2:01	Soybean	4	65	12:1	2.5	97.1	Gomes et al. [113]
Mg-Al HT	3:01	Soybean	9	65	15:1	7.5	67	Xie et al. [114]
1.5% K/Mg-Al HT	2.4:1	Palm	9	100	30:1	7	96.9	Trakarnpruk et al. [115]
Quintinite 3T	2:01	Canola	2	75	12:1	10	96	Kondamudi et al. [116]
Mg-Al HT	0.5-2.3	Sunflower	24	60	12:1	2	75	Navajas et al. [30]
K_2CO_3/Al-Ca HT	3:01	Soybean	2	65	13:1	2	87.4	Sun et al.[207]
FZ- HT	1.7:1	Mustard	5	65	12:1	7	93.4	Present study

For the optimization of methanol to oil molar ratio, transesterification was performed at 5 wt % catalyst concentration with methanol to oil molar ratio varying from 3:1 to 18:1 for 6 h and the result is shown in Fig. 6.4(B). Maximum conversion was obtained at optimum methanol to oil molar ratio of 12:1 and the order of conversion was FZ-HT (89.4%), C-HT (86.3%) and F-HT (67.1%), respectively. With further increase in methanol: oil molar ratio, conversion remained almost the same. Higher content of methanol inhibits the reaction rate by dissolution of glycerol further increasing the complexities in biodiesel separation reducing conversion [103].

The effect of catalyst concentration on biodiesel conversion is shown in Fig. 6.4(C). In general increase in catalyst concentration increases the rate of reaction, shifting the reaction equilibrium to products side resulting in higher conversion [3, 206]. As expected, with increase in catalyst concentration, conversion increased and reached a maximum value at 7 wt % of oil. When the catalyst concentration was further increased to 10 wt %, conversion decreased slightly. The order of conversion was FZ-HT (93.4%), C-HT (90.5%) and F-HT (71.2%), respectively. This could be due to the fact that, at higher catalyst concentrations, problems involving the mixing of reactant and catalyst increases resulting in meagre mixing in-turn increasing mass transfer resistance (some amount of the catalyst may remain unused) reducing conversion. Moreover, at a higher catalyst concentration, biodiesel products may get adsorbed on the surface of the catalyst, thus reducing conversion [37].

From the above it is clear that performance of catalyst FZ-HT was better when compared to C-HT and F-HT in the transesterification of mustard oil to produce a maximum biodiesel conversion of 93.4% and the optimum conditions of transesterification were; 12:1 methanol to oil molar ratio, 7 wt % catalyst concentration, reaction time of 6 h at temperature

of 65 ^{o}C. These values were in agreement with the literature. Wu et al. [103] reported that 30 wt % of CaO loaded Na-Y zeolite achieved a biodiesel yield of 95% with 3 wt % catalyst concentration, methanol to soybean oil molar ratio 9:1 for 3 h at 65 °C. Farooq et al. [206] tested the catalytic activity of Mo-Mn-Al_2O_3-15 wt % MgO catalyst using waste cooking oil. A maximum biodiesel yield of 91.4% was obtained in 4 h reaction time at temperature of 100 ^{o}C with methanol to oil molar ratio of 27:1. Sun et al. [207] studied the catalytic activity of K_2CO_3 loaded Al-Ca hydrotalcite in transesterification of soybean oil to obtain a biodiesel yield of 94.3% at the optimum conditions of methanol to oil molar ratio of 13:1, reaction temperature 65 °C, catalyst amount of 2 wt % and a reaction time of 2 h. A comparison of optimum parameters from literature with the present study is given in Table 6.2.

Chapter 7

Thermal Stability, Physical Properties, Chemical Composition and Degradation Kinetics of Biodiesel: A Comparative Study

Biodiesel;
Thermal stability;
Onset temperature;
Calorific value.

.

In this study, physico-chemical properties of synthesized mustard oil methylester (MOME) was determined using ASTM methods and was compared with standard biodiesel. Composition of mustard oil was also estimated by GC-MS. Thermal stability, onset temperatures and degradation kinetics of MOME was studied at different heating rates and was compared with the thermal behavior of raw mustard oil. Obtained results are shown below

7.1 Physical properties of mustard oil methylester

In order to assess the quality of mustard oil methyl ester (MOME), the biodiesel obtained was analyzed for its physical properties and results are shown in Table 7.1. The table also shows the comparison data with refined mustard oil (RMO), biodiesel and diesel [4, 208]. The MOME obtained has water content of 0.05% with specific gravity of 0.904 and has viscosity of 7.2 cP which is slightly higher than standard biodiesel (1.9 cP to 6 cP). Flash point of MOME is in the range with biodiesel, cloud points and pour points are slightly higher with an acid value of 0.06 mg of KOH g^{-1}. The calorific value of MOME was found to be 36.2 MJ Kg^{-1} with ash content less than 0.01%. A significant decrease in sulfur content was observed for MOME when compared with RMO. From the above it is clear that the MOME has similar characteristic properties to that of standard biodiesel and could be used as fuel when blended with diesel. The chemical composition of the refined mustard oil (RMO) was determined by using GC-MS as explained in section 2.3 and the results are shown in Table 7.2. The major composition of mustard oil was found to be linoleic acid (C18:2) 32.1% and erucic acid (C22:1) 32.8% respectively, along with other minor components like myristic (C14:0), palimitic (C16:0) and heneicosylic (C20:0) acids.

Table 7.1 Physico-chemical properties of refined mustard oil (RMO), mustard oil methyl ester (MOME), bio-diesel and diesel as per ASTM standards.

Physical properties	Raw material		Bio-diesel [4]	Diesel [208]	ASTM Standard
	RMO [208]	MOME Present study			
pH	4.7	5.4	—	5.6	—
Water content (% vol)	0.02	0.03	0.05	0.05	D 1796-94
Specific gravity (gm cc^{-1})	0.918	0.904	0.87- 0.9	0.84	D 1298-85
Viscosity @ 40 ^oC (cP)	52.6	7.2	1.9 - 6.0	2.7	D 445
Flash point (^oC)	321	197	130 min	60	D 93-90
Fire point (^oC)	355	210	—	65	D 93-90
Pour point (^oC)	—	2	-15	-35	D 97-93
Cloud point (^oC)	-4	14	-3 to -12	-20	D 2500-91
Acid value (mg KOH g^{-1})	1.41	0.067	0.08	0.062	D 664-89
Refractive index	1.468	1.454	1.454	1.465	—
Calorific value (MJ Kg^{-1})	33.9	36.2	38 - 43	42.5	D 240-92
Ash content (wt %)	<0.03	<0.01	0.02	0.01	D 482-91
Ultimate analysis (wt %)					
C	61.2	70.3	77	85.72	ASTM D5291-96
H	4.4	4.1	12	13.2	
N	4.12	0.4	--	0.18	
S	1.34	0.07	0.05	0.05	
O	28.9	25.6	11	0.85	
H/C molar ratio	0.86	0.69	1.8	1.85	
O/C molar ratio	0.35	0.27	0.11	0.01	

Table 7.2 Fatty acid composition of refined mustard oil (RMO).

Fatty acid	%
C 14:0	3.1
C 16:0	1.1
C 18:1	6.5
C 18:2	32.1
C 18:3	1.57
C 20:0	5.0
C 20:1	1.3
C 20:2	1.4
C 22:0	3.0
C 22:1	32.8
C 23:0	1.3

7.2 FTIR analysis

The MOME obtained was analyzed for its functional group from FTIR analysis and the results are shown in Fig. 7.1. From the infrared spectra of MOME, a broad band at 3444 cm^{-1} is observed due to the presence of hydroxyl group. This was due to the scanty drying of biodiesel. Presence of unsaturation was shown by small band at 3007 cm^{-1} which is due to –HC=CH– stretching vibrations. Two sharp peaks at 2922 cm^{-1} and 2852 cm^{-1} represent the presence of asymmetric and symmetric –CH– stretching vibrations. The –C=O, –C–O stretching vibrations at 1744 cm^{-1} and in between 1160-1236 cm^{-1} confirms the formation of ester peaks. Sharp peak at 721 cm^{-1} represents the presence of –HC– deformation of methyl group [70, 208].

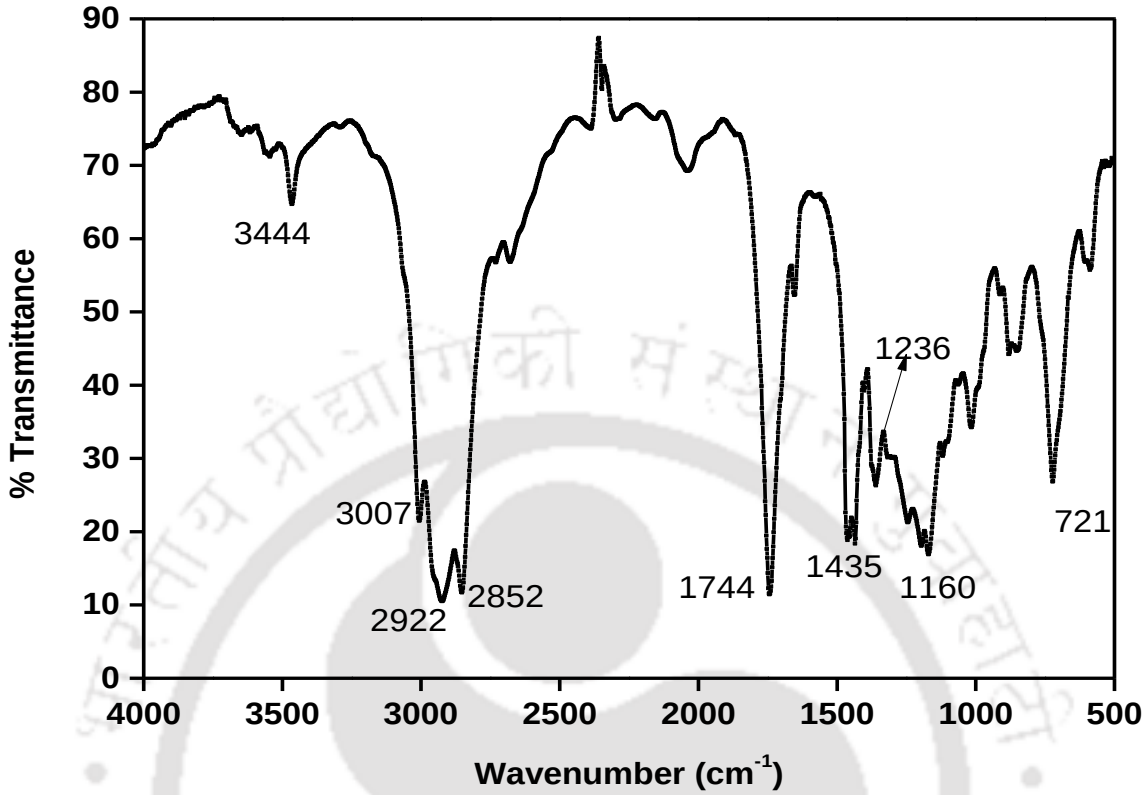

Fig. 7.1 FTIR spectra of mustard oil methyl ester.

7.3 Thermal stability and degradation kinetics of MOME

Studies regarding the thermal behavior and stability of the synthesized biodiesel was determined based on onset temperature (T_{onset}) using TGA at different heating rates (10, 20, 30 50 and 100 $^{o}C\ min^{-1}$). From Fig. 7.2(A) it is clear that thermal degradation of biodiesel followed a single stage decomposition with T_{onset} ranging from 153 to 272 ^{o}C signifying the start of thermal decomposition and it increased with increasing in heating rate. This could be due to the early decomposition of poly and mono unsaturated fatty acids. A total mass loss of 89% was observed at temperatures ranging from 153 to 435 ^{o}C. The peak temperatures (T_{peak}) at which maximum mass loss occurs was determined by DTG curves (Fig. 7.2(B)). The nature of TG curve with corresponding DTG peaks gives the number of stages of the thermal

degradation. The increasing rate of thermal decomposition resulted in increase of peak temperatures from 266 to 323 ^{o}C with increase in heating rate, shifting the DTG curves to higher temperature values. This could be due to faster release of volatiles at higher heating rates. Table 7.3 shows the comparison of MOME onset, offset and peak temperatures with raw mustard oil. The presence of unconverted mustard oil can be observed with the appearance of small hump after 512 to 600 ^{o}C. Offset temperatures (T_{offset}) which represents the end of thermal degradation was in the range of 536 to 568 ^{o}C.

Table 7.3 Comparison of onset, peak and offset temperatures of MOME and mustard oil

Heating Rate (^{o}C min^{-1})	Mustard oil (^{o}C)			MOME (^{o}C)		
	T_{onset}	T_{peak}	T_{offset}	T_{onset}	T_{peak}	T_{offset}
100	395	491	553	272	323	568
50	371	465	525	253	315	560
30	361	451	505	219	319	552
20	346	441	499	197	291	543
10	334	425	484	153	266	536

From the above it is clear that the synthesized biodiesel is thermally stable up to 150 ^{o}C and has major mass loss region in the temperature range of 153 to 435 ^{o}C when compared to refined mustard oil which is thermally stable up to 330 ^{o}C with the region of major mass loss between 334 to 553 ^{o}C which assures the removal of glycerol from mustard oil after transesterification [208]. The DSC thermograms of biodiesel from -30 to 450 ^{o}C at heating rate of 10 and 20 ^{o}C was shown in Fig. 7.2(C). The plot shows an endothermic event up to 9 ^{o}C, beyond that a sharp increase in heat flow occurs which is due to exothermic nature of the reaction. This particular temperature can be considered as pour point of biodiesel [126].

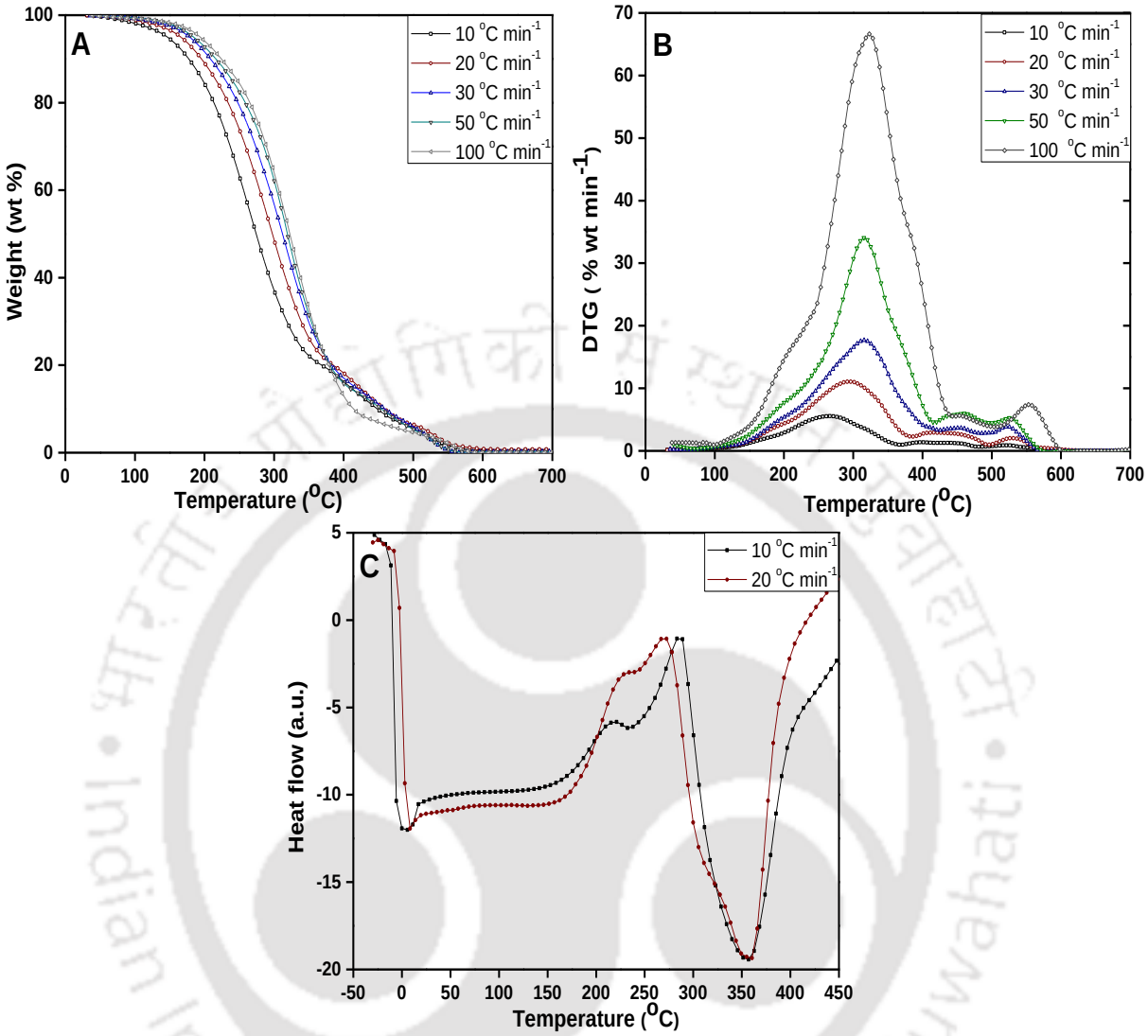

Fig. 7.2 Profiles of (A) TGA, (B) DTG and (C) DSC of biodiesel at different heating rates.

Iso-conversional Friedman, Kissinger, Flynn - Wall - Ozawa (FWO) and modified Coats - Redfern methods were used to determine the activation energy of the synthesized biodiesel in the conversion range of $0.2<X<0.9$ and are shown in Fig. 7.3 (A, B, C and D) respectively. The detailed derivation of kinetic equations was reported in our previous work [208]. With varying conversion variation in activation energy (Table 7.4) was observed over a range of 83.6 to 206.5 KJ mole^{-1} and the average values of activation energy were determined

as 142.4, 117.3, 131.9 and 129.1 KJ mole^{-1} with regression coefficients of 0.95, 0.99, 0.96 and 0.95 for Friedman, Kissinger, Flynn - Wall - Ozawa and modified Coats - Redfern methods, respectively.

As expected, the activation energy obtained from Kissinger method was less when compared to other methods. The values of activation energy derived from FWO and modified Coats - Redfern methods were almost same displaying good fitness of the model. When these methods were compared with Friedman and Kissinger method, the error percentage in the calculation of activation energy was found to be much higher (> 6%) showing the inadequate fitness of the model. From the above it is clear that the average value of activation energy of biodiesel is 130.5 KJ mole^{-1}. When compared with the activation energy of raw mustard oil (149.5 KJ mole^{-1}) [208], a signification reduction on the value of activation energy was observed in nitrogen atmosphere.

Table 7.4 Calculated values of activation energy of MOME using different models.

Method	**E_a*/ R^2**	**Conversion (X)**								**Average**
		0.2	**0.3**	**0.4**	**0.5**	**0.6**	**0.7**	**0.8**	**0.9**	
Friedman	E_a	88.9	93.1	105.1	123.5	153.5	180.1	212.8	182.5	142.4
	R^2	0.95	0.92	0.92	0.94	0.96	0.97	0.99	0.95	0.98
FWO	E_a	87.8	96.6	90.72	106.6	128.8	151.1	187.6	206.4	131.9
	R^2	0.96	0.96	0.94	0.94	0.96	0.97	0.98	0.98	0.96
Coats - Redfern	E_a	83.9	92.7	86.2	102.6	125.7	148.7	186.3	205.6	129.1
	R^2	0.95	0.95	0.92	0.94	0.95	0.97	0.98	0.97	0.95

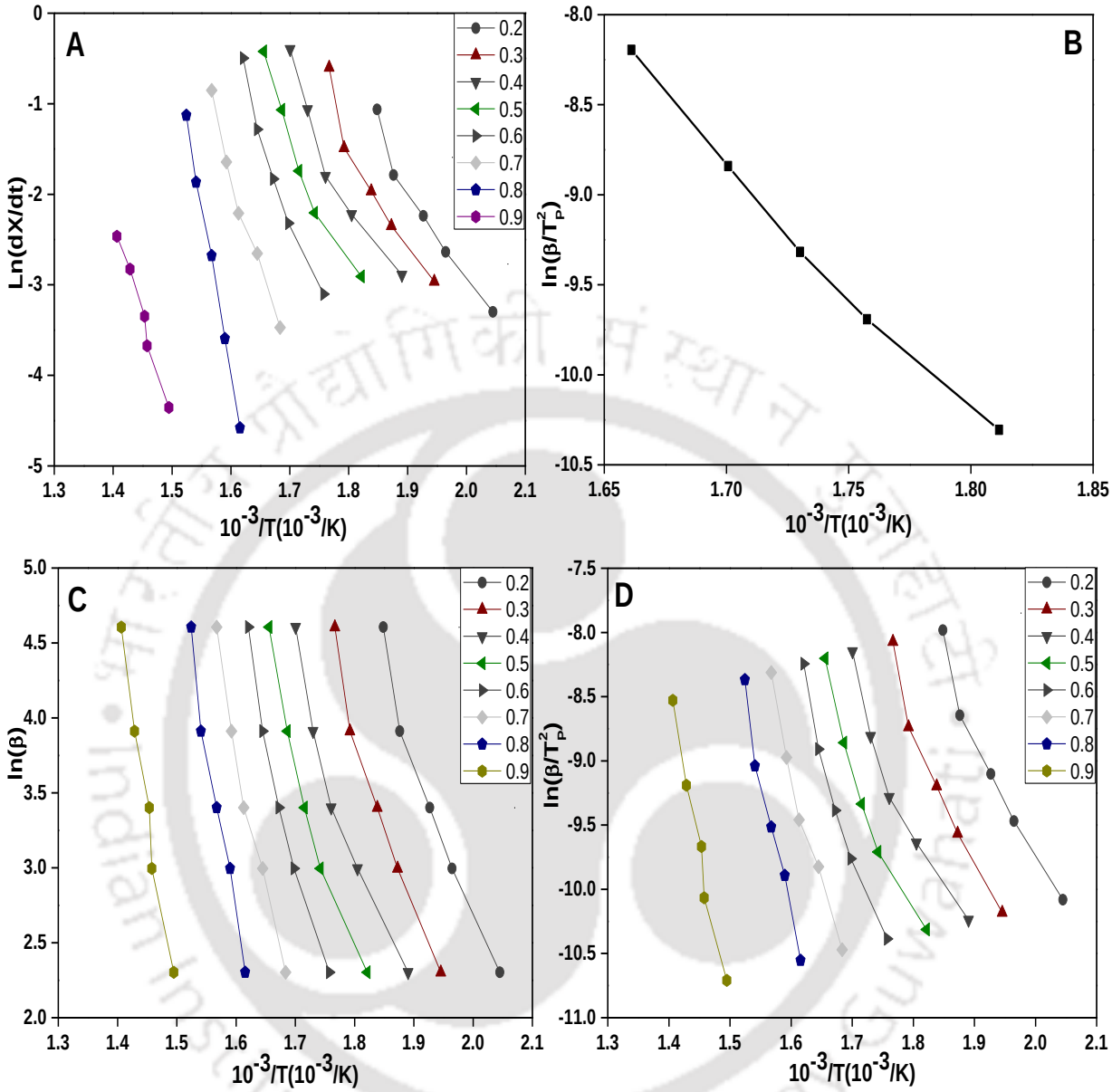

Fig. 7.3 Iso-conversional plot of (A) Friedman method, (B), Kissinger method, (C) F-W-O method and (D) modified Coats–Redfern method at varying conversion.

Chapter 8

Conclusion and Scope of Further Research

Future scope;

Cost analysis.

This chapter summarizes the conclusions drawn from various chapters presented in this thesis. Also, some suggestions towards the scope for future research were also outlined.

8.1 Conclusions

This work dealt with the preparation, characterization of different types of catalyst using flyash as starting material and their activity was evaluated in transesterification of mustard oil. Morphological characterization studies including FESEM, TGA, XRD, XRF, BET, CEC, TPR, FTIR and basicity have indicated that the synthesized catalyst possessed the desired characteristics for its application in biodiesel production. When the synthesized catalyst was used for transesterification of mustard oil, it provided higher yields with adequate product quality. The major conclusions obtained from this study are summarized below.

Physico-Chemical Properties and Thermal Degradation Studies of Commercial Oils in Nitrogen Atmosphere

1. Physical property analysis depicted that free fatty acid content in non-edible oils (2.82 to 19.74 mg KOH g^{-1}) were more than edible (0.56 to 2.11 mg KOH g^{-1}) oils resulting in higher acid value. Ash content of non-edible oils was higher than edible oils.
2. ^{1}H NMR analysis proved that except sesame, olive and mahua, all the other oils were rich in olefinic groups.
3. TGA of soybean, mustard, olive and karanja oils were performed in nitrogen atmosphere at different heating rates of 10, 20, 30, 50 and 100 ^{o}C min^{-1} from 25 to 600 ^{o}C. The results showed a single stage decomposition for all the samples when nitrogen medium was used.

4. The average value of the activation energy was determined to be 145.9, 150.6, 144.4 and 157.4 KJ mole^{-1} for mustard, soybean, olive and karanja oils, respectively. The order of activation energy was observed as; karanja > soybean > mustard > Olive.
5. It was envisaged that during thermal degradation of said oils, the calculated activation energy were less in nitrogen atmosphere than that of obtained in presence of oxidation.

Utilization of Flyash as Heterogeneous Catalyst for Transesterification

1. A study on the synthesis and characterization of heterogeneous base catalyst by impregnation of animal bone powder on flyash is presented in this paper.
2. Three different catalysts (C30, C20 and C10) varying the concentrations of flyash and bone powder was synthesized and its activity was evaluated in transesterification of mustard oil.
3. Response surface methodology was adopted to study the optimum value of biodiesel yield among bone powder concentration, catalyst concentration and methanol to oil molar ratio. Two factor interaction model was found to be a significant fit.
4. The optimum conditions obtained from RSM were at bone powder concentration of 10 wt %, 9.6 wt % catalyst concentration and 5.5:1 methanol/oil molar ratio would have biodiesel yield of 90.4%.
5. The above results were validated and from the experimental results of the optimum conditions an error of 2.8% was found.

Selective Preparation of Zeolite X and A from Flyash and its use as Catalyst for Biodiesel Production.

1. A single phase and highly crystalline zeolites X and A were synthesized from Indian flyash and condition was optimized (flyash/NaOH ratio 1:1.2; fusion and

crystallization time of 1 and 12 h; fusion, crystallization and calcination temperatures of 550 ^{o}C, 110 ^{o}C and 800 ^{o}C, respectively.

2. The CEC value of the synthesized UZ-X (168.2 meq/100g) and AZ-X (352.7 meq/100g)increased to UZ-KX (276.5 meq/100g) and AZ-KX (380.6 meq/100g), respectively when ion-exchanged with potassium.
3. Zeolite A had the highest CEC of 536.3 meq/100g. Si/Al ratio of 2 results in the formation of zeolite X and lower Si/Al ratios favoring formation of zeolite A.
4. The catalytic activity of synthesized zeolite (AZ-KX) was studied for transesterification of mustard oil and maximum conversion of 84.6% was obtained at 5 wt % catalyst loading, 12:1 methanol to oil molar ratio, reaction time of 7 h at 65 ^{o}C.

Preparation and Characterization of Hydrotalcite with Bifunctional Properties from Flyash for Transesterification

1. The present study successfully demonstrated the synthesis of hydrotalcite like materials from modified flyash. Three different hydrotalcite catalysts (C-HT, FZ-HT and F-HT) were synthesized with Mg/Al ratio varying from 1.3 to 2.3.
2. The surface area and total pore volume of FZ-HT was found to be higher when compared to other catalysts. The average particle size of 0.35, 0.93 and 6 µm, respectively was found for C-HT, FZ-HT and F-HT.
3. Activity of FZ-HT catalyst was observed better when compared to C-HT and F-HT in transesterification of mustard oil to produce a maximum biodiesel yield of 93.4% and the optimum conditions of transesterification were; 12:1 methanol to oil molar ratio, 7 wt % catalyst concentration, reaction time of 6 h at temperature of 65 ^{o}C.

Thermal stability, physical properties, chemical composition and degradation kinetics of biodiesel: A Comparative study.

1. The MOME obtained has water content of 0.05% with specific gravity of 0.904 and has viscosity of 7.2 cP which is slightly higher than standard biodiesel (1.9 cP to 6 cP).
2. The calorific value of MOME was found to be 36.2 MJ Kg^{-1} with ash content less than 0.01%.
3. The values of onset temperatures and activation energy was compared with mustard oil. The thermal degradation of biodiesel followed a single stage decomposition with T_{onset} ranging from 153 to 272 ^{o}C signifying the start of thermal decomposition and it increased with increasing in heating rate.
4. The average values of activation energy were determined as 142.4, 117.3, 131.9 and 129.1 KJ $mole^{-1}$ with regression coefficients of 0.95, 0.99, 0.96 and 0.95 for Friedman, Kissinger, Flynn - Wall - Ozawa and modified Coats - Redfern methods, respectively.
5. When compared with the activation energy of raw mustard oil (149.5 KJ $mole^{-1}$), the activation energy of MOME was found to be less (130.5 KJ $mole^{-1}$).

In summary, the thesis outlines the efficacy of flyash based catalyst for transesterification of mustard oil. The obtained data is anticipated to serve as reference data for furthering research in the field of catalysis and its application.

8.2 Recommendations for future work

Research findings in this work provided a good number of insights with respect to synthesis and characterization of diferent type of catalysts from flyash for transesterification of mustard oil. Few research areas for future work are presented as follows:

1. Use of Coats-Redfern Integral method of analysis might result result in a better comparative study in the estimation of model kinetics.
2. DSC could be a good analytical tool for analyzing the cold flow properties of commercial oils and the comparison of these properties with experimental methods could help in the better understanding of their thermal behavior.
3. Estimation of optimum paraameters for the transesterification by using ANN can be done in future
4. Effect of water: fusion mixture during hydrothermal treatement on different types of zeolite formation can also be studied.
5. The effect of basicity on Mg:Al (>2.3) and methods to imrove this ratio on formation of different types of hydrotalcites can be of great interest in future.
6. Estimation of thermodynamic propersties like Enthalpy, Entropy, Gibbs free energy and specific heat of biodiesel can ne helpul in the better understanding of the kinetics of transesterification.
7. Rigerious cost analysis for catalyst synthesis and transesterification needs to be studied as well in the near future to precisely define the benchmarks associated to technologies for biodiesel production.

References

[1] Conti JJ, Diefenderfer JR, Napolitano SA, Schaal AM, Turnure JT. Annual Energy Outlook with projections to 2040. 2015. (http://www.eia.gov/forecasts/aeo/assumptions/)

[2] Population Reference Bureau. 2014. (www.prb.org)

[3] Lam MK, Lee KT, Mohamed AR. Homogeneous, heterogeneous and enzymatic catalysis for transesterification of high free fatty acid oil waste cooking oil to biodiesel A review. Biotechnol Adv 2010;28:500–18.

[4] Leung DYC, Wu X, Leung MKH. A review on biodiesel production using catalyzed transesterification. Appl Energy 2010;87:1083–95.

[5] Atabani A. E, Silitonga A. S, Badruddin IA, Mahlia TMI, Masjuki HH, Mekhilef S. A comprehensive review on biodiesel as an alternative energy resource and its characteristics. Renew Sustain Energy Rev 2012;16:2070–93.

[6] History of biodiesel. (http://www.home-Made-Biodiesel.com/history-of-Biodiesel.html, Http://www.biodiesel.com/index.php/biodiesel/history_of_biodiesel_fuel/).

[7] Dias JM, Alvim-Ferraz MCM, Almeida MF. Comparison of the performance of different homogeneous alkali catalysts during transesterification of waste and virgin oils and evaluation of biodiesel quality. Fuel 2008;87:3572–8.

[8] Samart C, Sreetongkittikul P, Sookman C. Heterogeneous catalysis of transesterification of soybean oil using KI/mesoporous silica. Fuel Process Technol 2009;90:922–5.

[9] Kouzu M, Kasuno T, Tajika M, Sugimoto Y, Yamanaka S, Hidaka J. Calcium oxide as a solid base catalyst for transesterification of soybean oil and its application to biodiesel production. Fuel 2008;87:2798–806.

[10] Rodrigues RC, Ayub MAZ. Effects of the combined use of thermomyces lanuginosus and rhizomucor miehei lipases for the transesterification and hydrolysis of soybean oil. Process Biochem 2011;46:682–8.

[11] Ginting MSA, Tazli Azizan M, Yusup S. Alkaline in situ ethanolysis of Jatropha curcas. Fuel 2012;93:82–5.

[12] Taufiq-Yap YH, Lee HV, Hussein MZ, Yunus R. Calcium-based mixed oxide catalysts for methanolysis of Jatropha curcas oil to biodiesel. Biomass Bioenerg 2011;35:827–34.

[13] Olutoye MA, Hameed BH. Synthesis of fatty acid methyl ester from crude jatropha (Jatropha curcas Linnaeus) oil using aluminium oxide modified Mg-Zn heterogeneous catalyst. Bioresour Technol 2011;102:6392–8.

[14] Veljković VB, Avramović JM, Stamenković OS. Biodiesel production by ultrasound-assisted transesterification: State of the art and the perspectives. Renew Sustain Energy Rev 2012;16:1193–209.

[15] Tamalampudi S, Talukder MR, Hama S, Numata T, Kondo A, Fukuda H. Enzymatic production of biodiesel from Jatropha oil: A comparative study of immobilized-whole cell and commercial lipases as a biocatalyst. Biochem Eng J 2008;39:185–9.

[16] Liang J, Ren X, Wang J, Jinag M, Li Z. Preparation of biodiesel by transesterification from cottonseed oil using the basic dication ionic liquids as catalysts. J Fuel Chem Technol 2010;38:275–80.

[17] Qian J, Wang F, Liu S, Yun Z. In situ alkaline transesterification of cottonseed oil for production of biodiesel and nontoxic cottonseed meal. Bioresour Technol 2008;99:9009–12.

[18] Shu Q, Zhang Q, Xu G, Nawaz Z, Wang D, Wang J. Synthesis of biodiesel from cottonseed oil and methanol using a carbon-based solid acid catalyst. Fuel Process Technol 2009;90:1002–8.

[19] Chattopadhyay S, Karemore A, Das S, Deysarkar A, Sen R. Biocatalytic production of biodiesel from cottonseed oil: Standardization of process parameters and comparison of fuel characteristics. Appl Energy 2011;88:1251–6.

[20] Hameed BH, Lai LF, Chin LH. Production of biodiesel from palm oil (Elaeis guineensis) using heterogeneous catalyst : An optimized process. Fuel Process Technol 2009;90:606–10.

[21] Jitputti J, Kitiyanan B, Rangsunvigit P, Bunyakiat K, Attanatho L, Jenvanitpanjakul P. Transesterification of crude palm kernel oil and crude coconut oil by different solid catalysts. Chem Eng J 2006;116:61–6.

[22] Noiroj K, Intarapong P, Luengnaruemitchai A, Jai-In S. A comparative study of KOH/Al_2O_3 and KOH/NaY catalysts for biodiesel production via transesterification from palm oil. Renew Energy 2009;34:1145–50.

[23] Zhang X, Huang W. Catalysts derived from waste slag for transesterification. J Nat Gas Chem 2011;20:299–302.

[24] Wang L, Tang Z, Xu W, Yang J. Catalytic transesterification of crude rapeseed oil by liquid organic amine and co-catalyst in supercritical methanol. Catal Commun 2007;8:1511–5.

[25] Rashid U, Anwar F. Production of biodiesel through optimized alkaline-catalyzed transesterification of rapeseed oil. Fuel 2008;87:265–73.

[26] Tang S, Wang L, Zhang Y, Li S, Tian S, Wang B. Study on preparation of Ca/Al/Fe_3O_4 magnetic composite solid catalyst and its application in biodiesel transesterification. Fuel Process Technol 2012;95:84–9.

[27] Schuchardt U, Vargas RM, Gelbard G. Alkylguanidines as catalysts for the transesterification of rapeseed oil. J Mol Catal A Chem 1995;99:65–70.

[28] Lukić I, Krstić J, Jovanović D, Skala D. Alumina/silica supported K_2CO_3 as a catalyst for biodiesel synthesis from sunflower oil. Bioresour Technol 2009;100:4690–6.

[29] Cerro-Alarcón M, Corma A, Iborra S, Martínez C, Sabater MJ. Methanolysis of sunflower oil using gem-diamines as active organocatalysts for biodiesel production. Appl Catal A Gen 2010;382:36–42.

[30] Navajas A, Campo I, Arzamendi G, Hernández WY, Bobadilla LF, Centeno MA, et al. Synthesis of biodiesel from the methanolysis of sunflower oil using PURAL ® Mg – Al hydrotalcites as catalyst precursors. Appl Catal B Environ 2010;100:299–309.

[31] Ramos MJ, Casas A, Rodríguez L, Romero R, Pérez Á. Transesterification of sunflower oil over zeolites using different metal loading: A case of leaching and agglomeration studies. Appl Catal A Gen 2008;346:79–85.

[32] Sun H, Han J, Ding Y, Li W, Duan J, Chen P, et al. One-pot synthesized mesoporous Ca/SBA-15 solid base for transesterification of sunflower oil with methanol. Appl Catal A Gen 2010;390:26–34.

[33] Jiménez-López A, Jiménez-Morales I, Santamaría-González J, Maireles-Torres P. Biodiesel production from sunflower oil by tungsten oxide supported on zirconium doped MCM-41 silica. J Mol Catal A Chem 2011;335:205–9.

[34] Leung DYC, Guo Y. Transesterification of neat and used frying oil: Optimization for biodiesel production. Fuel Process Technol 2006;87:883–90.

[35] Wang Y, Ou S, Liu P, Xue F, Tang S. Comparison of two different processes to synthesize biodiesel by waste cooking oil. J Mol Catal A Chem 2006;252:107–12.

[36] Guan G, Kusakabe K, Yamasaki S. Tri-potassium phosphate as a solid catalyst for biodiesel production from waste cooking oil. Fuel Process Technol 2009;90:520–4.

[37] Lou WY, Zong MH, Duan ZQ. Efficient production of biodiesel from high free fatty acid-containing waste oils using various carbohydrate-derived solid acid catalysts. Bioresour Technol 2008;99:8752–8.

[38] Azócar L, Ciudad G, Heipieper HJ, Muñoz R, Navia R. Improving fatty acid methyl ester production yield in a lipase-catalyzed process using waste frying oils as feedstock. J Biosci Bioeng 2010;109:609–14.

[39] Ramadhas AS, Jayaraj S, Muraleedharan C. Biodiesel production from high FFA rubber seed oil. Fuel 2005;84:335–40.

[40] Sahoo PK, Das LM, Babu MKG, Naik SN. Biodiesel development from high acid value polanga seed oil and performance evaluation in a CI engine. Fuel 2007;86:448–54.

[41] Bhatti H, Hanif M, Qasim M, Ataurrehman. Biodiesel production from waste tallow. Fuel 2008;87:2961–6.

[42] Ilgen O. Dolomite as a heterogeneous catalyst for transesterification of canola oil. Fuel Process Technol 2011;92:452–5.

[43] Chaturvedi RK, Mal N, Nagabhushana KS. Process for production of biodiesel, US2011/0144375A1 2011.

[44] Chakraborty R, Bepari S, Banerjee A. Transesterification of soybean oil catalyzed by fly ash and egg shell derived solid catalysts. Chem Eng J 2010;165:798–805.

[45] Babajide O, Musyoka N, Petrik L, Ameer F. Novel zeolite Na-X synthesized from fly ash as a heterogeneous catalyst in biodiesel production. Catal Today 2012;190:54–60.

[46] Suppes GJ, Dasari MA, Doskocil EJ, Mankidy PJ, Goff MJ. Transesterification of soybean oil with zeolite and metal catalysts. Appl Catal A Gen 2004;257:213–23.

[47] Supamathanon N, Wittayakun J, Prayoonpokarach S. Properties of Jatropha seed oil from Northeastern Thailand and its transesterification catalyzed by potassium supported on NaY zeolite. J Ind Eng Chem 2011;17:182–5.

[48] Shu Q, Yang B, Yuan H, Qing S, Zhu G. Synthesis of biodiesel from soybean oil and methanol catalyzed by zeolite beta modified with La^{3+}. Catal Commun 2007;8:2159–65.

[49] Ojha K, Pradhan NC, Samanta AN. Alkylation of phenol with tert-butyl alcohol over a catalyst synthesized from coal fly ash. J Chem Technol Biotechnol 2006;81:659–66.

[50] Alam J, Akhtar MN. Fly ash utilization in different sectors in Indian scenario. Int J Emerg Trends Eng Dev 2011;1:1–14.

[51] Blissett RS, Rowson NA. A review of the multi-component utilisation of coal fly ash. Fuel 2012:1–23.

[52] Santos JCO, Santos IMG, Souza AG, Prasad S, Santos AV. Thermal stability and kinetic study on thermal decomposition of commercial edible oils by thermogravimetry. J Food Sci 2002;67:1393–8.

[53] Arora S, Bagoria R, Kumar M. Effect of alpha-tocopherol (vitamin E) on the thermal degradation behavior of edible oils. J Therm Anal Calorim 2009;102:375–81.

[54] Souza AG De, Santos JCO, Conceição MM, Silva MCD, Prasad S. A thermoanalytic and kinetic study of sunflower oil. Brazilian J Chem Eng Chem Eng 2004;21:265–73.

[55] Vecchio S, Cerretani L, Bendini A, Chiavaro E. Thermal decomposition study of monovarietal extra virgin olive oil by simultaneous thermogravimetry/differential scanning calorimetry: relation with chemical composition. J Agric Food Chem 2009;57:4793–800.

[56] Haryati T, Che Man YB, Asbi A., Ghazali HM, Buana L. Determination of iodine value of palm oil by differential scanning calorimetry. J Am Oil Chem Soc 1997;74:939–42.

[57] Tan CP, Che Man YB. Differential scanning calorimetric analysis of edible oils: Comparison of thermal properties and chemical composition. J Am Oil Chem Soc 2000;77:143–55.

[58] Souza AG, Silva D, Teixeira G. Thermal and kinetic evaluation of cotton oil biodiesel. J Therm Anal Calorim 2013;90:945–9.

[59] Thurgood J, Ward R, Martini S. Oxidation kinetics of soybean oil/anhydrous milk fat blends: A differential scanning calorimetry study. Food Res Int 2007;40:1030–7.

[60] Jain S, Sharma MP. Application of thermogravimetric analysis for thermal stability of Jatropha curcas biodiesel. Fuel 2012;93:252–7.

[61] Chouhan APS, Sarma AK. Modern heterogeneous catalysts for biodiesel production: A comprehensive review. Renew Sustain Energy Rev 2011;15:4378–99.

[62] Vujicic D, Comic D, Zarubica a., Micic R, Boskovic G. Kinetics of biodiesel synthesis from sunflower oil over CaO heterogeneous catalyst. Fuel 2010;89:2054–61.

[63] Dehkordi AM, Ghasemi M. Transesterification of waste cooking oil to biodiesel using Ca and Zr mixed oxides as heterogeneous base catalysts. Fuel Process Technol 2012;97:45–51.

[64] Alastuey A, Herna E, Querol X, Moreno N, Uman JC, Plana F, et al. Synthesis of zeolites from coal fly ash : an overview. Int J Coal Geol 2002;50:413–23.

[65] Xie W, Zhao L. Aminopropylsilica as an environmentally friendly and reusable catalyst for biodiesel production from soybean oil. Fuel 2013;103:1106–10.

[66] Chakraborty R, Bepari S, Banerjee A. Application of calcined waste fish (Labeo rohita) scale as low-cost heterogeneous catalyst for biodiesel synthesis. Bioresour Technol 2011;102:3610–8.

[67] Sharma M, Khan AA, Puri SK, Tuli DK. Wood ash as a potential heterogeneous catalyst for biodiesel synthesis. Biomass Bioenerg 2012;41:94–106.

[68] Chen KT, Wang JX, Dai YM, Wang PH, Liou CY, Nien CW, et al. Rice husk ash as a catalyst precursor for biodiesel production. J Taiwan Inst Chem Eng 2013;44:622–9.

[69] Smith SM, Oopathum C, Weeramongkhonlert V, Smith CB, Chaveanghong S, Ketwong P, et al. Transesterification of soybean oil using bovine bone waste as new catalyst. Bioresour Technol 2013;143:686–90.

[70] Roschat W, Kacha M, Yoosuk B, Sudyoadsuk T, Promarak V. Biodiesel production based on heterogeneous process catalyzed by solid waste coral fragment. Fuel 2012;98:194–202.

[71] Chouhan APS, Sarma AK. Biodiesel production from Jatropha curcas L. oil using Lemna perpusilla Torrey ash as heterogeneous catalyst. Biomass Bioenerg 2013;55:386–9.

[72] Viriya-empikul N, Krasae P, Nualpaeng W, Yoosuk B, Faungnawakij K. Biodiesel production over Ca-based solid catalysts derived from industrial wastes. Fuel 2012;92:239–44.

[73] Boey PL, Maniam GP, Hamid SA. Biodiesel production via transesterification of palm olein using waste mud crab (Scylla serrata) shell as a heterogeneous catalyst. Bioresour Technol 2009;100:6362–8.

[74] Nakatani N, Takamori H, Takeda K, Sakugawa H. Transesterification of soybean oil using combusted oyster shell waste as a catalyst. Bioresour Technol 2009;100:1510–3.

[75] Hu S, Wang Y, Han H. Utilization of waste freshwater mussel shell as an economic catalyst for biodiesel production. Biomass Bioenerg 2011;35:3627–35.

[76] Boro J, Thakur AJ, Deka D. Solid oxide derived from waste shells of Turbonilla striatula as a renewable catalyst for biodiesel production. Fuel Process Technol 2011;92:2061–7.

[77] Boey PL, Maniam GP, Hamid SA, Ali DMH. Utilization of waste cockle shell (Anadara granosa) in biodiesel production from palm olein: Optimization using response surface methodology. Fuel 2011;90:2353–8.

[78] Jain D, Khatri C, Rani A. Synthesis and characterization of novel solid base catalyst from fly ash. Fuel 2011;90:2083–8.

[79] Kotwal MS, Niphadkar PS, Deshpande SS, Bokade VV, Joshi PN. Transesterification of sunflower oil catalyzed by flyash-based solid catalysts. Fuel 2009;88:1773–8.

[80] Babajide O; Petrik L, Musyoka N, Amigun B, Ameer F. Use of coal flyash as a catalyst in the production of biodiesel. Pet Coal 2010;52:261–72.

[81] Davis R. New perspectives on basic zeolites as catalysts and catalyst supports. J Catal 2003;216:396–405.

[82] Kovacheva P, Predoeva a, Arishtirova K, Vassilev S. Oxidative methylation of toluene with methane using X zeolite catalyst modified with alkali earth oxides. Appl Catal A Gen 2002;223:121–8.

[83] Dutta K, Bowers C. Synthesis of Zeolites A and X : Influence of cosolvents. Zeolites 1991;11:507–10.

[84] Roozeboom F, Robson HE, Chan SS. Laser raman study on the crystallization of zeolites A, X and Y. Zeolites 1983;3:321–8.

[85] Cundy CS, Cox PA. The hydrothermal synthesis of zeolites: Precursors, intermediates and reaction mechanism. Microporous Mesoporous Mater 2005;82:1–78.

[86] Zhou M, Rownaghi A., Hedlund J. Synthesis of mesoporous ZSM-5 zeolite crystals by conventional hydrothermal treatment. RSC Adv 2013;3:15596.

[87] Auer H, Hofmann H. Pillared clays: characterization of acidity and catalytic properties and comparison with some zeolites. Appl Catal A Gen 1993;97:23–38.

[88] Fernandes Machado NRC, Malachini Miotto DM. Synthesis of Na–A and –X zeolites from oil shale ash. Fuel 2005;84:2289–94.

[89] Rios C, Williams C, Fullen M. Nucleation and growth history of zeolite LTA synthesized from kaolinite by two different methods. Appl Clay Sci 2009;42:446–54.

[90] Fan Y, Zhang F, Zhu J, Liu Z. Effective utilization of waste ash from MSW and coal co-combustion power plant — Zeolite synthesis. J Hazard Mater 2008;153:382–8.

[91] Rayalu S, Meshram SU, Hasan MZ. Highly crystalline faujasitic zeolites from flyash. J Hazard Mater 2000;77:123–31.

[92] Majchrzak-Kucęba I, Nowak W. A thermogravimetric study of the adsorption of CO_2 on zeolites synthesized from fly ash. Thermochim Acta 2005;437:67–74.

[93] Chang H, Shih W. A general method for the conversion of fly ash into zeolites as ion exchangers for cesium. Ind Eng Chem Res 1998;37:71–8.

[94] Hollman GG, Steenbruggen G. A two-step process for the synthesis of zeolites from coal fly ash. Fuel 1999;78:1225–30.

[95] Zhang M, Zhang H, Xu D, Han L, Niu D, Zhang L, et al. Ammonium removal from aqueous solution by zeolites synthesized from low-calcium and high-calcium fl y ashes. Desalination 2011;277:46–53.

[96] Wang C, Li J, Sun X, Wang L, Sun X. Evaluation of zeolites synthesized from fly ash as potential adsorbents for wastewater containing heavy metals. J Environ Sci 2009;21:127–36.

[97] Adamczyk Z, Bialecka B. Hydrothermal synthesis of zeolites from Polish coal fly ash. Polish J Environ Stud 2005;14:713–9.

[98] Mishra T, Tiwari SK. Studies on sorption properties of zeolite derived from Indian fly ash. J Hazard Mater 2006;137:299–303.

[99] Ruiz C, Juan R, Hern S. Ion exchange uptake of ammonium in wastewater from a Sewage Treatment Plant by zeolitic materials from fly ash. J Hazard Mater 2009;161:781–6.

[100] Leclercq E, Finiels A, Moreau C. Transesterification of rapeseed oil in the presence of basic zeolites and related solid catalysts. JAOCS 2001;78:1161–5.

[101] Intarapong P, Luengnaruemitchai A, Jai-in S. Transesterification of palm oil over KOH / NaY zeolite in a packed-bed reactor. Int J Renew Energy Res 2011;1:271–80.

[102] Kusuma RI, Hadinoto JP, Ayucitra A, Soetaredjo FE, Ismadji S. Natural zeolite from Pacitan Indonesia, as catalyst support for transesterification of palm oil. Appl Clay Sci 2013;74:121–6.

[103] Wu H, Zhang J, Wei Q, Zheng J, Zhang J. Transesterification of soybean oil to biodiesel using zeolite supported CaO as strong base catalysts. Fuel Process Technol 2013;109:13–8.

[104] Aliyu A, Lomsahaka E, Hamza A. Production of biodiesel via NaOH catalyzed transesterification of mahogany seed oil. Adv Appl Sci Res 2012;3:615–8.

[105] Jamil CAZ, Muslim A. Performance of KOH as a catalyst for transesterification of Jatropha Curcas oil. Int J Eng Res Appl 2012;2:635–9.

[106] Fukuda H, Kondo A, Noda H. Biodiesel fuel production by transesterification of oils. J Biosci Bioeng 2001;92:405–16.

[107] Boro J, Deka D, Thakur AJ. A review on solid oxide derived from waste shells as catalyst for biodiesel production. Renew Sustain Energy Rev 2012;16:904–10.

[108] Boey PL, Ganesan S, Maniam GP, Khairuddean M. Catalysts derived from waste sources in the production of biodiesel using waste cooking oil. Catal Today 2012;190:117–21.

[109] Ngamcharussrivichai C, Nunthasanti P, Tanachai S, Bunyakiat K. Biodiesel production through transesterification over natural calciums. Fuel Process Technol 2010;91:1409–15.

[110] Wang JX, Chen KT, Wen BZ, Liao YH Ben, Chen CC. Transesterification of soybean oil to biodiesel using cement as a solid base catalyst. J Taiwan Inst Chem Eng 2012;43:215–9.

[111] Purnomo CW, Salim C, Hinode H. Synthesis of pure Na–X and Na–A zeolite from bagasse fly ash. Microporous Mesoporous Mater 2012;162:6–13.

[112] Deng X, Fang Z, Liu Y, Yu CL. Production of biodiesel from Jatropha oil catalyzed by nanosized solid basic catalyst. Energy 2011;36:777–84.

[113] Gomes JFP, Puna JFB, Gonçalves LM, Bordado JCM. Study on the use of MgAl hydrotalcites as solid heterogeneous catalysts for biodiesel production. Energy 2011;36:6770–8.

[114] Xie W, Peng H, Chen L. Calcined Mg – Al hydrotalcites as solid base catalysts for methanolysis of soybean oil. J Mol Catal A Chem 2006;246:24–32.

[115] Trakarnpruk W, Porntangjitlikit S. Palm oil biodiesel synthesized with potassium loaded calcined hydrotalcite and effect of biodiesel blend on elastomer properties. Renew Energy 2008;33:1558–63.

[116] Kondamudi N, Mohapatra SK, Misra M. Quintinite as a bifunctional heterogeneous catalyst for biodiesel synthesis. Appl Catal A Gen 2011;393:36–43.

[117] Liu Q, Wang C, Qu W, Wang B, Tian Z, Ma H, et al. The application of Zr incorporated Zn-Al dehydrated hydrotalcites as solid base in transesterification. Catal Today 2014;234:161–6.

[118] Cantrell DG, Gillie LJ, Lee AF, Wilson K. Structure-reactivity correlations in MgAl hydrotalcite catalysts for biodiesel synthesis. Appl Catal A Gen 2005;287:183–90.

[119] Jain S, Sharma MP. Thermal stability of biodiesel and its blends: A review. Renew Sustain Energy Rev 2011;15:438–48.

[120] Jain S, Sharma M. Oxidation and thermal behavior of Jatropha curcas biodiesel influenced by antioxidants and metal contaminants. Int J Eng Sci Technol 2011;3:65–75.

[121] Oliveira LE, Giordani DS, Paiva EM, De Castro HF, Da Silva MLCP. Kinetic and thermodynamic parameters of volatilization of biodiesel from babassu, palm oil and mineral diesel by thermogravimetric analysis (TG). J Therm Anal Calorim 2013;111:155–60.

[122] Nautiyal P, Subramanian KA., Dastidar MG. Kinetic and thermodynamic studies on biodiesel production from Spirulina platensis algae biomass using single stage extraction-transesterification process. Fuel 2014;135:228–34.

[123] Cursaru D, Mihai S. Evaluation of thermal stability of biodiesel synthesized from different edible oils by thermogravimetric analysis. Rev Chim 2013;64:1156–9.

[124] Conconi CC, Crnkovic PM. Thermal behavior of renewable diesel from sugar cane, biodiesel, fossil diesel and their blends. Fuel Process Technol 2013;114:6–11.

[125] Zhao H, Cao Y, Orndorff W, Cheng Y-H, Pan W. Thermal behaviors of soy biodiesel. J Therm Anal Calorim 2012;109:1145–50.

[126] Borugadda VB, Goud VV. Thermal, oxidative and low temperature properties of methyl esters prepared from oils of different fatty acids composition: A comparative study. Thermochim Acta 2014;577:33–40.

[127] Lin R, Zhu Y, Tavlarides LL. Effect of thermal decomposition on biodiesel viscosity and cold flow property. Fuel 2014;117:981–8.

[128] Shivakumar, Srinivasa Pai P, Rao BRS. Artificial Neural Network based prediction of performance and emission characteristics of a variable compression ratio CI engine using WCO as a biodiesel at different injection timings. Appl Energy 2011;88:2344–54.

[129] Ma F, Hanna MA. Biodiesel production : a review. Bioresour Technol 1999;70:1–15.

[130] Xue J, Grift TE, Hansen AC. Effect of biodiesel on engine performances and emissions. Renew Sustain Energy Rev 2011;15:1098–116.

[131] Berrios M, Skelton RL. Comparison of purification methods for biodiesel. Chem Eng J 2008;144:459–65.

[132] Agarwal AK. Biofuels (alcohols and biodiesel) applications as fuels for internal combustion engines. Prog Energy Combust Sci 2007;33:233–71.

[133] Gary JH, Handwerk GE. Petroleum Refining Technology and Economics. Marcel Bekker,Inc 2001.

[134] Rao B. Modern Petroleum Refining Processes. Oxford & Ibh Publishing Co Pvt Ltd; 1984.

[135] Refractive index 2015:495677 (http://www.britannica.com/print/topic/495677).

[136] Hoekman SK, Broch A, Robbins C, Ceniceros E, Natarajan M. Review of biodiesel composition, properties, and specifications. Renew Sustain Energy Rev 2012;16:143–69.

[137] Hoekman SK, Robbins C. Review of the effects of biodiesel on NOx emissions. Fuel Process Technol 2012;96:237–49.

[138] Broido A. A simple, sensitive graphical method of treating thermogravimetric analysis data. J Polym Sci 1969;7:1761–73.

[139] Ramos P, Nelo C, Soriano M, Caro B, Mazzuco LM, Grac M. Quantification of soybean oil ethanolysis with ^{l}H NMR. JAOCS 2013;81:1111–4.

[140] Wu J, Lu X, Tang W, Kong H, Zhou S, Xu G. Application of comprehensive two-dimensional gas chromatography-time-of-flight mass spectrometry in the analysis of volatile oil of traditional Chinese medicines. J Chromatogr A 2004;1034:199–205.

[141] Condon JB. Surface area and porosity determination by physisorption measurement and theory. Elesevier 2006.

[142] Musyoka NM, Petrik LF, Fatoba OO, Hums E. Synthesis of zeolites from coal fly ash using mine waters. Miner Eng 2013;53:9–15.

[143] Gross-Lorgouilloux M, Soulard M, Caullet P, Patarin J, Moleiro E, Saude I. Conversion of coal fly ashes into faujasite under soft temperature and pressure conditions: Influence of additional silica. Microporous Mesoporous Mater 2010;127:41–9.

[144] Qiu B, Yi X, Lin L, Fang W, Wan H. The hydrocracking of n-decane over bifunctional Ni-$H_3PW_{12}O_{40}/SiO_2$ catalysts. Catal Today 2008;131:464–71.

[145] Singh AK, Fernando SD. Transesterification of soybean oil using heterogeneous catalysts. Energy & Fuels 2008;22:2067–9.

[146] Muñoz V, Zotin FMZ, Palacio LA. Copper–aluminum hydrotalcite type precursors for NOx abatement. Catal Today 2014;250:173–9.

[147] Rungsuk D, Apiratikul R, Pavarajarn V, Pavasant P. Zeolite synthesis from fly ash from coal-fired power plant by fusion. Sustain. Energy Environ 2006;042:2–6.

[148] Yang Q, Wu S, Lou R, Lv G. Analysis of wheat straw lignin by thermogravimetry and pyrolysis–gas chromatography/mass spectrometry. J Anal Appl Pyrolysis 2010;87:65–9.

[149] Friedman HL. Kinetics of thermal degradation of char-forming plastics from thermogravimetry. Application to a phenolic plastic. J Polym Sci Part C Polym Symp 1964;6:183–95.

[150] Yao F, Wu Q, Lei Y, Guo W, Xu Y. Thermal decomposition kinetics of natural fibers: Activation energy with dynamic thermogravimetric analysis. Polym Degrad Stab 2008;93:90–8.

[151] Burnham AK, Braun RL. Global kinetic analysis of complex materials. Energy & Fuels 1999;13:1–22.

[152] Coats AW, Redfern JP. Kinetic parameters from thermogravimetric data. Nature 1964;201:68–9.

[153] Brown ME, Maciejewskib M, Nomen SVR, Sempere J, Burnham A. thermochimica acta Computational aspects of kinetic analysis Part A : The ICTAC kinetics project-data , methods and results. Thermochim Acta 2013:125–43.

[154] Blaine RL, Kissinger HE. Homer Kissinger and the Kissinger equation. Thermochim Acta 2012;540:1–6.

[155] Joseph H. Flynn LAW. A quick, direct method for the determination of activation energy from thermogravimetric data. Polym Lett 1966;4:323–8.

[156] Takeo Ozawa. A new method of analyzing thermogravimetric data. Bull Chem Soc Jpn 1965;38:1881–6.

[157] Doyle CD. Series Approximations to the Equation of Thermogravimetric Data. Nature 1965;207:290–1.

[158] John N. Coupland and D. Julian McClements. Physical properties of liquid edible oils. JAOCS 1997;74:1559–64.

[159] Carareto NDD, Kimura CYCS, Oliveira EC, Costa MC, Meirelles AJA. Flash points of mixtures containing ethyl esters or ethylic biodiesel and ethanol. Fuel 2012;96:319–26.

[160] Mejía JD, Salgado N, Orrego CE. Effect of blends of diesel and palm-castor biodiesels on viscosity, cloud point and flash point. Ind Crops Prod 2013;43:791–7.

[161] Khodier SA. Refractive index of standard oils as a function of wavelength and temperature. Opt Laser Technol 2002;34:125–8.

[162] Ajiwe VIE, Ajaibola VO and Martins CMAO. Biodiesel fuels from palm oil, palm oil methylester and ester-diesel blends. Bull Chem Soc Ethiop 2003;17:19–26.

[163] Roberto M, Regina A, Ambrozin P, Santos S, Fabiana E, Pereira-filho ER, et al. Evaluation of biodiesel – diesel blends quality using ^{1}H NMR and chemometrics. Talanta 2009;78:660–4.

[164] S, Sevgi Sensoz, Ilknur Demiral HFG. Olive bagasse (Olea europea L .) pyrolysis. Bioresour Technol 2006;97:429–36.

[165] Lin SY, Wang SL. Advances in simultaneous DSC-FTIR microspectroscopy for rapid solid-state chemical stability studies: some dipeptide drugs as examples. Adv Drug Deliv Rev 2012;64:461–78

[166] Blissett RS, Rowson NA. A review of the multi-component utilisation of coal fly ash. Fuel 2012;97:1–23.

[167] Obadiah A, Swaroopa GA, Kumar SV, Jeganathan KR, Ramasubbu A. Biodiesel production from palm oil using calcined waste animal bone as catalyst. Bioresour Technol 2012;116:512–6.

[168] Zabeti M, Daud WMAW, Aroua MK. Biodiesel production using alumina-supported calcium oxide: An optimization study. Fuel Process Technol 2010;91:243–8.

[169] Zarei A, Amin NAS, Talebian-Kiakalaieh A, Zain NAM. Immobilized lipase-catalyzed transesterification of Jatropha curcas oil: Optimization and modeling. J Taiwan Inst Chem Eng 2014;45:444–51.

[170] Zabeti M, Daud WMAW, Aroua MK. Optimization of the activity of CaO/Al_2O_3 catalyst for biodiesel production using response surface methodology. Appl Catal A Gen 2009;366:154–9.

[171] Lee HV, Yunus R, Juan JC, Taufiq-Yap YH. Process optimization design for jatropha-based biodiesel production using response surface methodology. Fuel Process Technol 2011;92:2420–8.

[172] Noordin M., Venkatesh V., Sharif S, Elting S, Abdullah A. Application of response surface methodology in describing the performance of coated carbide tools when turning AISI 1045 steel. J Mater Process Technol 2004;145:46–58.

[173] Ashri KRD. Effective process parameters of mustard oil biodiesel - A review and analysis. Int J Emerg Technol 2014;5:99–106.

[174] Singh S, Sharma S, Mohapatra SK, Kundu K. Optimization of cotton seed methyl ester and mustard methyl ester from transesterification process. Int J Eng Sci Res Technol 2013;2:2027–31.

[175] Bouaid A, Diaz Y, Martinez M, Aracil J. Pilot plant studies of biodiesel production using Brassica carinata as raw material. Catal Today 2005;106:193–6.

[176] Zapata N, Vargas M, Reyes JF, Belmar G. Quality of biodiesel and press cake obtained from Euphorbia lathyris, Brassica napus and Ricinus communis. Ind Crops Prod 2012;38:1–5.

[177] Jham GN, Moser BR, Shah SN, Holser RA., Dhingra OD, Vaughn SF, et al. Wild brazilian mustard (brassica juncea l.) seed oil methyl esters as biodiesel fuel. J Am Oil Chem Soc 2009;86:917–26.

[178] Jazie AA, Pramanik H, Sinha ASK. Egg shell waste-catalyzed transesterification of mustard oil : optimization using response surface methodology (RSM). Int. Conf. Power Energy Syst., 2012;56:52–7.

[179] Yang Z, Xie W. Soybean oil transesterification over zinc oxide modified with alkali earth metals. Fuel Process Technol 2007;88:631–8

[180] Wdowin M, Franus M, Panek R, Badura L, Franus W. The conversion technology of fly ash into zeolites. Clean Technol Environ Policy 2014;16:1217–23.

[181] Franus W, Wdowin M, Franus M. Synthesis and characterization of zeolites prepared from industrial fly ash. Environ Monit Assess 2014;186:5721–9.

[182] Shigemoto N, Hayashi H, Miyaura K. Selective formation of Na-X zeolite from coal fly ash by fusion with sodium hydroxide prior to hydrothermal reaction. J Mater Sci 1993;28:4781–6.

[183] Ríos RCA, Williams CD, Roberts CL. A comparative study of two methods for the synthesis of fly ash-based sodium and potassium type zeolites. Fuel 2009;88:1403–16.

[184] Catalfamo P, Corigliano F, Primerano P, Di Pasquale S. Study of the pre-crystallization stage of hydrothermally treated amorphous aluminosilicates through the composition of the aqueous phase. J Chem Soc Faraday Trans 1993;89:171–5.

[185] Pengthamkeerati P, Satapanajaru T, Chularuengoaksorn P. Chemical modification of coal fly ash for the removal of phosphate from aqueous solution. Fuel 2008;87:2469–76.

[186] Ojha K, Pradhan NC, Samanta AN. Zeolite from fly ash: synthesis and characterization. Bull Mater Sci 2004;27:555–64.

[187] Querol X, Lbpez-soler A, Fernhdez-turiel JL. Synthesis of zeolites by alkaline of ferro-aluminous fly ash activation. Fuel 1995;74:1226–31.

[188] Xie W, Huang X. Synthesis of biodiesel from soybean oil using heterogeneous KF/ZnO catalyst. Catal Letters 2006;107:53–9.

[189] Singh S, Patel A. 12-Tungstophosphoric acid supported on mesoporous molecular material: synthesis, characterization and performance in biodiesel production. J Clean Prod 2014;72:46–56.

[190] Sánchez M, Navas M, Ruggera JF, Casella ML, Aracil J, Martínez M. Biodiesel production optimization using γAl_2O_3 based catalysts. Energy 2014;73:661–9.

[191] Feyzi M, Khajavi G. Investigation of biodiesel production using modified strontium nanocatalysts supported on the ZSM-5 zeolite. Ind Crops Prod 2014;58:298–304.

[192] Shu Q, Yang B, Yuan H, Qing S, Zhu G. Synthesis of biodiesel from soybean oil and methanol catalyzed by zeolite beta modified with La^{3+}. Catal Commun 2007;8:2159–65.

[193] SathyaSelvabala V, Selvaraj DK, Kalimuthu J, Periyaraman PM, Subramanian S. Two-step biodiesel production from Calophyllum inophyllum oil: optimization of modified β-zeolite catalyzed pre-treatment. Bioresour Technol 2011;102:1066–72.

[194] Rocha J, Del Arco M, Rives V, Ulibarri MA. Reconstruction of layered double hydroxides from calcined precursors: a powder XRD and 27Al MAS NMR study. J Mater Chem 1999;9:2499–503.

[195] Tynjälä P, Pakkanen TT. Acidic properties of ZSM-5 zeolite modified with Ba^{2+}, Al^{3+} and La^{3+} ion-exchange. J Mol Catal A Chem 1996;110:153–61.

[196] Di Cosimo JI, Díez VK, Xu M, Iglesia E, Apesteguía CR. Structure and surface and catalytic properties of Mg-Al basic oxides. J Catal 1998;178:499–510.

[197] Hickey L, Kloprogge JT, Frost RL. The effects of various hydrothermal treatments on magnesium-aluminium hydrotalcites. J Mater Sci 2000;35:4347–55.

[198] Kloprogge JT, Hickey L, Frost RL. Heating stage Raman and infrared emission spectroscopic study of the dehydroxylation of synthetic Mg-hydrotalcite. Appl Clay Sci 2001;18:37–49.

[199] Liu X, Fan B, Gao S, Li R. Transesterification of tributyrin with methanol over MgAl mixed oxides derived from MgAl hydrotalcites synthesized in the presence of glucose. Fuel Process Technol 2013;106:761–8.

[200] Rey F, Forns V, Rojo JM. Thermal decomposition of hydrotalcites. An infrared and nuclear magnetic resonance spectroscopic study. J Chem Soc Faraday Trans 1992;88:2233.

[201] Kanezaki E. Thermal behavior of the hydrotalcite-like layered structure of Mg and Al-layered double hydroxides with interlayer carbonate by means of in situ powder HTXRD and DTA/TG. J Chem Soc Faraday Trans, 1998;106:279–84.

[202] Roelofs JCA, van Bokhoven JA, van Dillen AJ, Geus JW, De Jong KP. The thermal decomposition of Mg-Al hydrotalcites: effect of interlayer anions and characteristics of the final structure. Chem A Eur J 2002;8:5571–9.

[203] Hosoglu F, Faye J, Mareseanu K, Tesquet G, Miquel P, Capron M, et al. High resolution NMR unraveling Cu substitution of Mg in hydrotalcites–ethanol reactivity. Appl Catal A Gen 2014:1–9.

[204] Xu S, Liao MC, Zeng HY, Zhang ZQ, Liu XJ, Zhu P-H. Ultrafine hydrotalcite particles prepared with novel technology to improve the flame retardancy of polypropylene. Appl Clay Sci 2015;108:215–21.

[205] Oh JM, Hwang SH, Choy JH. The effect of synthetic conditions on tailoring the size of hydrotalcite particles. Solid State Ionics 2002;151:285–91.

[206] Farooq M, Ramli A, Subbarao D. Biodiesel production from waste cooking oil using bifunctional heterogeneous solid catalysts. J Clean Prod 2013;59:131–40.

[207] Sun C, Qiu F, Yang D, Ye B. Preparation of biodiesel from soybean oil catalyzed by Al-Ca hydrotalcite loaded with K_2CO_3 as heterogeneous solid base catalyst. Fuel Process Technol 2014;126:383–91.

[208] Volli V, Purkait MK. Physico-chemical properties and thermal degradation studies of commercial oils in nitrogen atmosphere. Fuel 2014:1010–9

International Journals:

1. **Volli V**, Purkait MK. Selective preparation of zeolite X and A from flyash and its use as catalyst for biodiesel production. J Haz Mat. 2015;297:101-111.
2. Bhandari R, **Volli V**, Purkait MK. Preparation and characterization of flyash based mesoporous catalyst for transesterification of soybean oil. J Env Chem Eng. 2015;3:906-914
3. **Volli V**, Purkait MK. Physico-chemical properties and thermal degradation studies of commercial oils in nitrogen atmosphere. Fuel 2014;117:1010–9.

Manuscripts Communicated:

1. **Volli V**, Purkait MK. Preparation and characterization of hydrotalcite with bifunctional properties from flyash and use as heterogeneous catalyst. Clean Technol Environ Policy (under review)
2. **Volli V**, Purkait MK. Utilization of flyash as heterogeneous catalyst for transesterification. J Ind & Eng Chem. (under review)

National Conference:

1. **Volli V**, Purkait MK. Physico-chemical properties and thermal degradation studies of commercial oils in nitrogen atmosphere. Reflux (2013).